ÇUKUROVA UNIVERSITY
INSTITUTE OF NATURAL AND APPLIED SCIENCES

PhD THESIS

Bülent BÜYÜKGÜZEL

HYBRID GLOBAL MAXIMUM POWER POINT TRACKING SYSTEM FOR SOLAR PANELS

DEPARTMENT OF ELECTRICAL AND ELECTRONICS ENGINEERING

ADANA-2022

ABSTRACT

PhD THESIS

HYBRID GLOBAL MAXIMUM POWER POINT TRACKING SYSTEM FOR SOLAR PANELS

Bülent BÜYÜKGÜZEL

ÇUKUROVA UNIVERSITY
INSTITUTE OF NATURAL AND APPLIED SCIENCES
DEPARTMENT OF ELECTRICAL AND ELECTRONICS ENGINEERING

Supervisor : Assoc. Prof. Dr. Murat AKSOY
Year: 2022, Pages: 129
Jury : Assoc. Prof. Dr. Murat AKSOY
: Prof. Dr. Mehmet KARAKILÇIK
: Prof. Dr. Ahmet TEKE
: Assoc. Prof. Dr. M. Mustafa SAVRUN
: Asst. Prof. Dr. Zehan KESİLMİŞ

Due to the nonlinearity of the power-voltage (P-V) characteristic, maximum power can be obtained from the PV panel at a single operating point called the Maximum Power Point (MPP). This point, which varies depending on environmental and load conditions, must be determined continuously by a system known as the Maximum Power Point Tracking (MPPT) system. The situation where some parts of the PV panel receive different radiation due to obstructions such as dirt, clouds and trees is called partial shading. In the absence of partial shading, the P-V curve has only one maximum power point, while in the case of partial shading, multiple local maximum power points occur. Determining the highest value (global maximum power point GMPP) among these points and operating the PV panel at this point is a problem that classical MPPT systems cannot solve. As a result, in the case of partial shading, it is necessary to employ GMPP tracking systems capable of locating the GMPP. In this thesis study, a new bypass diode-based hybrid MPPT system is designed, which uses currents passing through the bypass diodes to estimate the location of the GMPP and then searches only around this location using the Particle Swarm Optimisation (PSO) algorithm.

Keywords: MPPT, GMPPT, Hybrid MPPT, Partial Shading, Bypass Diode

ÖZ

DOKTORA TEZİ

SOLAR PANELLER İÇİN HİBRİD GLOBAL MAKSİMUM GÜÇ NOKTASI TAKİP SİSTEMİ

Bülent BÜYÜKGÜZEL

ÇUKUROVA ÜNİVERSİTESİ
FEN BİLİMLERİ ENSTİTÜSÜ
ELEKTRİK - ELEKTRONİK MÜHENDİSLİĞİ ANABİLİM DALI

Danışman : Doç. Dr. Murat AKSOY
Yıl : 2022, Sayfa: 129
Jüri : Doç. Dr. Murat AKSOY
: Prof. Dr. Mehmet KARAKILÇIK
: Prof. Dr. Ahmet TEKE
: Doç. Dr. M. Murat SAVRUN
: Dr. Öğr. Üyesi Zehan KESİLMİŞ

PV panelden, güç-gerilim (P-V) karakteristiğinin doğrusal olmaması nedeniyle, Maksimum Güç Noktası (MGN) olarak adlandırılan, tek bir çalışma noktasında maksimum güç elde edilebilir. Çevresel koşullar ve yük durumuna göre yeri değişen bu noktanın Maksimum Güç Noktası Takip (MGNT) sistemi olarak adlandırılan bir sistem tarafından sürekli olarak belirlenmesi gerekmektedir. PV panelin bazı bölümlerinin kir, bulut, ağaç gibi engelleyiciler nedeniyle farklı ışınım alması durumu kısmi gölgelenme olarak adlandırılır. Kısmi gölgelenmenin olmadığı durumda P-V eğrisinde sadece bir maksimum güç noktası bulunurken kısmi gölgelenme durumunda birden fazla lokal maksimum güç noktası meydana gelmektedir. Bu noktalar arasından en yüksek değerli olan (global maksimum güç noktası GMGN) tespit edilerek PV panelin bu noktada çalıştırılması klasik MGNT sistemlerinin çözemediği bir problemdir. Bu nedenle kısmi gölgelenme durumunda, global maksimum güç noktasını bulabilen GMGN takip sistemlerinin kullanılması gereklidir. Bu tez çalışmasında bypass diyotlarından geçen akımlar kullanılarak GMGN'nin yerini tahmin eden ve daha sonra sadece bu yer etrafında Parçacık Sürü Optimizasyonu (PSO) algoritması kullanarak arama yapan bypass diyot tabanlı yeni bir hibrit MGNT sistemi tasarlanmıştır.

Anahtar Kelimeler: MGNT, GMGN, Hibrit MGNT, Kısmi Gölgelenme, Baypas Diyot

EXTENDED ABSTRACT

The gradual decrease in fossil fuels used as energy sources and the increase in negative environmental effects due to the use of these fuels cause an increasing concern in the world. This concern has resulted in an increase in the use of renewable energy resources, which are constantly renewed and do not deplete over time, and have a very low environmental impact when compared to fossil fuels. Wind, photovoltaic (PV), geothermal, and tidal energy are among the renewable energy sources that have seen significant advancements in recent years.

Among renewable energy sources, the amount of increase in the use of photovoltaic systems has the highest value. According to 2021 data, the total installed power of PV systems worldwide is 942 GW, a 22 % increase over the previous year (Gibb, et al., 2022).

Photovoltaic energy has a significant disadvantage in terms of efficiency. Besides being renewable and sustainable, aside from the low efficiency of PV panels, which are the main components used in energy conversion, the use of other components, such as DC/AC inverters, which are required for energy production, is not increasing quickly enough due to the high investment costs caused by the low efficiency.

Consumers who invest in PV systems intend to maximize their economic gain by generating as much power as possible and transferring it to a distribution network that is exclusive to them or to which other consumers are also connected. As a result, the greatest expectation from PV systems is that they produce the most energy possible and thus recover the money spent on the investment as soon as possible.

The production cost of PV panels used in energy conversion was \$0.67/W in 2015, but it has since dropped to \$0.26/W in 2021. On the other hand, technological advancements in semiconductors and other components used in power electronics cause the investment and operating costs of power generation facilities to decrease, as do the investment return times (Feldman, Dummit, Zuboy, & Margolis, 2022).

Despite the decrease in production costs, the energy conversion efficiency of PV panels remains low, necessitating the extraction of the maximum amount of energy possible from the panels, i.e., operating them at maximum efficiency. One of the most significant causes of efficiency loss is operating the PV panel at a power point other than the MPP. The MPPT system is in charge of pulling the operating point, which varies depending on load resistance and environmental conditions, such as irradiance and temperature, to the maximum power point at that time. The success of the MPPT system in locating and maintaining the MPP is another critical parameter that affects the overall system's efficiency.

Assume that all panels connected in series receive the same amount of radiation. In this case, a single maximum power point will emerge on the P-V curve and MPPT systems using traditional search algorithms will successfully find and track this point. However, in the case of partial shading, where some panels receive less irradiance than others for whatever reason, multiple maximum power points will emerge. This situation is a problem that traditional search algorithms cannot solve, necessitating the use of meta-heuristic algorithms capable of locating global optimum points.

Research on MPPT systems has focused on this topic, with numerous algorithms proposed in the literature in recent years. Even though these algorithms have different advantages over one another, the speed with which they reach the global maximum power point and their ability to follow this point are the points that must be developed for all algorithms (Ali, et al., 2020; Liu, Chen, & Huang, 2015; Kumar, Nema, Nema, & Verma, 2020; Yang, Zhang, Yu, Shu, & Fang, 2017).

Reaching the right MPP point as soon as possible for the MPPT system is a desirable feature as it directly affects the system efficiency. The time it takes for the MPPT system to reach the MPP point increases the amount of energy lost during this time. For this reason, researches on algorithms that will shorten the search time as much as possible while reaching the MPP point of the algorithms used are increasing.

In recent years, the use of heuristic algorithms has been used very often in determining the GMP point. However, due to the large search spaces of these algorithms, the access time to the GMP point is quite long.

Therefore, the energy losses in the dynamic state are quite high. On the other hand, as the scanning process is repeated due to frequently changing operating conditions, losses are repeated and efficiency decreases.

So, using heuristic algorithms alone in MPPT systems is quite problematic in terms of applicability. The success of heuristic algorithms in detecting the GMP point is indisputable. It is clear that the search range should be narrowed as much as possible in order to shorten the search time, which negatively affects the system efficiency.

In this regard, the importance of hybrid systems, in which different algorithms are used together in the same MPPT system to develop some features, is growing.

In the present thesis study, a new MPPT system was designed and simulated by utilizing the current flowing through the bypass diode used to prevent the low irradiated panel from causing excessive power loss by limiting the current of the series-connected PV array in the event of partial shading.

The currents passing through the bypass diodes in a situation close to the short circuit state are measured in this developed system, and the location of the global maximum power point is approximated by using irradiance values and then these values.

The estimated location of the global maximum power point is used as the offset value of the search space of the Particle Swarm Optimization (PSO) algorithm in the second step. The PSO algorithm's search space is shifted around the predicted location of the global maximum power point on the P-V curve, allowing for a search with a small number of particles in a small area. In this manner, unlike conventional MPPT systems using the PSO algorithm, only a subset of the P-V curve is scanned, rather than the entire P-V curve. Since the scanning area is smaller than in other PSO algorithms, it requires fewer particles and, thus, fewer iterations.

GENİŞLETİLMİŞ ÖZET

Enerji kaynağı olarak kullanılan fosil yakıtların giderek azalması ve bu yakıtların kullanımı sonucunda ortaya çıkan olumsuz çevresel etkilerdeki artış, dünyada giderek artan bir endişeye neden olmaktadır. Bu endişe, sürekli olarak yenilenen ve yaşam boyu tükenmeyen, çevresel etkileri ise fosil yakıtlarla kıyaslandığında oldukça az olan yenilenebilir enerji kaynaklarının kullanımının artmasına neden olmuştur. Son yıllarda kullanımı artan yenilebilir enerji kaynakları arasında rüzgâr, fotovoltaik (PV), jeotermal ve gel-git enerjilerinin kullanımında önemli gelişmeler olmuştur.

Fotovoltaik sistemlerin kullanımındaki artış miktarı yenilenebilir enerji kaynakları içerisinde en yüksek değere sahiptir. 2019 yılı verilerine göre, dünya genelindeki PV sistemlerin toplam 942 GW kurulu güce sahip olduğu, bir önceki yıla göre ise %22'lik bir artışı göstermiştir (Gibb, et al., 2022).

Fotovoltaik Enerji, yenilenebilir ve sürdürülebilir olmasının yanında verimlilik gibi çok önemli bir dezavantajı da vardır. Enerji dönüşümünde kullanılan ana bileşen olan PV panellerin verimliliklerinin düşük olmasının yanında, enerji üretimi için gerekli olan DC/AC eviriciler gibi diğer bileşenlerin verimliliklerinin de düşük olmasından kaynaklanan yüksek yatırım maliyetleri nedeniyle kullanımı yeterince hızlı bir şekilde artmamaktadır.

PV sistemlerine yatırım yapan tüketiciler, mümkün olan maksimum gücün üretilerek bunu sadece kendilerine ait veya diğer tüketicilerin de bağlı olduğu bir dağıtım ağına aktarmak suretiyle olası maksimum ekonomik kazancı elde etmeyi planlamışlardır. Bu nedenle, PV sistemlerinden en büyük beklenti mümkün olan maksimum enerjinin üretilmesi ve bu sayede yatırım için harcanan paranın olabildiğince kısa sürede geri kazanılmasıdır.

Enerji dönüşümünde kullanılan PV panellerin üretim maliyeti 2015 yılında 0.67$/W iken 2021 yılında 0.26$/W'a düşmüştür. Diğer taraftan güç elektroniğinde kullanılan yarıiletken ve diğer bileşenlerde ortaya çıkan teknolojik gelişmeler, enerji üretim tesislerinin yatırım ve işletme maliyetlerinin giderek azalmasına ve yatırım geri dönüşüm sürelerinin de giderek kısalmasına neden olmaktadır (Feldman, Dummit, Zuboy, & Margolis, 2022).

Üretim maliyetlerinde yaşanan bu düşüşe karşın, PV panellerin enerji dönüşüm verimliliklerinin halen düşük olması nedeniyle panellerden mümkün olan maksimum enerjinin elde edilmesi yani maksimum verimde çalıştırılmasını zorunlu kılmaktadır. PV panelin maksimum güç noktasından farklı bir noktada çalıştırılması ise verim kaybının en önemli sebeplerinden birisidir. Işınım ve sıcaklık gibi çevresel koşulların yanında yük direncine de bağlı olarak değişen çalışma noktasının o andaki maksimum güç noktasına çekilmesi görevini MPPT sistemi üstlenir. MPPT sisteminin maksimum güç noktasını bulmadaki ve takip etmedeki başarısı da tüm sistemin verimliliğine etki eden çok önemli diğer bir parametredir.

Seri bağlı tüm panellerin aynı miktarda radyasyon aldığını varsayalım. Bu durumda, P-V eğrisi üzerinde tek bir maksimum güç noktası ortaya çıkacak ve geleneksel arama algoritmalarını kullanan MPPT sistemleri bu noktayı başarıyla bulup izleyecektir. Ancak, bazı panellerin diğer panellere göre herhangi bir nedenle daha az ışınım aldığı kısmi gölgelenme durumunda ise birden fazla maksimum güç noktası ortaya çıkacaktır. Bu durum, klasik arama algoritmalarının üstesinden gelemeyecekleri bir problemdir ve meta-sezgisel algoritmalar gibi global optimum noktalarını bulma yeteneğine sahip algoritmaların kullanımını zorunlu kılar.

Son yıllarda MPPT sistemleri konusunda yapılan araştırmalar bu alanda yoğunlaşmış ve literatürde çok sayıda algoritma önerilmiştir. Ancak, bu algoritmaların birbirlerine göre farklı üstünlükleri bulunsa da global maksimum güç noktasına erişim hızı ve bu noktayı takip edebilme becerileri tüm algoritmalar için geliştirilmesi gereken noktalardır (Ali, et al., 2020; Liu, et al., 2015; Kumar, et al., 2020; Yang, et al., 2017).

MPPT sisteminin doğru MPP noktasına mümkün olan en kısa sürede ulaşması sistem verimini doğrudan etkilediği için istenilen bir özelliktir. MPPT sisteminin MPP noktasına ulaşma süresi, bu esnada kaybedilen enerji miktarını arttırmaktadır. Bu nedenle kullanılan algoritmaların MPP noktasına erişirken arama zamanını olabildiğince kısaltacak algoritmaların konusunda yapılan araştırmalar giderek artmaktadır.

Son yıllarda sezgisel algoritmaların kullanımı GMP noktasının belirlenmesinde çok sıklıkla kullanılmaktadır. Ancak bu algoritmaların aram uzaylarının büyüklüğü nedeniyle GMP noktasına erişim süresi oldukça uzun olmaktadır. Bu nedenle dinamik durumdaki enerji kayıpları oldukça yüksek olmaktadır. Diğer taraftan sık değişen çalışma koşulları nedeniyle tarama işlemi yinelendiği için kayıplarda yinelenmekte ve verim düşmektedir.

Bu nedenle sezgisel algoritmaların tekbaşlarına MPPT sistemlerinde kullanılması uygulanabilirlik açısından oldukça problemlidir.

Sezgisel algoritmaların GMP noktasını tespit etmedeki başarıları tartışmasızdır. Sistem verimini olumsuz olarak etkileyen arama süresinin kısaltılması için arama aralağının olabildiğince daraltılması gerektiği açıktır.

Birtakım özelliklerin geliştirilmesi için aynı MPPT sisteminde birbirinden farklı algoritmaların bir arada kullanıldığı karma sistemlerin önemi bu açıdan giderek artmaktadır.

Bu tez çalışmasında, kısmi gölgelenme durumunda az ışınım alan panelin seri bağlı PV dizisinin akımını sınırlayarak aşırı güç kaybına neden olmasının engellenmesi amacıyla kullanılan bypass diyotundan geçen akımdan faydalanılarak yeni bir MPPT sistemi tasarlanmış ve simülasyonu yapılmıştır.

Geliştirilen bu sistemde kısa devre durumuna yakın bir durumda bypass diyotlarından geçen akımlar ölçülerek önce ışınım değerleri sonra bu değerler kullanılarak global maksimum güç noktasının yeri yaklaşık olarak tahmin edilmektedir.

İkinci aşamada global maksimum güç noktasının tahmini yeri Parçacık Sürü Optimizasyonu (PSO) algoritmasının arama uzayınınım ofset değeri olarak kullanılmıştır. PSO algoritmasının arama uzayı, P-V eğrisi üzerinde global maksimum güç noktasının tahmin edilen yeri civarına kaydırılarak sınırlı bir alanda sınırlı bir parçacık sayısı ile arama yapılması sağlanmıştır. Bu sayede, PSO algoritmalı klasik MPPT sistemlerinin aksine tüm bir P-V eğrisi değil P-V eğrisi üzerindeki sınırlı bir alan taranmaktadır. Tarama alanı PSO kullanan diğer algoritmalara göre daha küçük olması nedeniyle de daha az sayıda parçacık ve dolayısıyla daha az iterasyon gerektirmektedir.

ACKNOWLEDGEMENTS

I would like to express my heartfelt thanks to my supervisor, Assoc. Prof. Dr. Murat AKSOY for his help, support, invaluable advice and guidance throughout this thesis.

I would like to thank to Prof. Dr. Ahmet TEKE, Prof. Dr. Mehmet KARAKILÇIK, Assoc. Prof. Dr. M. Mustafa SAVRUN and Asst. Prof. Dr. Zehan KESİLMİŞ for accepting to be a member of the examining committee for my thesis.

Finally, I would like to thank my beloved wife, Rana and my one and only son, Batuhan, who motivated, encouraged and supported me throughout my thesis and even during the difficult days, we are going through.

This thesis is dedicated to two most precious people in my life, Rana and Batuhan.

CONTENTS **PAGE**

LIST OF TABLES **PAGE**

LIST OF FIGURES **PAGE**

LIST OF SYMBOLS AND ABBREVIATIONS

Symbols	Description
h	: Planck’s constant
k	: Boltzmann’s constant
σ	: Stefan-Boltzmann’s constant
λ	: Photon’s wavelength
c	: Speed of light
f	: Frequency
E_g	: Band gap energy
q	: Charge of an electron
I	: Current
I_{PH}	: Photon generated current
I_D	: Diode current
I_0	: Diode saturation current
I_{SC}	: Short circuit current
I_{MPP}	: Maximum power point current
V	: Voltage
V_T	: Thermal voltage
V_{OC}	: Open circuit voltage
V_D	: Diode voltage
V_{MPP}	: Maximum power point voltage
R_S	: Serial resistance
R_{SH}	: Shunt resistance
n,n_1,n_2	: Diode ideality factor
A	: Combined diode ideality factor
n_s	: number of the series connected cell
D	: Duty cycle

α_{ISC} : Temperature coefficient of I_{SC}

α_{VOC} : Temperature coefficient of V_{OC}

G : Irradiance

Abbreviations	**Description**
PV	: Photovoltaic
MPP	: Maximum Power Point
MPPT	: Maximum Power Point Tracking
LMPP	: Local Maximum Power Point
GMPP	: Global Maximum Power Point
GMPPT	: Global Maximum Power Point Tracking
STC	: Standard Test Condition
AM	: Air Mass
NOCT	: Nominal Operating Cell Temperature
PSC	: Partial Shading Condition
PS	: Shading Pattern
NN	: Neural Network
BD	: Bypass Diode
BDC	: Bypass Diode Current
IC	: Incremental Conductance
PWM	: Pulse With Modulation
PID	: Proportional-Integral-Derivative
P&O	: Perturb and Observe
HC	: Hill Climbing
GA	: Genetic Algorithm
DE	: Differential Evolution
MDE	: Modified Differential Evolution
CS	: Cuckoo Search

ACO	: Ant Colony Optimization
BOA	: Butterfly Optimization Algorithm
GWO	: Grey Wolf Optimization
ABCO	: Artificial Bee Colony Optimization
BSA	: Bat Search Algorithm
FA	: Firefly Algorithm
SA	: Simulated Annealing
PSO	: Particle Swarm Optimization
NREL	: National Renewable Energy Laboratory

1. INTRODUCTION

A photovoltaic cell is a semiconductor element that uses the photovoltaic effect to convert the energy carried by photons of sunlight into electrical energy. The PV cell is essentially a p-n junction made up of p-type and n-type semiconductors like a diode. When sunlight strikes a *p* or *n*-type semiconductor, the photons' energy causes free *electron-hole* pairs, known as charge carriers, to appear in the semiconductor. The electric field that exists between the *p* and *n* regions separates these *electron-hole* pairs, allowing them to accumulate in different regions and creating a potential difference between the two ends.

1.1. The *p-n* Junction

When an *n-type* semiconductor in which electrons are the majority carriers, and a *p-type* semiconductor in which the holes are the majority carriers, are metallurgically combined, the resulting structure is a p-n junction.

Electrons and holes in the *n* and *p*-type regions diffuse from the majority to the minority side immediately after the merger. As shown in Figure 1.1, a region forms on both sides of the junction line in which the donor and acceptor atoms are ionized in opposite polarity due to electron and hole recombination passing to the opposite side. A *built-in voltage* occurs between the two sides of the junction point due to the polarity of the ionized atoms in this region depleted of majority carriers. This voltage difference, also known as the built-in potential barrier, creates an electric field in the junction area, preventing the majority of carriers from passing through to the other side. Thanks to this electric field arising in the depletion region, the p-n junction only conducts current in one direction; that is, it works as a diode (Luque & Hegedus, 2003).

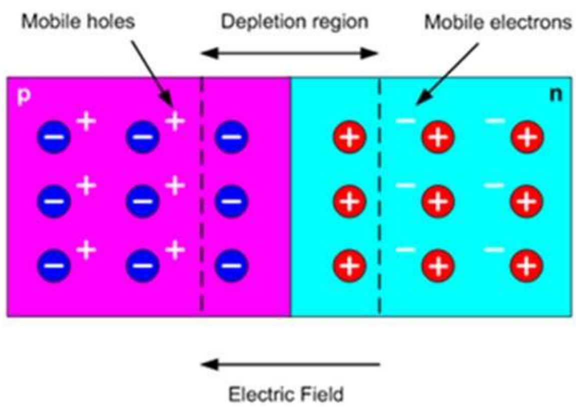

Figure 1.1 Build-in electric field of the p-n junction

1.2. The *p-n* Junction Diode

When a voltage is applied to the ends of a *p-n* junction in a direction that decreases the electric field in the depleted region, i.e., the *p*-side is positive with respect to the *n*-side, the width of the depleted region decreases. In this case, free electrons and holes have crossed the potential barrier, allowing current to flow between the terminals. On the contrary, when a voltage is applied such that the *p* side is negative and the *n* side is positive, the width of the depleted region expands, causing no current to flow and only a very small current, known as reverse saturation current, to flow. This current is generated by minority carriers that are thermally generated and are carried to the opposite side by the electric field. Equation (1.1) expresses the relationship between the voltage applied to the *p-n* diode terminals and the current flowing through them, and

Figure 1.2 depicts the I-V characteristic of the *p-n* diode (Gilbert, 2004).

$$I_D = I_0\left[\exp\left(\frac{qV_D}{nkT}\right) - 1\right] \tag{1.1}$$

where,

- I_O, reverse saturation current (A),
- I_D, diode current (A),

- q, electron charge (1.602×10^{-19} C),
- n, diode ideality factor,
- V_D, diode voltage (V),
- k, Boltzmann's constant (1.381×10^{-23} J/K),
- T, junction temperature in Kelvin (K).

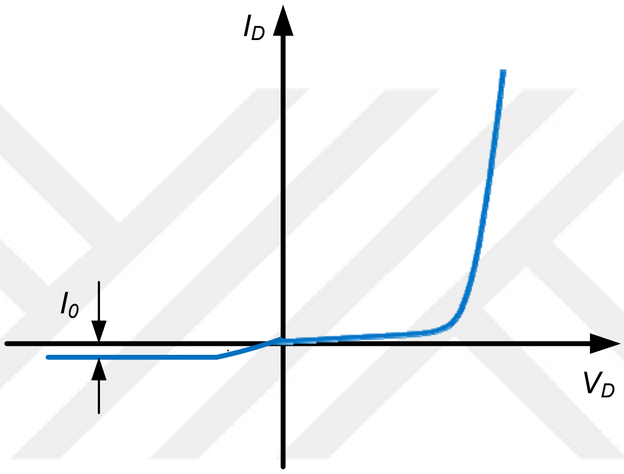

Figure 1.2 I-V Characteristics of the p-n junction diode

1.3. PV Cell

Figure 1.3 shows the physical structure of a PV cell. Metal strip contacts are placed at regular intervals on the top layer to allow light to pass through. Following these metal contacts are a thin n-type semiconductor layer and a thicker p-type semiconductor layer. The metal connected with the p-type semiconductor is placed at the bottom.

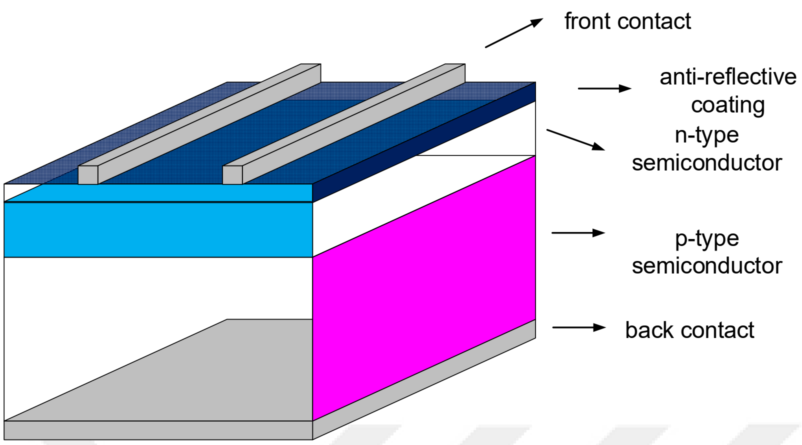

Figure 1.3 Physical structure of PV cell

Sunlight contains photons with varying wavelengths and energy levels that match these wavelengths. When sunlight strikes a semiconductor material, photons with energies less than the semiconductor layer's band gap energy cannot interact with the semiconductor material, and if the layer is in a light-transmitting structure, they pass through the layer. Photons with energies equal to or greater than the band gap energy cause electrons they collide with to enter the conduction band, i.e., the free state, and the excess energy is converted into heat. In the semiconductor, photons with energies greater than the band gap energy form *electron-hole* pairs, as shown in Figure 1.4.

These free electrons and holes are distributed evenly throughout the silicon crystal structure. After an average lifetime of 1 ms, some electrons and holes recombine and release their energy as heat. If these moving charge carriers approach the *p-n* junction boundary, the electric field in the depleted region will push the electrons to the *n* region and the holes to the *p* region. In other words, the electric field in the depletion region causes the separation of electron-hole pairs in both regions of the PV Cell as a result of the collision of photons and the accumulation of holes in the p region and electrons in the n region. This charge accumulation in the *p* and *n* regions results in a potential difference between the leads of the PV cell and an electric current flowing over a connected load (Gilbert, 2004).

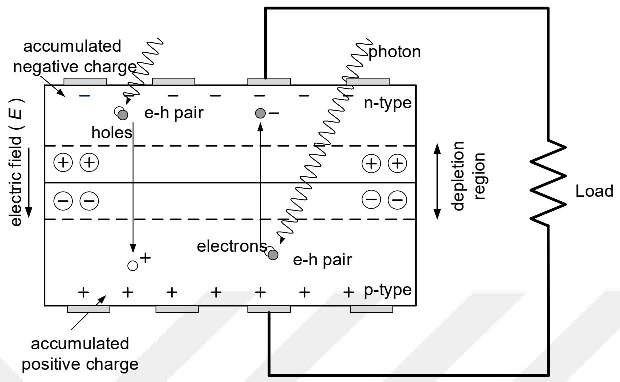

Figure 1.4 Photon, electron and electric field interaction within the p-n junction

1.4. Basic Parameters of the PV Cell and Its I-V curve

Figure 1.5 depicts the simplest equivalent circuit of the PV cell, which has a *p-n* diode structure. This equivalent circuit represents the ideal situation in which losses are not considered. The current produced by the photons is shown in the circuit by the current source I_{PH}. The value of this current is directly proportional to the amount of irradiance falling on the PV cell (Wenham, Green, Watt, Corkish, & Sproul, 2013).

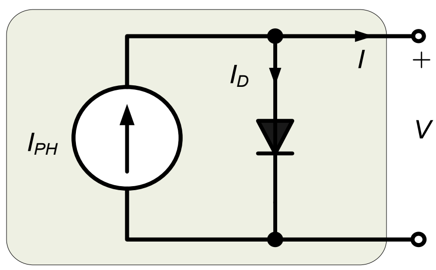

Figure 1.5 Equivalent circuit of the ideal PV cell

The power-voltage relationship of the PV cell can be written as follows using the equivalent circuit of the PV cell;

$$I = I_{PH} - I_0\left[\exp\left(\frac{qV}{nkT}\right) - 1\right] \tag{1.2}$$

Figure 1.6 depicts a PV cell's I-V characteristics and basic parameters. Examining the I-V characteristic reveals that the PV Cell acts as a current source at low voltage levels and as a voltage source at high voltage levels. The Equation (1.2) can also be used to understand the non-linear relationship between the PV Cell's output current and voltage. The nonlinearity of the current-voltage relationship leads to the nonlinearity of the generated power-voltage relationship. As a result, the PV Cell can only transfer maximum power to the load at one point. This point is called as the maximum power point (MPP), while the obtained power is called as the maximum power (P_{MPP}). Power gradually decreases on either side of the maximum power point, so the variation of power with voltage is zero at this point. In MPP, current and voltage values are denoted as I_{MPP} and V_{MPP}, respectively. When the PV cell terminals are short-circuited, the current is referred to as the short-circuit current (I_{SC}), and when they are open-circuit, the voltage at the terminals is referred to as the open-circuit voltage (V_{OC}). There is no power transfer from the PV cell to the outside in either case. If a load other than these two situations is connected to the ends of the PV cell, power will be transferred to the connected load.

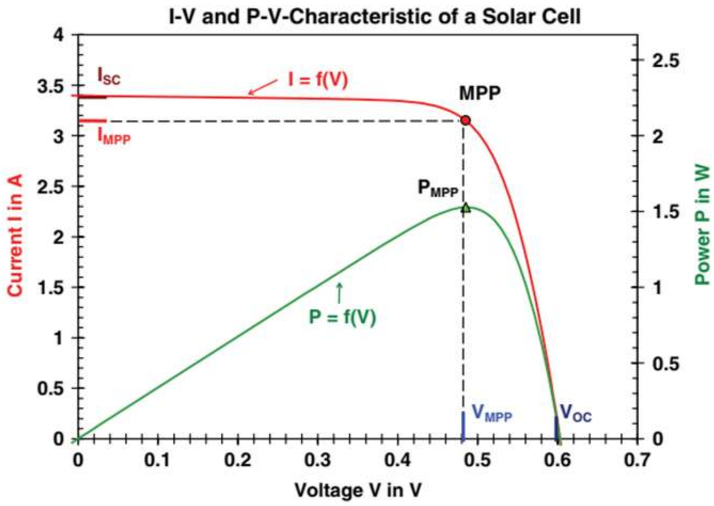

Figure 1.6 The I-V and P-V curves of the PV Cell and its basic parameters

1.5. Effect of The Irradiance and Temperature on the I-V Characteristic

The most important environmental elements impacting the basic parameters of PV cells are temperature and irradiance. The effect of these on the I-V and P-V characteristics is shown in Figure 1.7. The relationship between temperature, $I_{SC,}$ and V_{OC} is linear, as shown in Equations (1.3) and (1.4). On the other hand, V_{OC} changes logarithmically with irradiance, whereas I_{SC} changes linearly (Villalva, Gazoli, & Filho, 2009). The power produced by the PV Cell declines with temperature because the change of V_{OC} with temperature is higher and negative than that of I_{SC}.

$$I_{SC}\big|_{G} = \left(\frac{G}{G_0}\right) I_{SC}\big|_{STC}$$
$$V_{OC} = \frac{kT}{q}\ln\left(\frac{I_{SC}}{I_0}+1\right) \qquad (1.3)$$

$$V_{OC}\big|_T = V_{OC} + \alpha_{VOC}\left(T - T_{STC}\right)$$
$$I_{SC}\big|_T = I_{SC}\left(1 + \alpha_{ISC}\left(T - T_{STC}\right)\right) \tag{1.4}$$

where; $\propto_{VOC}$ and $\propto_{ISC}$ stand for the temperature coefficients of V_{OC} and I_{SC}, respectively, G stands for the irradiance value, and G_0 stands for the irradiance value under standard test conditions (STC). The irradiance value is applied as 1000 W/m^2, the spectral distribution of the irradiance as 1.5, so the air mass (AM) as 1.5, and the temperature as 25 C° in standard test conditions. AM defines the thickness of the atmosphere through which the light falling on the PV panel passes. AM1 indicates that light enters the atmosphere perpendicularly, while AM1.5 indicates that it enters at an angle of about 48°.

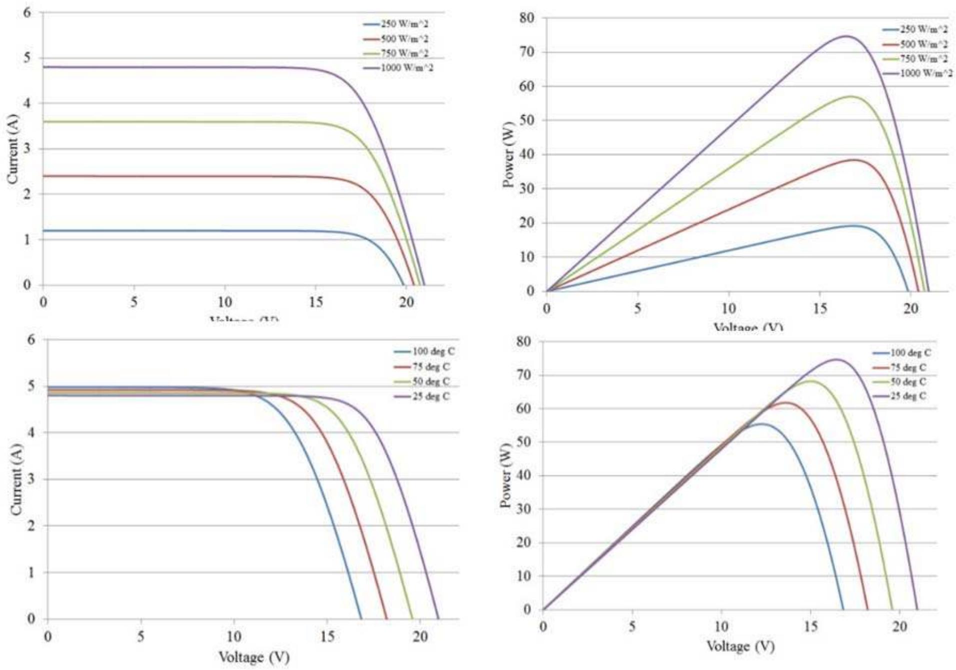

Figure 1.7 Effect of The Irradiance and Temperature on The I-V and P-V curves

1.6. Module, String, Array

A single PV cell cannot be utilized alone in most applications due to the open-circuit voltage of roughly 0.6 V. More than one PV Cell is connected in series to enhance the open-circuit voltage to more useful levels, and a PV module/panel is realized by encasing it in a protective sheath against external causes.

The basic building block of PV applications is this structure, known as a module or panel. Array structures are created by connecting modules in series to generate higher voltages and strings in parallel to obtain greater currents, as shown in Figure 1.8. All these structures can be called *PV Source.*

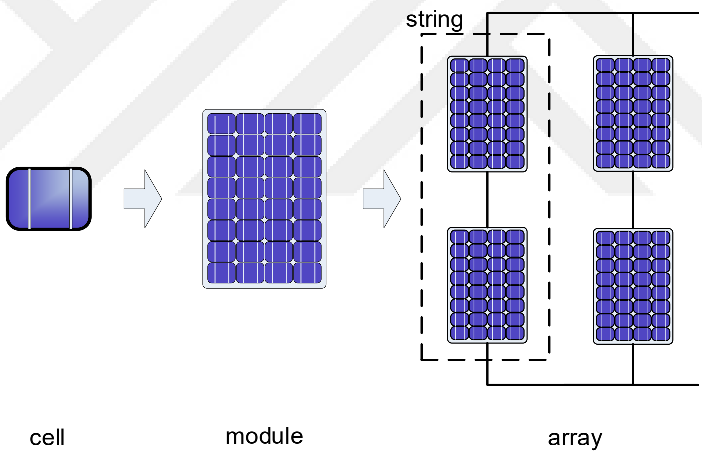

Figure 1.8 Photovoltaic Cell, Module, String, Array

1.7. Maximum Power Point Tracking

As previously stated, the I-V and P-V characteristics of the PV source (cell, module, string, or array) are non-linear. As a result, for a particular temperature and irradiance value, maximum power may be generated from the PV source only at one point inside the operational zone, i.e., in the range of 0-V_{OC}. The voltage of

MPP changes greatly with temperature, and the current value changes significantly with irradiance, as illustrated in Figure 1.9.

It is obvious that; V_{MPP}/I_{MPP} is the value of the load resistor (optimal load resistance) that determines the maximum power point as the operating point. The I-V characteristic will change if the external circumstances (irradiance and temperature) change; hence the location of the MPP and the value of the optimum load resistance will change as well. The PV source will function at a different operating point than the maximum power point if the load connected to the PV source and the optimal load value are not the same, and maximum power transfer from the PV source to the load will be impossible. When a different load resistor is coupled to a PV source with an optimum load resistor, the same thing happens. Maximum power transfer will not be achievable in this situation because the operating point will be different from MPP even if the environmental conditions stay the same.

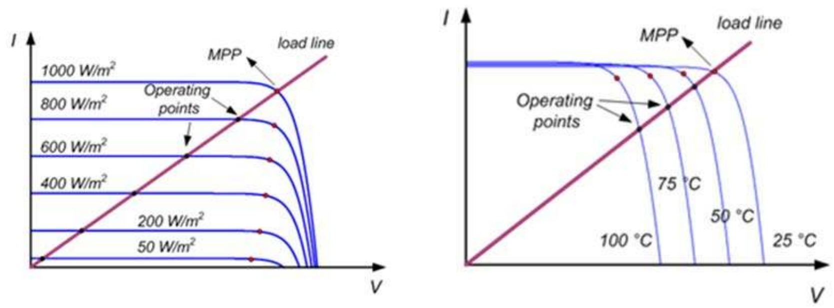

Figure 1.9 Location of the MPP at different irradiance and temperature

It is clear that the highest efficiency from a PV source can be obtained only at MPP and that the efficiency will drop at operating points other than the maximum power point. This is an undesirable situation for PV sources with low energy conversion efficiency. The efficiency of a PV source is defined as:

$$\eta = \frac{V_{PV} \bullet I_{PV}}{\int_0^\infty P(\lambda)\,d\lambda} \tag{1.5}$$

where, the power density at a given λ wavelength is denoted by $P(\lambda)$. In other words, the efficiency of a PV source is the ratio of the power from the source to the power supplied by the sunlight falling on it.

As shown in Figure 1.10, the maximum power point must be determined for each scenario of environmental conditions and/or load resistance. The operating point must be adjusted to obtain the most power from the PV source. A matching circuit should be installed between the PV source and the load resistor, and the operating point should be controlled by an appropriate control system to acquire maximum power. This procedure is called Maximum Power Point Tracking (MPPT).

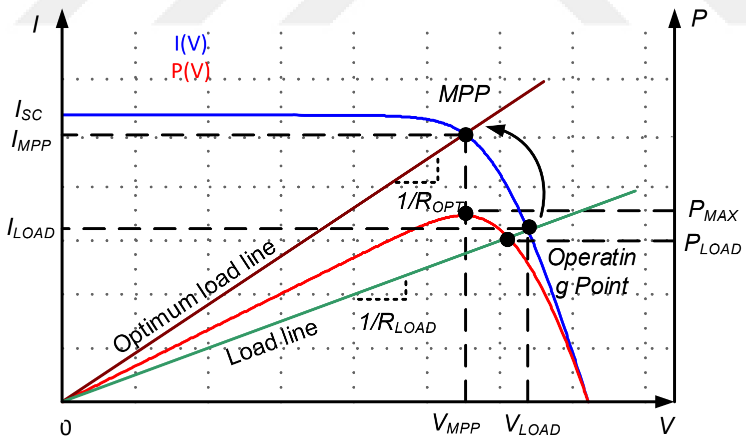

Figure 1.10 Operating points of the load connected PV source

By adjusting the pulse/period ratio (D) of a DC/DC converter connected between the load resistor and the source, as shown in Figure 1.11, the resistance seen by the PV source can be adjusted according to the changing position of the maximum power point due to changing environmental conditions and/or changing load resistance. At a steady state, assuming the DC/DC converter is lossless, the voltage conversion ratio *M(D)* can be stated as:

$$M(D) = \frac{V_{out}}{V_{in}} \quad (1.6)$$

The load resistance connected to the PV Cell, or the resistance *Ri,* which is seen at the DC/DC converter's input, can be defined as:

$$R_i = \frac{R_{Load}}{\left(M(D)\right)^2} \quad (1.7)$$

The input resistance can be modified by adjusting the pulse/period ratio of the switching signal applied to the DC/DC converter, as shown in Equation (1.7).

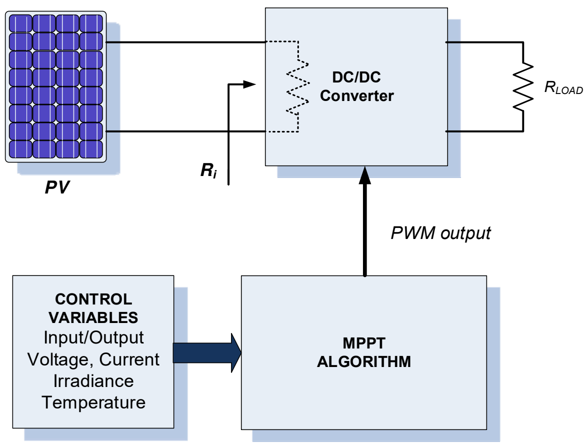

Figure 1.11 MPPT system connected to PV Source

The MPPT system is a dynamic system that always ensures maximum power from the system by eliminating the non-overlapping of the operating point and MPP of the PV Cell due to changing environmental conditions and changing load resistance. In other words, the MPPT system is a *dynamic optimization* system. The PV system must be regularly monitored to optimize, and the DC/DC converter's pulse/period ratio must be modified if a correction is deemed required upon analyzing the received data. The evaluation of the data received from the system, that is, the optimization process is performed by the algorithms used in the MPPT system. These algorithms are also known as MPPT Algorithms or methods/techniques. Most of these algorithms are implemented using both hardware and software, while some use analogue structures only.

In MPPT systems, very different structures are used as DC/DC converters. The voltage conversion ratio of the DC/DC converter utilized determines the variable range of resistance seen by the PV source, as depicted in Equation (1.7). Table 1.1 depicts the relationship between load resistance and input resistance for common DC/DC converter architectures.

Table 1.1 Variation range of the R_i according to converter type

Converter Type	R_i	Interval of the R_i
Buck	R_L/D^2	$R_L < R_i < \infty$
Boost	$(1-D)^2 R_L$	$0 < R_i < R_L$
Buck-Boost	$(1-D)^2 R_L/D^2$	$0 < R_i < \infty$

Despite the numerous studies on MPPT algorithms and DC/DC converter topologies in the literature, the goal is always to run the PV source at maximum efficiency.

1.8. Partial Shading

As previously stated, the voltage of a single PV cell is insufficient for many applications. As a result, after connecting multiple PV cells in series, a structure known as a module is constructed by encasing it in a protective sheath. However, the serial connection of PV cells brings with it a very big problem.

When some of the cells connected in a series get less irradiance (nonuniform irradiance) than others due to factors such as clouds, shadowing from surrounding structures, or pollution, it is called partial shading (PS). Partial shading will cause cells to exhibit lower I_{PH} currents, hence, lower I_{SC} currents than cells that receive more irradiance. Because the cells are coupled in series, the array's operating current will be limited to the lowest I_{SC} current. If the PV array is short-circuited, the *p-n* structure in cells with I_{SC} values greater than the lowest I_{SC} value will be forward polarized due to the current that cannot be transferred to the load, while the cell with the lowest I_{SC} value will be reversely polarized, as shown in Figure 1.12. In other words, this cell will be used as a load by other cells, resulting in power consumption. In fact, the excess power produced in other cells will be consumed in this cell. This causes the cell with the lowest I_{SC} to heat up, resulting in hot spots on the array. However, if the reverse voltage applied to the cell exceeds the *p-n* structure's breaking voltage in the opposite direction, the cell will be permanently damaged.

In addition to the power reduction and hot spot issues that occur with partial shading, exposing partially shaded cells to end voltages higher than the reverse breaking point voltage is a significant issue that should be avoided.

In the event that partially shaded cells reach short circuit currents, bypassing them by any means will be the most appropriate solution to all these problems. If the current flowing through a PV array reaches the short-circuit current of a partially shaded cell, the terminal voltage of that cell is zero, whereas when the string is forced to carry more current by connecting a lower load resistor or shorting it, the terminal voltage rises in the opposite direction.

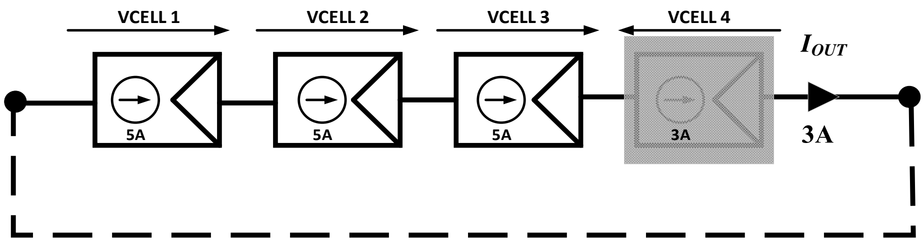

Figure 1.12. PV string under partial shading and output current of the string

If a diode is connected in parallel to the terminals of the PV cell in such a way that it is reverse biased under normal irradiance, this diode will be forward biased in case of shadowing. In case of partial shading, the diode will turn on, and this cell will be bypassed. The array current will no longer be limited by the shaded cell once this diode, known as the bypass diode, turns on and provides an additional current path. Because the bypass process also prevents the partially shaded cell from being used as a load, no hot spots will occur, the breaking voltage limits in the opposite direction will not be exceeded, and the cell will not sustain permanent damage.

Although the use of a bypass diode prevents the string current from being limited in the event of partial shading and thus reducing available power, another issue arises.

Figure 1.13 shows a PV string with four modules that receive different amounts of irradiance due to partial shading on one of the modules. The bypass diodes in this string will turn on or off based on the string current value, which varies with the operating point. In other words, the bypass diodes of modules in which I_{SC} current is less than the string current will be activated. As a result, the I-V characteristic of a partially shaded PV array will differ significantly from that of a PV array receiving uniform irradiance. I-V and P-V curves of this PV string are depicted in Figure 1.14. The I-V curve has a two-step structure because, after a certain current value due to two different irradiance values, the bypass diode of the fourth cell turns on and bypasses the cell, and thus the string current is not limited by the fourth cell and continues to increase. The I-V curve's two-step structure indicates two distinct maximum power points. This situation is clearly depicted in the P-V curve. The number of steps in the I-V curve, and thus the number of maximum power points, that is, the points with $dP/dV = 0$, will increase as the number of cells receiving different irradiance increases. The highest-rated power point is known as the Global Maximum Power Point (GMPP), while the others are known as the Local Maximum Power Points (LMPP). Figure 1.14 depicts that the maximum power obtained from the PV source is P3 if the bypass diode is not used, whereas the maximum power obtained is a higher value (P2) if the bypass diode is used. If the bypass diode is not used, the available power and system efficiency will gradually decrease as the amount of shading of the PV source exposed to partial shading increases. As a result, even though it complicates the optimization algorithms, the use of a bypass diode is required for system efficiency.

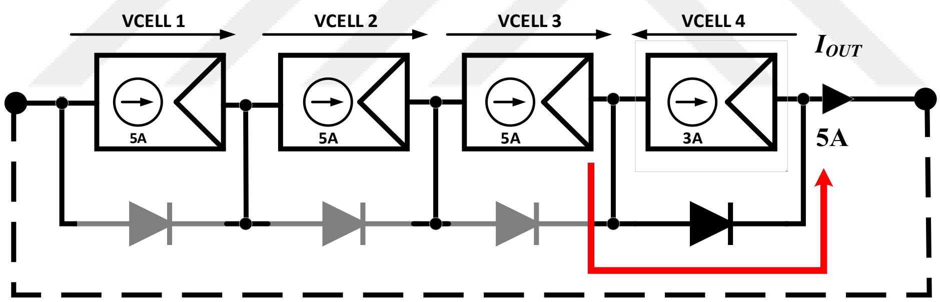

Figure 1.13 Bypassing of the shaded cell using diode

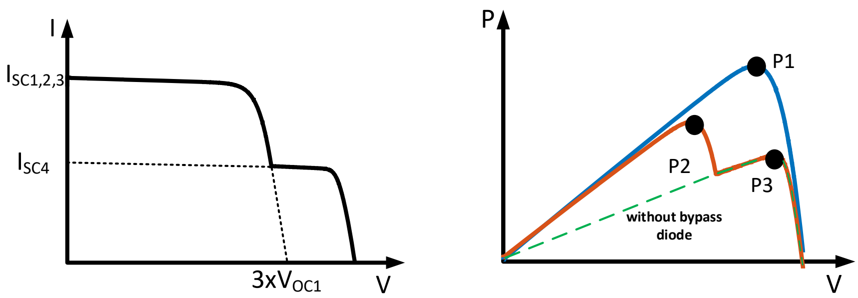

Figure 1.14 I-V and P-V curves under shaded PV string

Conventional MPPT systems generally observe the change in power by changing the voltage conversion ratio of the DC/DC converter and consider the first maximum power point found as GMPP. While these systems are capable of successfully determining the maximum power point in PV systems with a single maximum power point, such as the P1 point in Figure 1.14, they can give incorrect results in the case of partial shading where more than one maximum power point occurs. Since these systems are designed for PV sources that operate under uniform irradiance, they cannot distinguish the global maximum power point, such as the P2 point shown in Figure 1.14, from multiple maximum power points.

As a result, a more complex search or optimization algorithm that can find the global optimum in general in MPPT systems to be designed for PV sources operating under partial shading is required.

2. PV CELL MODELLING

The examination of the behaviour of PV sources in different operating conditions using simulations in a computer environment plays an important role in PV System research.

It is critical to use models that accurately reflect the characteristics of the PV source, particularly when designing MPPT systems in computer-aided design (CAD) studies that use circuit-based simulation tools such as PSPICE, PSIM, or general-purpose simulation tools such as MATLAB. It is always preferable to have a model that closely mimics the behaviour of the PV source, that is, using a real PV source that is precisely matched to the I-V data measured under different environmental conditions (irradiance and temperature).

The nonlinearity of the relationship between the output current and voltage due to the *p-n* junction structure is the most difficult challenge in modelling the PV Cell, which is the simplest PV source. The non-linear I-V relationship necessitates the use of non-linear components in the model's construction. Another difficulty is incorporating the effects of environmental conditions on the I-V characteristic into the model.

Various models for PV Cells have been proposed in the literature, as have numerous methods for determining the components of these models. The accuracy, complexity, and adaptability to changing environmental conditions of these models vary.

The equivalent circuit structure, which includes both linear and nonlinear components, is the most popular among the approaches used for modelling the PV Cell, such as Neural Network (AbdulHadi, Al-Ibrahim, & Virk, 2004; Karatepe, Boztepe, & Colak, 2006), curve fitting (Andrei, Ivanovici, Predusca, Diaconu, & Andrei, 2012), and Thevenin equivalent circuit (Chatterjee & Keyhani, 2011).

The PV Cell equivalent circuit-based model is typically built with one or more current sources, resistors, and diodes. The most widely used equivalent circuit-based models are the Single Diode Model (SDM) and Double Diode Model (DDM), depicted in Figure 2.1. If the SDM contains only a current source and a D1 diode, it is referred to as the Ideal Single Diode Model (ISDM), and if the R_S is included, it is referred to as the Simplified Single Diode Model (SSDM).

Despite a wide variety of PV Cell modelling techniques being available, SDM is widely regarded as the model with the best balance of accuracy and simplicity (Villalva, Gazoli, & Filho, 2009).

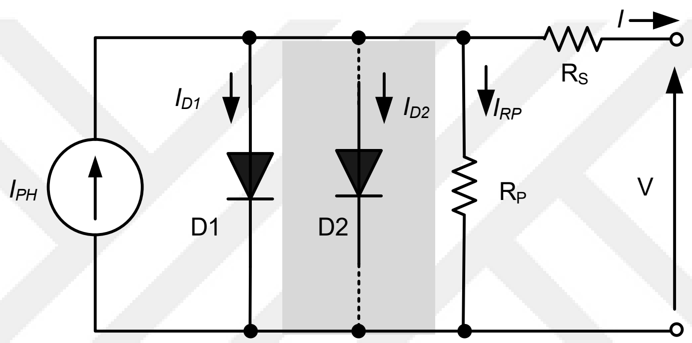

Figure 2.1 Single and Double Diode Model of the PV cell

2.1. Single Diode Model

In the model shown in Figure 2.1, where only the D1 diode is included, the current source I_{PH} shows the photon-induced current caused by the light hitting the PV cell, and the D1 diode shows the diffusion-induced losses. The series resistance is the sum of the *p*-type and n-type semiconductor resistances, as well as the resistances of the semiconductor-metal junction and metal contacts. Parallel resistance, on the other hand, describes leakage currents caused by material defects in the crystal structure, especially in the edge regions of the PV cell.

Using Figure 2.1, the relationship between the voltage and current between the output terminals of the PV cell can be expressed as the equation given below;

$$I = I_{PH} - I_D - I_{RP} = I_0\left[\exp\left(\frac{q(V + I \cdot R_S)}{nkT}\right) - 1\right] - \frac{V + IR_S}{R_P} \tag{2.1}$$

2.2. Double Diode Model

As previously stated, electron-hole pairs in the p-n structure produced by light striking the PV Cell are separated by the electric field located at the p-n junction and pushed towards the *p* and *n* regions by the electric field. However, recombination destroys some of these free electrons and holes before they can pass to the opposite region of the junction. This phenomenon is known as recombination, and it refers to the loss of carriers produced by light, which reduces the efficiency of the PV cell.

As shown in Figure 2.1, a second diode is added to the model to account for the recombination effect in the junction region, which becomes dominant, especially at low voltages. The relationship between the voltage and current between the terminals of the PV cell can be expressed in the Double Diode Model as follows;

$$\begin{aligned} I &= I_{PH} - I_{D1} - I_{D2} - I_{RP} \\ I &= I_{01}\left(\exp\left(\frac{q(V + I \cdot R_S)}{n_1 kT}\right) - 1\right) - I_{02}\left(\exp\left(\frac{q(V + I \cdot R_S)}{n_2 kT}\right) - 1\right) \\ &\quad - \frac{V + I \cdot R_S}{R_P} \end{aligned} \tag{2.2}$$

In this equation, n_1 and n_2 represent the quality factors of diodes D1 and D2, respectively, and I_{01} and I_{02} represent the reverse saturation currents of diodes D1 and D2, respectively.

2.3. Model of The PV Module

As can be seen in Figure 2.2, models of the structures, such as string and array, can be developed by using a single diode PV Cell model. If it is assumed that n_S number of cells connected in series and that each cell is exposed to the same irradiance and temperature, I_{PH} and I_O values of all cells will be the same. It can be easily found that the series resistance of the module is $n_S \cdot R_S$ and parallel resistance is $n_s \cdot R_P$ by using Thevenin's theorem. Terminal voltage of the series connected PV cell string will be $n_s{\cdot}V_D$.

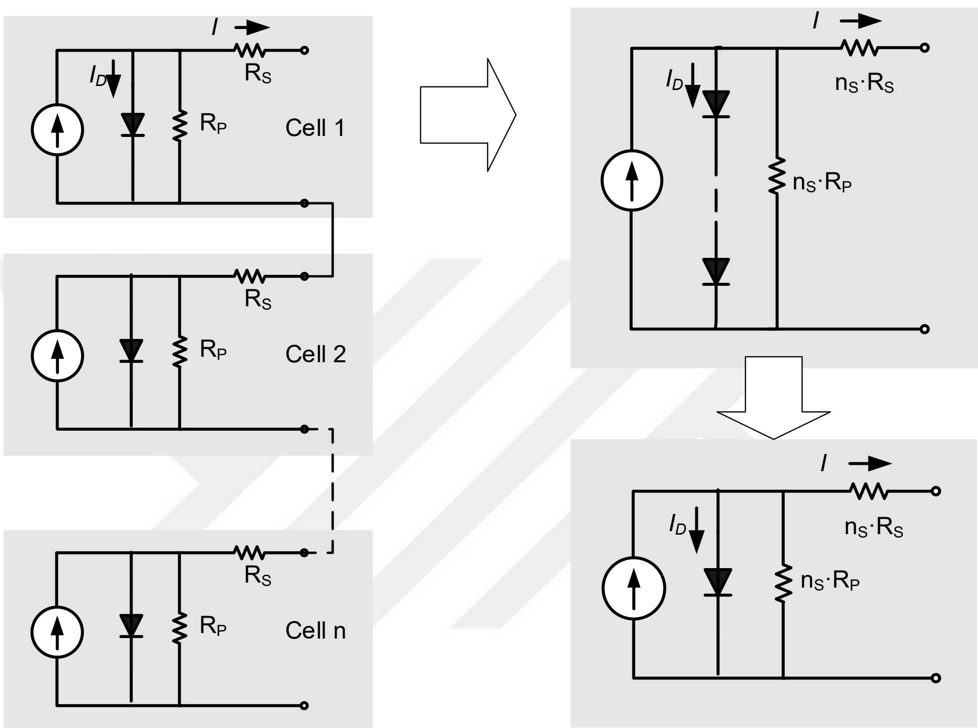

Figure 2.2 SDM of The PV Module

2.4. Parameter Estimation for the SDM

All equivalent circuit-based models contain a number of parameters that vary depending on the structure of the model. Accurate estimation/determination of these parameters, which can change depending on the temperature and irradiance value, is necessary for the accuracy of the model.

I_{PH}, I_0, R_S, n and R_P, are five parameters of the Single Diode Model that are required to be determined. For this reason, SDM is also called the five parameter model. In the literature, many methods have been proposed to determine/calculate these parameters using basic parameters, such as I_{SC} and V_{OC}, that are given in the datasheets of the manufacturers or obtained experimentally. These methods can be grouped into three main classes as analytical, numerical, and soft computing methods (Chatterjee & Keyhani, 2011; Tamrakar & Gupta, 2015). The accuracy of the obtained parameters differs according to the method used.

2.4.1. Analytical Methods

Commonly used analytical methods for determining SDM parameters only solve explicit mathematical equations and need much less computation time than other methods. These methods work well for both STC and varying environmental conditions (Tamrakar & Gupta, 2015).

A fully analytical solution was proposed by Chan and Phang (1987) using Equation (2.2) for extracting single and double diode model parameters and other equations derived from this equation for short circuit and open circuit cases. In some studies, since I_0 current can be neglected in the case of short circuit, solutions have been made by assuming that I_{PH} equals to I_{SC}. In the case of short circuit in some works, I_0 current can be neglected; solutions are generated assuming that I_{PH} equals to I_{SC} (Villalva, Gazoli, & Filho, 2009; Femia, Petrone, Spagnuolo, & Vitelli, 2017). Having obtained I_{PH} by using this approach, other parameter I_0 can be found by using open-circuit voltage. However, there are also studies stating that this approach will negatively affect the accuracy of the model (Sera, Teodorescu, & Rodriguez, 2007).

Jain and Kapoor (2004) suggested using the *Lambert W* function in order to determine the PV cell parameters. In this method, the current-voltage relationship of the PV module, which is expressed in a transcendental equation, is transformed into a $I = f(V)$ form using *the Lambert W* function, as expressed in Equation (2.3) , and the solutions are provided without using iteration (Di Piazza & Vitale, 2013).

$$I=-\frac{nV_T}{R_S}\text{Lambert } W\left[\frac{I_0 R_P R_S}{nV_T(R_P+R_S)}\exp\left(\frac{R_S\left(I_{PH}R_P+I_0R_P-V(R_P/R_S)\right)}{nV_T(R_P+R_S)}\right)\right] + \frac{I_{PH}R_P-I_0R_P-V}{\left(R_P+R_S\right)} \tag{2.3}$$

Similarly, Batzelis et al. (2014) have offered another feature that expresses the voltage according to the current by using *the Lambert W* function. Methods using the Lambert W function combine the versatility and accuracy provided by the single diode model with significantly faster and more accurate execution. Cubas et al. (2014) proposed an analytical method using the Lambert W function to transform the series resistance equation into an explicit equation. This method was used in order to analyse the performance of the commercial PV module in different irradiance and temperature levels.

2.4.2. Numerical Methods

The best approach to parameterization is to create a system of equations using the key parameters given in the manufacturer datasheets (Andrei, Ivanovici, Predusca, Diaconu, & Andrei, 2012; Mahmoud, Xiao, & Zeineldin, 2012; Siddique, Xu, & De Doncker, 2013). Due to the fact that PV source is *p-n* junction diode structure, and the relation of I-V is non-linear, the analytical expressions of the models are both non-linear and are implicit because they are neither $I = f(V)$ nor $V = f(I)$.

It is quite difficult to solve this system of equations, which is in the form of $I=f(I,\ V)$ and contains transcendental expressions analytically and can be solved much more easily with numerical methods. For this reason, the majority of scientific studies in the literature that develop methods for solving the PV model parameter definition problem are based on numerical solutions using iterative methods (Ayodele, Ogunjuyigbe, & Ekoh, 2016).

For the determination of the PV source parameters, many iterative methods were proposed in the literature. One of the most preferred methods among these methods is the Newton-Raphson method (NRM) (Shongwe & Hanif, 2015; Chin, Salam, & Ishaque, 2015; Villalva, Gazoli, & Filho, 2009). However, the incorrect selection of initial conditions greatly affects its accuracy and convergence. The study conducted by Villalva et al. (2009) and Moballegh (2014), chose the initial value of R_S as zero, and its value is increased until the difference between the data sheets and the calculated voltage value of the maximum power point (V_{MP}) was within an acceptable error range. Siddique (2013) and Rahman et al (2013) use the same idea. Instead of adjusting the value of R_S, they changed the value of the diode ideality factor between 1 and 2. Mahmoud et al (2013) proposed another method for determining the parallel resistance R_P, in which the other four parameters are calculated by a system of equations.

Defining the parameters of the PV model using the information given in the data sheets provided by the manufacturer of the PV source is a very advantageous method since there is no need to set up a measurement system. On the other hand, in the study of Sera et al. (2007), they determined five parameters of the single diode model, information in the manufacturer's data sheets, using an iterative method. Some stages of the parameter determination procedure contain similarities with analytical methods. They also examined the dependence of the study parameters on irradiance and temperature. This study has been summarized below.

The equation system below can be written using the Equation (2.1);

$$I_{SC} = I_{PH} - I_0 \exp\left(\frac{I_{SC}R_S}{n_s V_T}\right) - \frac{I_{SC}R_S}{R_P}$$

$$I_{MPP} = I_{PH} - I_0 \exp\left(\frac{V_{MPP} + I_{MPP}R_S}{n_s V_T}\right) - \frac{V_{MPP} + I_{MPP}R_S}{R_P}$$

$$I_{OC} = 0 = I_{PH} - I_0 \exp\left(\frac{V_{OC}}{n_s V_T}\right) - \frac{V_{OC}}{R_P} \tag{2.4}$$

$$\left.\frac{dP}{dV}\right|_{\substack{V=V_{MPP}\\ I=I_{MPP}}} = 0$$

$$\left.\frac{dI}{dV}\right|_{I=I_{SC}} = -\frac{1}{R_P}$$

Photo generated current I_{PH} and diode saturation current I_0 can be obtained based on this equation system.

$$\begin{aligned} I_{PH} &= I_0 \exp\left(\frac{V_{OC}}{n_s V_T}\right) + \frac{V_{OC}}{R_P} \\ I_0 &= \left(I_{SC} - \frac{V_{OC} - I_{SC}R_S}{R_P}\right)\exp\left(-\frac{V_{OC}}{n_s V_T}\right) \end{aligned} \tag{2.5}$$

The current at MP point I_{MPP} can be expressed as follows using Equations (2.4) and (2.5) together;

$$\begin{aligned} I_{MPP} = I_{SC} - \frac{V_{MPP} + I_{MPP}R_S - I_{SC}R_S}{R_P} - \\ \left(I_{SC} - \frac{V_{OC} - I_{SC}R_S}{R_P}\right)\exp\left(\frac{V_{MPP} + I_{MPP}R_S}{n_s \frac{nkT}{q}}\right) \end{aligned} \tag{2.6}$$

There are three unknowns, namely, *Rs*, R_P and *n,* in Equation (2.5), and two more equations are needed to find them. These two equations can also be derived using Equations (2.3) and (2.4).

$$\left.\frac{dP}{dV}\right|_{\substack{V=V_{MPP}\\ I=I_{MPP}}} = I_{MPP} + V_{MPP}\frac{-\dfrac{\left(I_{SC}R_P - V_{OC} + I_{SC}R_S\right)\exp\left(\dfrac{V_{MPP}+I_{MPP}R_S-V_{OC}}{n_sV_T}\right)}{n_sV_TR_P} - \dfrac{1}{R_P}}{1+\dfrac{\left(I_{SC}R_P - V_{OC} + I_{SC}R_S\right)\exp\left(\dfrac{V_{MPP}+I_{MPP}R_S-V_{OC}}{n_sV_T}\right)}{n_sV_TR_P} + \dfrac{R_S}{R_P}} \tag{2.7}$$

$$-\left.\frac{1}{R_P}\right|_{I=I_{SC}} = \frac{-\dfrac{\left(I_{SC}R_{SH} - V_{OC} + I_{SC}R_S\right)\exp\left(\dfrac{I_{SC}R_S-V_{OC}}{n_sV_T}\right)}{n_sV_TR_P} - \dfrac{1}{R_P}}{1+\dfrac{\left(I_{SC}R_{SH} - V_{OC} + I_{SC}R_S\right)\exp\left(\dfrac{I_{SC}R_S-V_{OC}}{n_sV_T}\right)}{n_sV_TR_P} + \dfrac{R_S}{R_P}} \tag{2.8}$$

These three unknowns are found iteratively using the flowchart shown in Figure 2-3 and Equations (2.6) and (2.7) (Sera, Teodorescu, & Rodriguez, 2007; Di Piazza & Vitale, 2013).

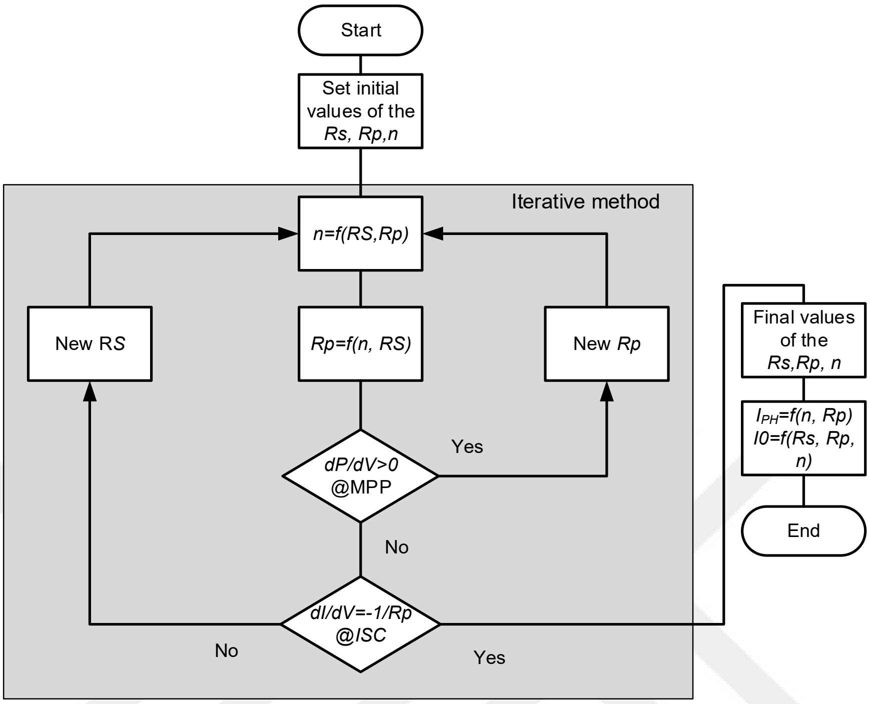

Figure 2.3 Flow chart for determining five parameters

2.4.3. Soft Computing Methods

In PV parameter estimation, methods such as evolutionary and artificial neural networks, in which artificial intelligence techniques are used, have been increasingly used in recent years due to their accuracy and reliability in order to overcome some of the problems encountered in analytical and iterative methods. Many methods have been proposed using some popular evolutionary algorithms, such as Genetic Algorithms (GA) (Saadaoui, Elyaqouti, Assalaou, & Lidaighbi, 2021) , Particle Swarm Optimization (PSO) (Fan, et al., 2022), Simplified Bird Mating Optimization (SBMO) (Askarzadeh & dos Santos Coelho, 2015) , Cat Swarm Optimization (CSO) (Guo, Meng, Sun, & Wang, 2016), Artificial Bee Swarm Optimization (ABSO) (Askarzadeh & Rezazadeh, 2013; Duy, Ho, & Dunnigan, 2020), Bacterial Aggregation (BA) (Awadallah, 2016), Flower Pollination Algorithm (FPA) (Alam, Yousri, & Eteiba, 2015; Prasanth Ram, Pillai, Rajasekar, & Kumar Chinnaiyan, 2020), Adaptive Mutational Differential Evolution (AMDE) (Muhsen, Ghazali, Khatib, & Abed, 2015), Differential Evolutionary Algorithm (DEA) (Kharchouf, Herbazi, & Chahboun, 2022) and Artificial Neural Network (ANN) (Bonanno, Capizzi, Graditi, Napoli, & Tina, 2012; Fathabadi, 2013; Karatepe, Boztepe, & Colak, 2006; Zhang, 2021).

2.4.4. Parameter Estimation Method of the Sandia National Laboratories

In the study of Hansen (2015), a new method has been proposed in which the previously mentioned analytical and numerical methods are used and the data obtained as a result of the measurements carried out in the external environment of Sandia National Laboratories for the estimation of the five parameters of SDM. In outdoor measurements using different PV panels, data of approximately 4500 I-V curves were obtained for each panel. These data are shared as open source by Sandia National Laboratories. In the study, primarily I_{SC} and V_{OC} temperature coefficients were obtained from I-V curves using the linear curve fitting method, and diode quality factor n was calculated by using V_{OC} value and *Lambert W* analytical method. R_S, R_P, I_{PH} and I_0 parameters are found by the iterative method.

2.5. Impact of the Irradiance and Temperature on The Parameters

Parameters belonging to a single diode model of a PV source are almost always gathered using data obtained under standard test conditions. For this reason, these parameters are only valid in STC, and the model created using the parameters will also give correct results only for STC. On the other hand, since the characteristics and model parameters of a PV source vary significantly with irradiance and temperature, these extracted parameters need to be adjusted for environmental conditions such as irradiance and ambient temperature other than STC when used in the model.

The relationship of model parameters with temperature and irradiance is defined as given in Equations (2.9) through (2.13) in many studies in the literature.

$$I_{SC}(G)=\frac{G}{G_{(STC)}}I_{SC(STC)}$$
$$I_{SC}(T)=I_{SC(STC)}+\alpha_{ISC}\left(T-T_{(STC)}\right) \qquad (2.9)$$
$$I_{SC}(G,T)=\frac{G}{G_{(STC)}}\left(I_{SC(STC)}+\alpha_{ISC}\left(T-T_{(STC)}\right)\right)$$

$$V_{OC}(G,T)=V_{OC,(STC)}+\frac{n_s kTn}{q}\ln\left(\frac{G}{G_{(STC)}}\right)+\alpha_{VOC}\left(T-T_{(STC)}\right) \qquad (2.10)$$

$$I_{PH}(G,T)=\frac{G}{G_{(STC)}}\left(I_{PH(STC)}+\alpha_{ISC}\left(T-T_{(STC)}\right)\right) \qquad (2.11)$$

$$I_0(T)=I_{0(STC)}\left(\frac{T}{T_{(STC)}}\right)^3\exp\left(\frac{qE_g}{nk}\left(\frac{1}{T_{(STC)}}-\frac{1}{T}\right)\right) \qquad (2.12)$$

$$R_S(G,T)=R_{S(STC)}$$
$$R_P(G)=\frac{G}{G_{(STC)}}R_{P(STC)} \qquad (2.13)$$

where, α_{ISC} (A/°C) is the temperature coefficient of short-circuit current, α_{VOC} (V/°C) is the temperature coefficient of the open circuit voltage.

In many studies in the literature, it has been stated that the diode quality factor for Silicon PV cells does not change with temperature and irradiance (Anani & Ibrahim, 2020; Carrero, Ramírez, Rodríguez, & Platero, 2011; De Soto, Klein, & Beckman, 2006; Siddique, Xu, & De Doncker, 2013; Villalva, Gazoli, & Ruppert Filho, 2009; Di Piazza & Vitale, 2013).

2.6. PV Model Implementation for Simulators

The electrical equivalent circuit of the PV cell in Figure 2.1 can be created by using linear and non-linear components such as resistance, diode, and current source in circuit-based simulation programs such as PSPICE, and its behaviour can be examined by simulating it like other electrical circuits. This method is generally more suitable for situations where environmental conditions and parameters are assumed to be constant. Some limitations of direct circuit setup can be overcome by using behavioural models.

The fact that any parameter can be changed instantly during the simulation is important in terms of the accuracy of the simulation result and provides the user with wider testing possibilities on the system in which the model is used.

Many commercial simulation programs, such as PSIM and MATLAB, have configurable embedded blocks that characterize PV sources and can take into account the effects of environmental conditions. Some simulators provided tools to gather model parameters by using basic data such as I_{SC}, V_{OC} and V_{MPP} given by the manufacturer. If the simulation program allows the use of user-defined mathematical expressions, it can be done easily, as in the PV source model.

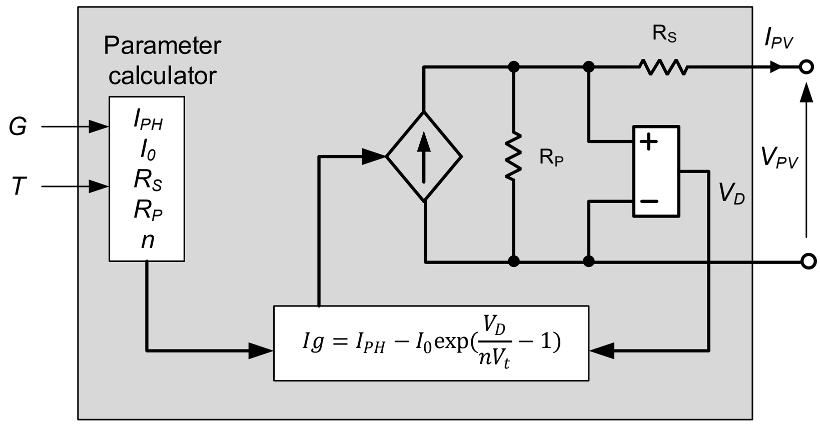

Figure 2.4 PV Model implementation for simulator

3. MPPT ALGORITHMS/ METHODS

One of the most important components of the MPPT system is the MPPT algorithm. The MPPT algorithm adjusts the duty cycle value of the DC/DC converter and brings the operating point of the PV source to the optimum value after evaluating the measured data in order to obtain maximum power from the PV source.

3.1. Classification of MPPT Algorithms

In the literature, there are many proposed methods/algorithms or techniques for tracking the maximum power point in PV systems. Different classifications have been made in the literature for many different methods proposed for MPPT. While MPPT techniques were classified as *online* (*direct* or *true seeking*) and *offline* (*indirect* or *quasi seeking*) in early studies (Salas, Olías, Barrado, & Lázaro, 2006), they were later classified as uniform irradiance and non-uniform irradiance due to the increasing number of studies on partial shading (Ali, et al., 2020).

Offline MPPT algorithms are also known as model-based algorithms. These algorithms are algorithms which are designed using basic parameters (V_{OC}, I_{SC}, I_{MPP}, V_{MPP}, P_{MPP}) obtained from data sheets provided by the manufacturer or as a result of measurements made. While some methods, such as Neural Network MPTT, use models based on these data, some methods, such as Constant Current MPPT use mathematical functions which are obtained purely empirically (Grunow, ve diğerleri, 2004).

As can be seen in Figure 3.1, offline algorithms cannot find out the location of the MPP precisely because they do not have a structure that generates feedback to correct the operating point by instantly calculating the power obtained from the PV source. Therefore, performance/efficiency to find and track maximum power point (*tracking efficiency*) of these methods, which are also named as *quasi seeking* algorithms, are limited.

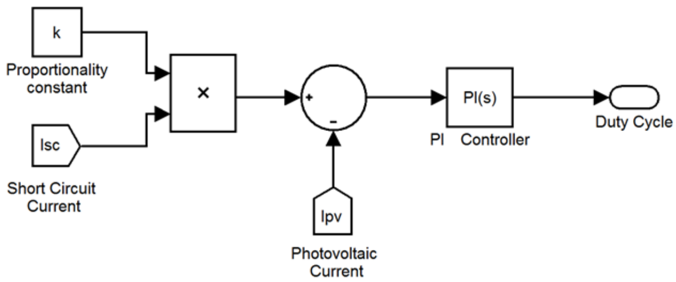

Figure 3.1 An Example of the Off-line MPPT/ Constant Current MPPT

As can be seen in Figure 3.2, algorithms called true seeking, online or direct MPPT find the duty cycle value required to maximize the power obtained from the PV source by instantly measuring the current and voltage values of the PV source or load resistor, and control DC/DC convertor with the PWM signal. Unlike offline algorithms, online algorithms do not need the model of the PV source for some calculations. For this reason, as their performance does not change according to the PV source used and environmental effects, their tracking efficiency/success is quite high when compared to offline algorithms.

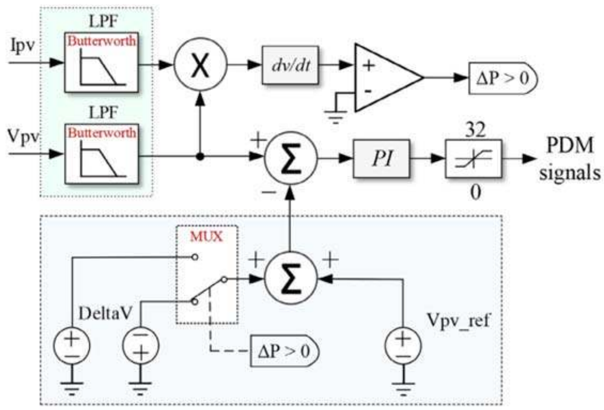

Figure 3.2 An Example of the Online MPPT / P&O MPPT

Uniform and nonuniform irradiance classification indicate whether an MPPT system is capable of distinguishing between global and local maximum power points that occur in case of nonuniform irradiance, such as partial shading. MPPT algorithms taking place under the Uniform Irradiance classification should only be operated under uniform irradiance because they can give erroneous results by evaluating the first reached local maximum power point as the global maximum power point in case of partial shading. Those under the nonuniform irradiance classification generally give accurate or approximate results under both uniform and nonuniform irradiance.

3.2. MPPT Algorithms for Uniform Irradiance

Many algorithms have been given in the literature that gives correct results when there is no partial shading, in other words, in the case of only one maximum power point on the PV curve. In this section, only commonly used algorithms are examined.

3.2.1. Constant-voltage and Constant-current MPPT

The Constant Voltage MPPT method, which is also known as *Fractional Open Circuit Voltage MPPT* is based on the assumption that V_{MPP} is in the range of 70-80% of the open-circuit voltage, which varies depending on the PV source.

The MPPT system measures the open circuit voltage by periodically disconnecting the PV source from the load. It then applies the calculated value using the measured open circuit voltage and the predetermined coefficient as a reference voltage to a PID (Proportional Integral Derivative) circuit whose output is connected to the DC/DC converter. PID circuit changes the duty cycle value of the DC/DC converter to the required value and brings the voltage of the PV source into to the accepted point as V_{MPP}.

The constant current MPPT method works similarly. In this method, short-circuit current I_{SC} substituted for V_{OC}, I_{MPP} substituted for V_{MPP}.

The tracking efficiency/success is limited since the coefficient used in both methods varies according to the PV source, and the system does not contain a feedback structure (Ramasamy & Suthanthira Vanitha, 2014; Tauseef & Nowicki, 2012; Esram & Chapman, 2007)

3.3. Current Based Analog MPPT with Pilot Cell

Büyükgüzel & Aksoy (2016) developed a new low-cost, simple, analogue, current-based MPPT system for a specific PV module and fixed load in their study. In the developed system, the irradiance exposure of the PV module was obtained by measuring the short circuit current of a pilot cell. With this irradiance value obtained from the pilot cell, the *irradiance*-R_{MPP} characteristic of the main PV module and the characteristic of the DC/DC converter are used to determine the location of the MPP effectively. In the study, KXOB22−4X3 as pilot cell, STP005 as PV module were used and SDM parameters of Main PV module were obtained by the method described in Section 2.4.2. The accuracy of the model created using the extracted parameters was confirmed using experimental measurement data. The designed system was simulated in the MATLAB environment, using both constant and variable irradiance profiles, and the results obtained were compared with the experimental results, and it was determined that they were completely compatible. The theory and working method on which the designed MPPT system is based are explained in detail below.

The relationship between the optimum load resistance R_{MPP}, which is the load resistance at the maximum power point of the PV module (STP005), and the irradiance to which the module is exposed is shown in Figure 3.3 (a). In Figure 3.3 (b), the relationship between the input resistance of the buck type DC/DC converter whose output is connected to a 30 Ω resistor and the duty cycle value is given.

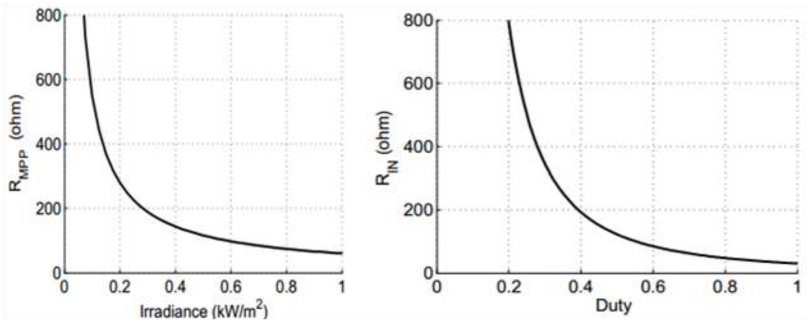

(a) (b)

Figure 3.3 *G*-R_{MPP} and *D*- R_{IN} relation for STP005 PV panel (T=25 °C)

As can be seen in Figure 1.11, the load resistance of the PV source in an MPPT system is actually the input resistance of the DC/DC converter. If the irradiance value of the PV module and the variation of R_{MPP} according to the irradiance are known, the location of the MP point can be determined by adjusting the duty cycle value of the DC/DC converter in accordance with the R_{MPP}-*Irradiance* curve.

In Figure 3.4, the relationship of the D_{MPP} (Duty cycle at MPP)– *Irradiance* is given for the PV system consisting of STP005 PV module and buck type DC/DC converter with 30 Ω load resistance connected. This graphic is obtained via MATLAB using *the Irradiance* − R_{MPP} and *Duty* − R_{IN} relationship given in Figure 3.3. Figure 3.4 shows the required value of the duty cycle, which must be applied to the DC/DC converter in order to obtain the R_{MPP} that actually needs to be at a certain irradiance value.

It is seen from Figure 3.4 that the D_{MPP} – *Irradiance* relationship is almost linear in the range of 0.2-1 kW/m^2 irradiance value, which is the beneficial region for PV systems in terms of energy production. On the other hand, as mentioned in the previous section, the relationship between the short-circuit current I_{SC} and irradiance is also completely linear.

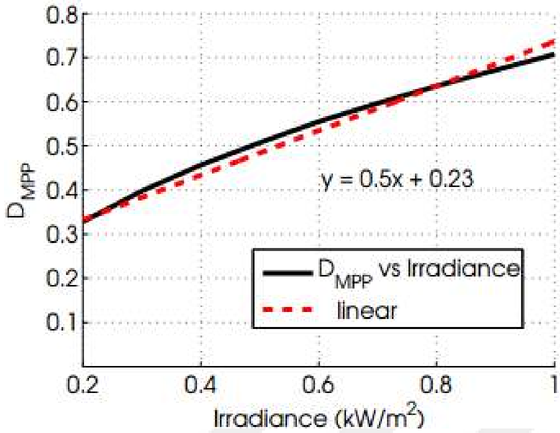

Figure 3.4 D_{MPP}- Irradiance relation of the main PV with best-fitting line.

I_{SC}- *Irradiance* curves are given for both Pilot PV and Main PV in Figure 3.3. If the short-circuit current of the Pilot PV, I_{SC-P}, is measured correctly and multiplied with an appropriate coefficient, the irradiance value to which the Main PV is exposed can be obtained. Then, the R_{MPP} value of the Main PV and thus the MP point can be followed by using this irradiance value and the R_{MPP}-*Irradiance*

There is also no need to measure the short-circuit current of the Main PV, as the method does not require the *ISC-Irradiance* characteristics of the Pilot PV and the Main PV to be similar to obtain the irradiance value of the Main PV. Therefore, unlike similar current-based methods, the efficiency of the system increases as the Main PV does not need to be short-circuited periodically to measure the short-circuit current.

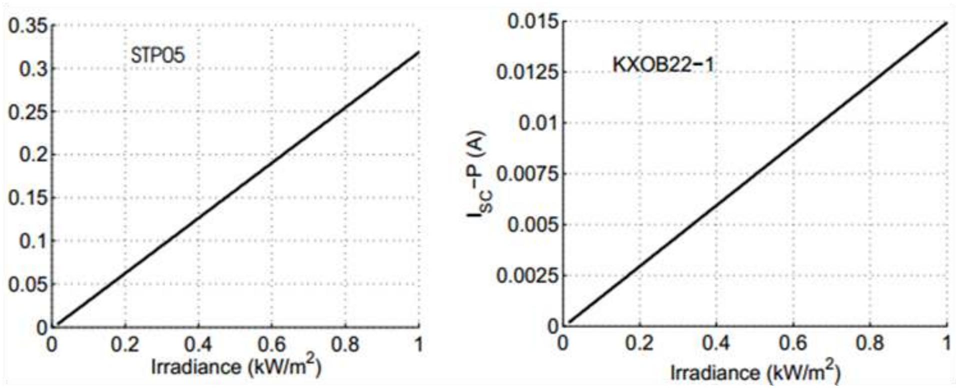

(a) (b)

Figure 3.5 *Irradiance-I_{SC}* characteristics of the main and pilot PV panels.

The functional block diagram of the developed analog system is given in Figure 3.6. The system consists of five main units: Pilot PV, Current to Voltage Converter (CVC), PWM controller, buck type DC/DC Converter and Main PV. In short, the system works as follows;

- To determine the irradiance level of the Main PV, I_{SC-P} is multiplied by a constant.
- The scaled I_{SC-P} value is applied as an offset value to a summing circuit to obtain the *Irradiance -D_{MPP}* characteristic, given in Figure 3.4.
- The result obtained is applied as the control voltage ($V_{CONTROL}$) to set the duty cycle value to the DC/DC converter.

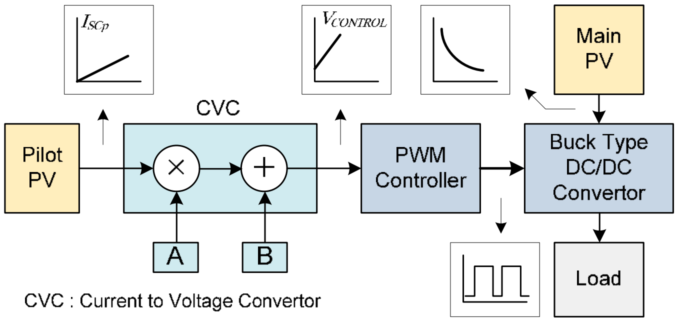

Figure 3.6 Functional block diagram of the proposed system.

Considering Figure 3.6, $V_{CONTROL}$ can be expressed as:

$$V_{CONTROL} = A \times I_{SC-P} + B \tag{3.1}$$

where, A and B are constants and are calculated as described below using experimental measurements and data obtained from MATLAB simulations using the model of the PV module.

The relationship between short-circuit current of the pilot PV using Figure 3.5 (b) ($I_{SC\text{-}P}$) and irradiance:

$$I_{SC-P} = 0.015G \qquad G = \frac{I_{SC-P}}{0.015} \tag{3.2}$$

D_{MPP} can be expressed as below by using Figure 3.4.

$$D_{MPP} = 0.5G + 0.23 \tag{3.3}$$

If Equation 3.2 is substituted in Equation 3.3;

$$D_{MPP} = 33.3I_{SC-P} + 0.23 \tag{3.4}$$

In Figure 3.7, the control voltage-duty cycle curve obtained as a result of experimental studies of the TL494 PWM controller used in the designed MPPT system is given. As a result of the curve fitting process using MATLAB and Figure 3.7, the control voltage $V_{CONTROL}$ can be expressed as follows;

$$V_{CONTROL} = 3.023 \times Duty + 0.61 \tag{3.5}$$

By substituting Equation (3.7) in Equation (3.8);

$$\begin{aligned} V_{CONTROL} &= 3.023(D_{MPP}) + 0.61 \\ &= 99.9 I_{SC-P} + 1.3 \end{aligned} \tag{3.6}$$

A = 99.9 Ω and B = 1.3 V are found using simulation and experimental results.

The CVC circuit designed using calculated A and B values is given in Figure 3.8. The CVC circuit is designed using only a single OPAMP.

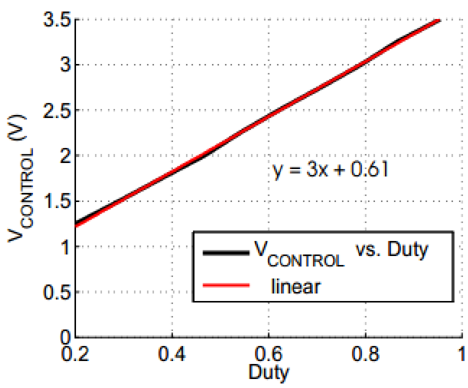

Figure 3.7 *D*- Control Voltage relation of the PWM controller

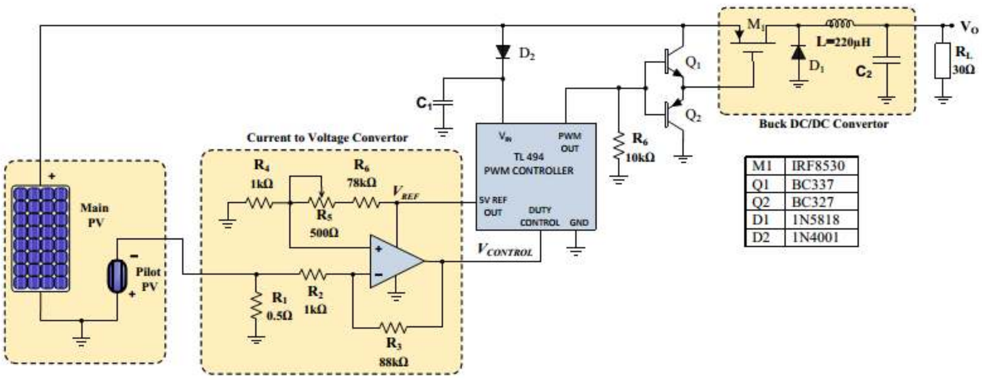

Figure 3.8 Designed analog-based MPPT circuit.

In case of the designed MPPT system is used and not used, power obtained from the PV module has been examined with simulation and experimental application, and the results obtained are given in Figure 3.9. The experimental results obtained regarding the tracking error and tracking efficiency of the system are given in Table 3.1.

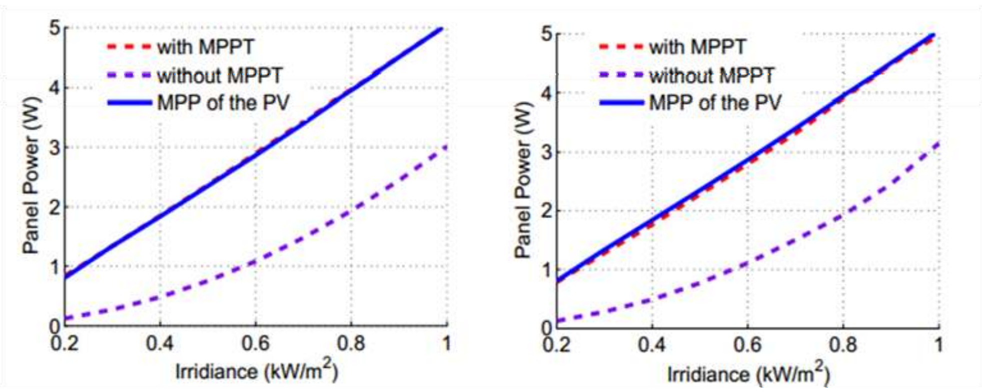

Simulation Experimental

Figure 3.9 Comparison of the output power of the PV

Table 3.1 MPPT system error and efficiency at different irradiance levels for T=25° C (experimental)

Irradiance (kW/m^2)	Expected MP_{PV} (W)	Actual P_{PV} (W)	Tracking Error%	Tracking η_{MPPT}%
0.2	0.84	0.79	5.95	94.05
0.3	1.33	1.28	3.76	94.24
0.4	1.84	1.77	3.80	96.20
0.5	2.37	2.28	3.80	96,20
0.6	2.89	2.80	3.11	96.89
0.7	3.43	3.32	3.21	96,79
0.8	3.96	3.91	1.26	98.74
0.9	4.50	4.48	0.44	99.56
1	5.05	4.98	1.39	98.61

One-day energy production of the MPPT system was calculated in the MATLAB environment using real irradiance data, and the system was compared with the classical P&O method. Comparison results are given in Table 3.2.

Table 3.2 Daily Energy production of the PV panel

Expected (Wh/day)	Proposed Method (Wh/day)	Energy Efficiency(%)	P&O Method (Wh/day)	Energy Efficiency(%)
20.7	20.6	99.5	20.5	99

3.4. Perturb and Observe (P&O)/ Hill Climbing (HC)

Perturb and Observe is the most widely used algorithm due to its simplicity and easy implementation. The P&O algorithm detects a certain change in the operating point voltage of the PV source (*perturb cycle*), periodically increases or decreases the duty cycle value of the DC/DC converter and observes the effect of this change on the power obtained from the PV source (*observe cycle*). If the resulting power is reduced, in other words, $\Delta P<0$, the change is made in the opposite direction in the next step.

As long as the change in power value is positive, the duty cycle value continues to be changed in the same direction. As it can be seen in Figure 3.10, since no stopping criterion is defined in the algorithm, even if the MP point is reached, it is passed beyond this point. The process is reversed as passing the MP point will cause a decrease in power. The process is reversed as passing the MP point will cause a decrease in power. This feature of the algorithm causes the operating point to continuously move back and forth around the MP point (Femia, Petrone, Spagnuolo, & Vitelli, 2017; Ahmed & Salam, 2014; Grunow, ve diğerleri, 2004). This oscillation around the MP point and its misconduct in case of rapid change of irradiance reduces the system efficiency (Salas, Olías, Barrado, & Lázaro, 2006; Jiang, Srivatsan, & Maskell, 2018).

Despite the voltage of the PV source is changed by a constant ΔV in each perturb step in the P&O method, the duty cycle of the DC/DC converter is changed by a constant ΔD in the Hill Climbing method. That is to say, P&O and HC are two different ways of doing the same basic method. Both methods are summarized in Table 3-3. There are also studies that change the value of ΔV or ΔD as the MP point is approached. Erroneous results can be obtained in both methods under rapidly changing irradiance conditions (Veerachary, Senjyu, & Uezato, 2001; Xiao & Dunford, 2004).

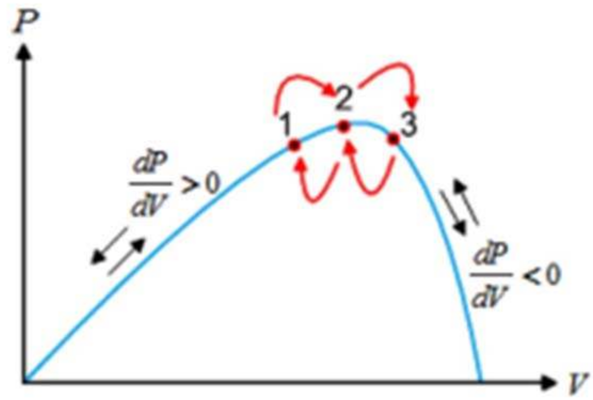

Figure 3.10 P&O algorithm decision principle

Table 3.3 Summary of P&O and HC

Perturbation	**Change in Power**	**Next Perturbation**
Positive	Positive	Positive
Positive	Negative	Negative
Negative	Positive	Negative
Negative	Negative	Positive

3.5. Incremental Conductance (INC)

The MPPT system, in the INC method, periodically measures the voltage and current of the PV source and calculates conductance (*I/V*) and incremental conductance *(*$\Delta I/\Delta V$) values and finds which way the operating point of the PV source should be shifted. Then it changes the duty cycle value of the DC/DC converter by means of changing it and shifts the operating point to the right place. System operation is summarized in Equation (3.7) and (3.8) (Grunow, ve diğerleri, 2004).

$$\frac{dP}{dV}=\frac{d(VI)}{dV}=I+V\frac{dI}{dV}\approx I+V\frac{\Delta I}{\Delta V} \tag{3.7}$$

$$\begin{aligned}
&\frac{dP}{dV}=0 \text{ if } \frac{\Delta I}{\Delta V}=-\frac{I}{V} \text{ ,(at MPP)}\\
&\frac{dP}{dV}>0 \text{ if } \frac{\Delta I}{\Delta V}>-\frac{I}{V} \text{ ,(left of MPP)}\\
&\frac{dP}{dV}<0 \text{ if } \frac{\Delta I}{\Delta V}<-\frac{I}{V} \text{ ,(right of MPP)}
\end{aligned} \tag{3.8}$$

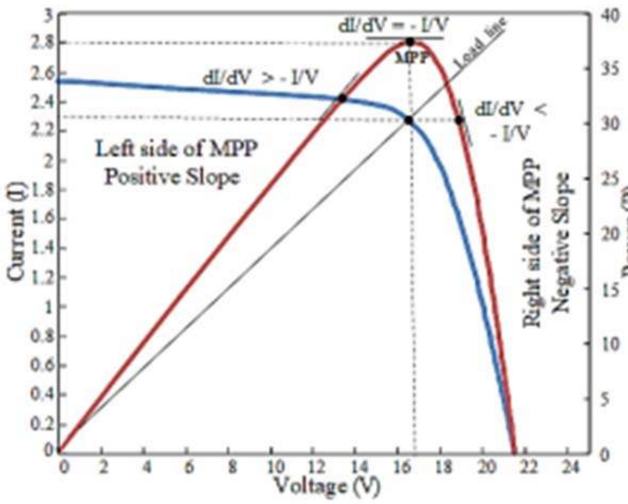

Figure 3.11 INC algorithm decision principle

As can be seen from the flowchart given in Figure 3.12, the biggest difference from the P&O system is that the MPPT system does not change its operating point when the environmental conditions and load conditions do not change (ΔV and ΔI equal 0). A mechanism that is not in the P&O method has been added to this system to stop the periodic change in PV voltage when the MPP is reached. Although it has advantages such as keeping up with rapidly changing irradiance values and not oscillating at the MP point, it is a difficult method to perform due to its complexity compared to P&O. (Kumar, Yadav, Singh, & Tiwari, 2018; Salas, Olías, Barrado, & Lázaro, 2006).

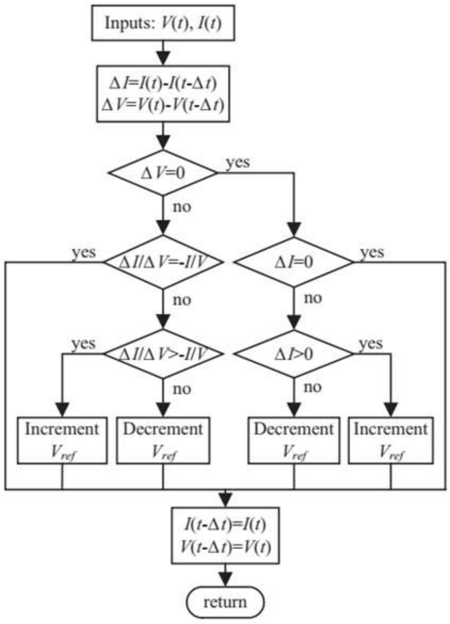

Figure 3.12 Flowchart of the INC Method

3.6. Other Methods for Uniform Irradiance

Except from widely used P&O, HC, INC methods, Beta (Jain & Agarwal, 2004; Pradeep, Mouli, Reddy, & Raju, 2015), Current Swep (Tsang & Chan, 2015; Moring & Pols, 2012), One Cycle Control (Fortunato, Giustiniani, Petrone, Spagnuolo, & Vitelli, 2008; Chatterjee & Keyhani, 2011), Ripple Correlation Control (Galtieri & Krein, 2018), System Oscillation (Ho, Chung, & Lo, 2004; Obaid, Cipcigan, & Muhssin, 2017), Linear Current Control (Mumtaz, et al., 2018), DC-link Capacitor Drop Control (Prasad, Myneni, & Kumar, 2018; Khatib, Elmenreich, & Mohamed, 2017), Analytical Solution (Kuperman, 2014), Constant Voltage (Leedy, Guo, & Aganah, 2012; Tauseef & Nowicki, 2012), Constant Current (Di, Yundong, & Qianhong, 2014; Anoop & Nandakumar, 2018), Lookup Table (Desai & Patel, 2007), Pilot Cell (Grunow, ve diğerleri, 2004; Büyükgüzel & Aksoy, 2016) methods are MPPT methods which take place in the literature and work under the uniform irradiance.

3.7. GMPPT-MPPT Algorithms For Nonuniform Irradiance

Partial shading can be overcome where conventional MPPT methods fail by using modified conventional MPPT methods (modified P&O, INC, HC), soft computing methods such as meta-heuristic, or mixed methods using some of these together.

These systems are also called Global Maximum Power Point Tracking (GMMPT) systems because of their ability to find the highest value, that is, the global maximum, among multiple maximum power points that occur due to partial shading in the PV characteristic of a PV source.

3.7.1. Meta-Heuristic MPPT Algorithms

Optimization is an iterative process based on extensive research among possible solutions to a problem to find the best (optimal) solution to a particular problem. The best solution may be to minimize the cost of a manufacturing process or maximize the efficiency of a system such as a PV system. The search process within the set of possible solutions mentioned in this definition divides the optimization algorithms/methods into two main classes as *Gradient Based* and *Direct Search algorithms*. *Gradient Based* algorithms use differential calculus operations during the search. For this reason, the function to be optimized, which is also defined as the objective function, must be continuous and differentiable. In an optimization process, if the objective function is continuous and differentiable, *Gradient Based* algorithms should be used if not continuous and differentiable, *Direct Search* algorithms should be used.

Most traditional optimization algorithms reach the optimum solution using the gradient or higher derivatives of the objective function. In contrast, *Direct Search* algorithm do not use the gradient of the objective function in solving the optimization problem. A *Direct Search* algorithm searches through a set of points around that point to find a better value (lower or higher) than the objective function's value at a given point. Today, the most used algorithms in this algorithm classification are meta-heuristic algorithms, which are generally nature-inspired algorithms.

The origin of word *heuristically* originates from the ancient Greek word *heuriskein*, which means the art of developing new strategies (rules) in order to solve problems. The Greek word *meta* suffix stands for high-level methodology. The term meta-heuristic was first used by Glover (1986).

A heuristic algorithm can be considered as a procedure for finding a solution for a given problem that is not necessarily optimal but can be considered good enough. Heuristic algorithms are generally considered to be iterative algorithms designed for a particular problem, where a new solution is sought at each iteration that may be even better than the previous best solution. When the algorithm terminates after a reasonable time, the solution it provides is the best of the solutions found during iterations. No guarantee can be given that the solution obtained is the optimum solution, but a well-designed heuristic algorithm can usually provide at least a near-optimal solution.

On the other hand, metaheuristic algorithms are iterative algorithms that are not designed to solve a particular problem, which combines two concepts of search space, such as global search and local search, and use learning strategies to structure the information obtained in order to reach a near-optimal solution.

Metaheuristic algorithms have been widely used in solving optimization problems of PV systems in recent years, as they have proven their effectiveness in solving complex optimization problems.

Metaheuristic optimization algorithms which are often inspired by nature, perform iterative computations by dividing the search space into two main phases to increase the probability of finding the global optimum solution to the problem. These two contradictory but complementary search mechanisms are called *diversification/exploration* and *condensation/exploitation.* The diversification process aims to perform a comprehensive global search in order to eliminate the possibility of getting stuck in a local optimum mostly through randomization within the search range. Condensation or exploitation usually aims to search near successful samples and find local best solutions by evaluating useful solution information stored in population memory.

3.7.1.1. Genetic Algorithm (GA)

A genetic algorithm is a nature-inspired algorithm that basically imitates the theory of natural selection. This algorithm has three main processes called selection, crossover, and mutation. Studies conducted have shown that GA, which can be used to determine the parameters of the PV model, can also be used to determine the MPP of PV systems under PSC (Smida & Sakly, 2015; Shaiek, Smida, Sakly, & Mimouni, 2013; Daraban, Petreus, & Morel, 2014; Hilali, Mardoude, Essahlaoui, Rahali, & El Ouanjli, 2022). However, it is complex and difficult to implement such an algorithm with a low-cost microcontroller because it requires high processing power. For this reason, it is necessary to use a microcontroller or DSP with high processing power for MPPT systems using GA.

3.7.1.2. Differential Evolution (DE)

Although the basic algorithm structure of differential evolution is similar to GA, it has a fundamental difference from GA. In the mutation/crossover operations used to generate a new population in DE, the difference between two or more vectors in the population is used to create a new vector.

Tey et al. (2018) proposed an advanced global search domain DE algorithm for the GMPPT system. Tajuddin et al. (2014) developed the DE (DynNP-DE) algorithm, which increases the accuracy and high convergence rate, which is a desired feature in GMPPT systems, whose population size changes dynamically. In the study by Ramli et al. (2015), a modified differential evolution (MDE) based MPPT algorithm, which can also be applied to low-cost microcontrollers, is proposed for PV systems under PSC. The proposed system can be applied to microcontrollers with low processing power since it does not contain random numbers and has only one parameter to be adjusted, and it can reach MPP in a maximum of 12 iterations for each situation.

3.7.1.3. Cuckoo search (CS)

The CS algorithm is a metaheuristic algorithm developed by Yang and Deb (2009) based on the vital behaviours and reproductive activities of cuckoos. The procedure for finding a nest for the cuckoo in the CS algorithm is characterized by *the Levy Flight* mechanism instead of a simple *random walk*.

Peng et al., (2018) proposed a GMPPT system that uses a deterministic CS (DCS) algorithm, which has some outstanding features such as simple structure and easy adjustment of parameters.

3.7.1.4. Ant Colony Optimization (ACO)

Ant colony optimization is one of the types of algorithms designed inspired by various living species and their behaviour in nature. The ACO algorithm, whose command values can be adjusted instantly according to changing environmental conditions, mimics the foraging behaviour of ants to determine the optimum location within the foraging area. Jiang et al. (2013) proposed a GMPPT system using ACO for large-scale PV sources.

One of the most important advantages of the ACO algorithm is that its convergence is independent of the initial positions of the population. However, the most important disadvantage is that positioning the ants away from the GMPP increases the probability of getting stuck in the local maximum (Li, Jin, Akram, Chen, & Ji, 2018).

3.7.1.5. Artificial Bee Colony Optimization (ABCO)

The ABCO algorithm introduced by Karaboğa (2005) mimics the foraging behaviour of bee colonies. The ABCO algorithm working in the MPPT system calculates the duty cycle value (D) of the DC/DC converter to change the operating point of the PV source as follows;

$$D(i) = D_{\min} + rand\left[0\ 1\right]\left(D_{\max} - D_{\min}\right)$$
$$D\left(i+1\right) = D\left(i\right) + \theta(i)\left(D\left(i\right) - D\left(i-1\right)\right) \tag{3.9}$$

where, Θ is a constant in the range [-1 1]. The ABCO algorithm is simple as it is flexible and only has two parameters to set. On the other hand, the convergence of the algorithm is independent of the initial conditions (Sawant, Lbhattar, & Bhattar, 2016).

3.7.1.6. Grey wolf optimization (GWO)

Grey wolf optimization (GWO) is a metaheuristic algorithm developed mainly by considering the hierarchies of grey wolves living in groups and their natural hunting behaviour. The GWO algorithm has three main steps that mimic the wolf pack's behaviour. These steps are expressed as hunting (searching), following the prey, encircling the prey, and attacking. The prey-encircling behaviour of grey wolves can be modelled as follows;

$$\vec{F} = \left|\vec{G}\vec{X}p(j) - \vec{X}p(j)\right|$$
$$\vec{X}(j+1) = \vec{X}p(j) - \vec{B}\vec{C} \tag{3.10}$$

In this model, *j* represents the current iteration, *F, G* and *B* represent coefficient vectors.

$$\vec{B} = 2\vec{a}\vec{r_1} - \vec{a}$$
$$\vec{G} = 2\vec{r}_2 \tag{3.11}$$

During the iteration processes, vector *a* is reduced from 2 to 0 linearly, and vectors r_1 and r_2 are random vectors that can take values in the range of [0 1] (Luo et al., 2019; Yang et al., 2017).

3.7.1.7. Bat search algorithm (BSA)

Bats use a feature called echolocation, which functions as a type of radar to detect obstacles and search for their prey during their flight at night. Bats emit sounds that can vary in frequency and amplitude. They listen to echoes returning from objects. They can determine their prey's direction and distance according to the return signal's direction and strength. On the other hand, bats display completely random behaviours while searching for their prey. Yang et al. (2010) developed a metaheuristic method, BSA, inspired by this feature of bats. The mathematical expression of this algorithm is given in summary in the equation below.

$$\begin{aligned} f_j &= f_{\min} + (f_{\max} - f_{\min}) \cdot a \\ v_j^{t+1} &= v_j^t + (x_j^{t+1} - x) f_j \\ x_j^{t+1} &= x_j^t + v_j^{t+1} \\ x_{new} &= x_{old} + \varepsilon K^t \end{aligned} \qquad (3.12)$$

where, *xj* and *vj* represent the position and speed of each bat that will be updated during the optimization process, ε represents a random number in the range of [-1 1], and *Kt* represents the average loudness. The average loudness decreases when prey is found by the bat.

Kaced et al. (2017) proposed a new MPPT method with very high static efficiency that can accurately detect GMPP using the BS algorithm.

3.7.1.8. Butterfly optimization algorithm (BOA)

A butterfly produces scents based on the food availability at that location as it moves from one location to another while foraging. Thanks to this scent, which can be felt by other butterflies, butterflies can share their personal information with other butterflies and create a collective social information network.

BOA is an algorithm that mimics the foraging and mating behaviour of butterflies. The algorithm has two main stages, namely, global and local. The global search phase is as expressed in Equation (3.13), and the local search phase is expressed in Equation (3.14).

$$x_i^{t+1} = x_i^t + (r^2 \bullet g * - x_i^t) x f_i \tag{3.13}$$

$$x_i^{t+1} = x_i^t + (r^2 \bullet x_j^t - x_i^t) x f_i \tag{3.14}$$

x represents the position of the butterfly, x_i^t represents the solution vector, *g** represents the optimum solution obtained in the ongoing iteration, f_i, *i* represents butterfly's scent level, *r* represents a random number in the range of [0 1] (Arora & Singh, 2019).

Aygül et al., (2019) proposed an MPPT system realized using BOA, and stated that the performance and convergence rate of this system is higher than the other two methods compared.

3.7.1.9. Firefly Algorithm (FA)

Thanks to a special chemical substance in their bodies, fireflies can emit a yellow light around them, and they can communicate with other fireflies. Fireflies convey their status during foraging (whether they have reached the food and the status of the food) to other fireflies by using these features.

The key parameter that determines the movements of fireflies is the brightness of the light they emit. If no firefly emits light in the firefly colony, each firefly moves randomly. In the case of fireflies emitting light, those that emit less light move towards those that emit more light.

Yang (2008) developed the Firefly Algorithm inspired by these behaviours of fireflies. The firefly algorithm is summarized in Equation 3.15.

$$r_{jk} = \left| X_j - X_k \right|$$
$$\beta(r) = \beta_0 e^{-\gamma (r_{jk})^n} \quad (3.15)$$
$$X_p^{i+1} = X_p^i + \beta(r)(X_j - X_k) + \alpha(rand - \frac{1}{2})$$

wheere, X_j and X_k represent the current position of the two fireflies, r_{jk} represents the distance between them, $\beta(r)$ represents attraction among fireflies, β_0 represents the initial value of attractiveness, γ represents the light absorption coefficient that can vary in the range of [0 10], α represents the randomization coefficient.

Sundareswaran, et al., (2015) proposed a new GMPPT system that uses a firefly algorithm for PV sources operating under partial shade. The implementation of the proposed MPPT system was carried out using an inexpensive microcontroller, and the results showed that GMPP tracking could be done successfully under different irradiance scenarios.

A GMPPT system using a modified firefly algorithm (MFA) with a linear relationship between the α and $\beta_0$coefficients is proposed by Teshome et al. (2016) and Farzaneh et al., (2018) in order to increase the search speed.

3.7.1.10. Simulated Annealing (SA)

The application of heat treatment (heating and cooling) in order to change the physical properties of a metal such as hardness is called annealing. The potential energy of the mass is minimized by optimizing the molecular arrangement of the metal particles by annealing. The SA algorithm put forward by Kirkpatrick, et al., (1983) generally adopts an iterative motion according to the variable temperature parameter, which mimics the annealing process of metals.

Wang et al., (2017) proposed a GMPPT system that uses the Enhanced SA algorithm with a higher convergence rate and tracking efficiency compared to the classical SA algorithm.

3.7.1.11. Particle Swarm Optimization (PSO)

It is one of the commonly used algorithms for PSO GMPPT systems. The PSO algorithm was also used in the GMPPT system designed in this thesis. Therefore, the PSO algorithm is explained in detail in this section.

PSO is a population-based optimization approach inspired by nature and developed by Kennedy and Eberhart in 1995. It is used to search the solution space of a problem in order to discover the best solution.

The fact that many animal swarms in nature, such as birds and fish, communicate with one another in numerous ways during various activities such as locating food, hunting, and escaping from predators boosts the speed and likelihood of achieving the objective. The PSO algorithm is based on this behaviour of animal swarms.

Any individual in a swarm is defined as a particle, and these particles correspond to candidate solutions of a problem to be optimized. The positions of the particles randomly placed in the search area at the beginning are updated according to both the best value they obtained and the best value obtained in the swarm so that the swarm moves towards the optimum solution. Meanwhile, certain particles in the swarm are randomly separated, preventing the algorithm from being locked in any local optimum (Ishaque & Salam, 2012; Sen, Pragallapati, Agarwal, & Kumar, 2018; Ram & Rajasekar, 2017). The PSO algorithm is mathematically summarized below.

Particle swarm **S**;

$$\mathbf{S} = \{x_1, x_2, ...x_N\}$$

N particles showing potential solutions for n dimensions;

$$x_i = \left(x_{i1}, x_{i2}, ..., x_{in}\right)^T \in A, \quad i = 1, 2, ..., N$$

The particles are transported through the search space at each iteration using a position shift termed velocity, which is represented as:

$$v_i = \left(v_{i1}, v_{i2}, ..., v_{in}\right)^T, \quad i = 1, 2, ..., , N$$

The velocity value of each particle is iteratively changed based on the information collected in earlier phases of the algorithm to guarantee that the particles reach any region of the search space and that the global optimum may be established. The best place that each particle has ever visited is saved in memory for this reason. The optimal particle locations are calculated as follows;

$$\mathbf{P} = \{p_1, p_2, ..., p_N\}$$

$$p_i(t) = \arg\max f_i(t)$$

In this equation, *t* donates the value of the iteration counter.

PSO is a social behaviour simulation model-based algorithm. The algorithm aims to reach the global optimum using the best position ever visited by all particles. As a result, an information exchange mechanism is required for the particles to relay their experiences to one another. If the index of the best position with the highest function value in the ***P*** vector, which holds the best locations of the particles in a particular iteration t, is indicated by *g*, it may be stated as follows;

$$p_g(t) = \arg\max f\left(p_i(t)\right)$$

This value indicates the global maximum value at iteration t since it is the best value selected by the herd at iteration t.

As a result of the previous statements, the traditional PSO algorithm is expressed as given in Equation (3.16);

$$v_{ij}(t+1) = v_{ij}(t) + c_1R_1\left(p_{ij}(t) - x_{ij}(t)\right) + c_2R_2\left(p_{gj}(t) - x_{ij}(t)\right)$$
$$x_{ij}(t+1) = x_{ij}(t) + v_{ij}(t+1) \qquad (3.16)$$
$$i = 1,2,...,N, \quad j = 1,2,...,n$$

where, *R1* and *R2* are random variables with uniform distributions in the range [0,1], while c_1 and c_2 are weight factors, sometimes known as cognitive and social parameters, respectively.

After the particles are updated and analyzed at each iteration, the optimal places in memory are likewise modified. Thus, at iteration t+1, the new optimum position of *xi* is defined as follows:

$$p_i(t+1) = \begin{cases} x_i(t+1), \text{ if } f(x_i(t+1)) \geq f(pi(t)) \\ p_i(t), \quad \text{otherwise} \end{cases}$$

The motion of any particle in the swarm, whose mathematical expression is given in Equation (3.16), is shown in Figure 3.13. In Figure 3.14, the flow chart of the PSO algorithm is given.

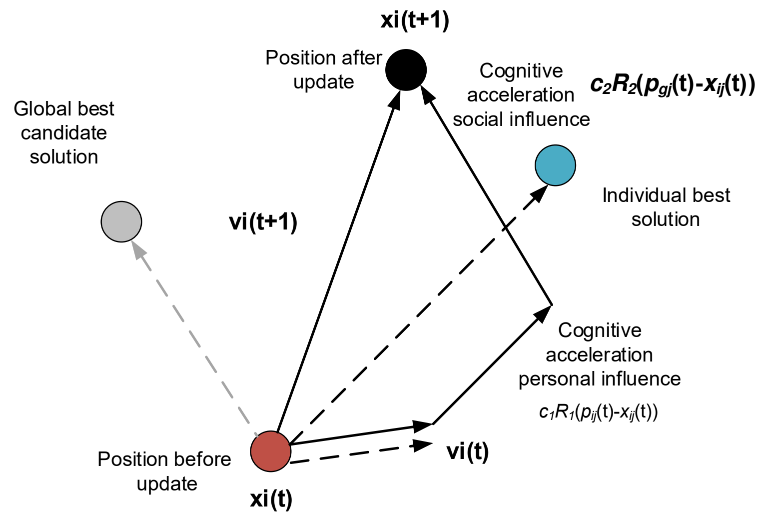

Figure 3.13 Movement of a particle in search space

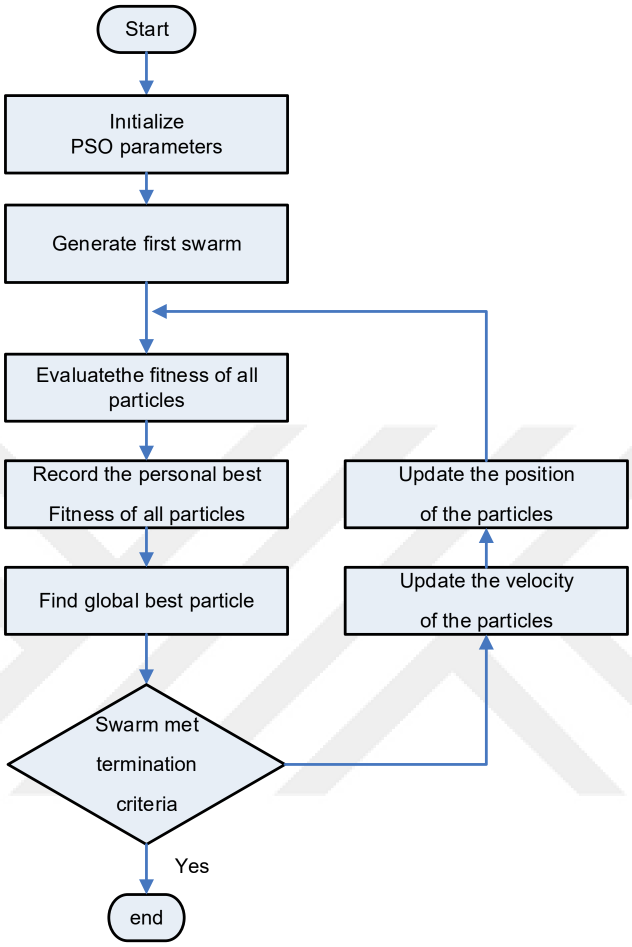

Figure 3.14 Flow chart of the PSO Algorithm

3.7.2. Inflection Voltages Based Methods

When the string current is higher than the short circuit current of any module in the string, the bypass diode of that module turns on. As Figure 3.15 shows, when the bypass diode turns on, a break occurs on the I-V curve, as the string voltage will remain relatively constant. The voltage value at which this break occurs is called the inflection voltage. As can be seen in Figure 3.15, the local maximum power points are located near the inflection points.

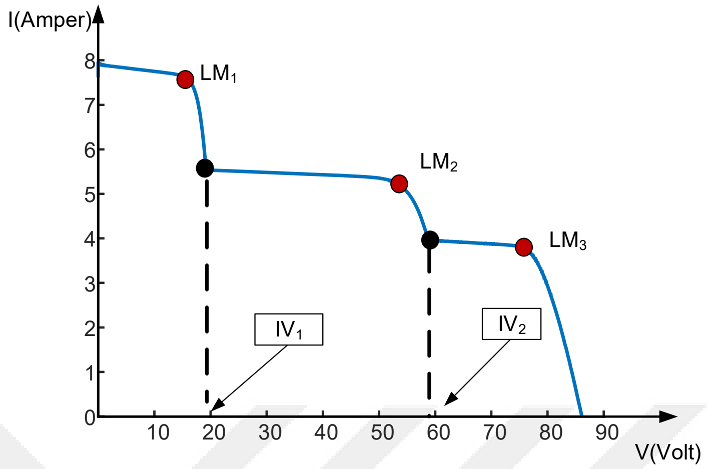

Figure 3.15 Inflection Voltages of the shaded PV string

In the Kesilmiş, Karabacak, & Aksoy (2020) study, the voltage values of the inflection points on the I-V curve were calculated as given in Equation (3.17).

$$V_{inf}\left[i\right] = i \times Va - \left(n - i\right) \times Vb \qquad ; \quad 1 \le i \le n \tag{3.17}$$

where, n is the number of modules in the array, i is the module number, Va is the open circuit voltage of the modules, and Vb is the conduction voltage of the bypass diodes.

In the proposed method, the voltage values of the local maximum power points are calculated by multiplying these voltage values with a coefficient k that varies according to the module, as given in Equation (3.18).

$$V_{IVM}\left[i\right] = k \times V_{inf}\left[i\right] \tag{3.18}$$

where, $V_{IVM}[i]$ is the voltage value of the local maximum power point of module i. After obtaining the voltage values of the local maximum power points, the PV array is adjusted to these voltage values, and the power value obtained at each local maximum power point is found. The largest of the obtained power values is the GMP point.

The study by Mobarak & Bauman (2021), is actually based on the inflection voltages method. This method uses parabolas with the vertex at the local maximum and passing through the V_{OC}, as shown in Figure 3.16. The LM_1 voltage is found by multiplying the V_{OC} with a coefficient, as in the fractional open circuit voltage method.

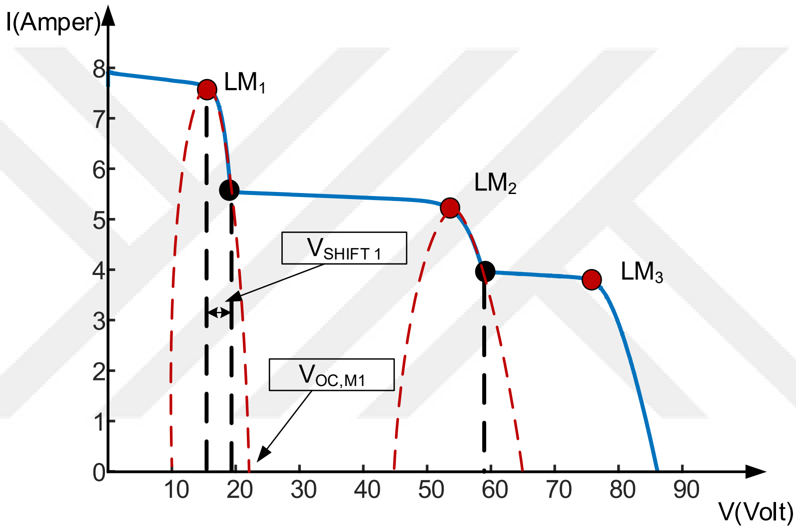

Figure 3.16 Parabolic Assumption Method

The V_{SHIFT} voltages are calculated by finding the intersection point of the parabola and short circuit currents using Equation (3.19). This voltage value is used to calculate the voltage value of the next local maximum power point and the power at that point. After calculating the power value at all local maximum points, the GMP point is found.

$$\left(x_i - V_{LM,i}\right)^2 = 4 f_i \left(y_i - I_{MPP,i}\right) \tag{3.19}$$

3.7.3. Two-Stage GMPPT Methods

More than one maximum power point (peak) occurs under partial shading (PSC) in the P-V characteristic of a PV source. The number of these peaks is directly related to the characteristic of the shading. Such a PV curve is divided into regions with a single peak in each section, and the global maximum can be reached if the location of the peak in each region can be determined using a conventional algorithm such as P&O or INC. In other words, the location of the GMP point can be found accurately by searching around the points where the GMP point is likely to be found using one of the classical search methods (Liu, Li, Wu, & Zhou, 2017; Gawande, Ghulaxe, Mahatme, Salvi, & Bagewadi, 2021). Although these methods are similar to mixed methods, they are called two-stage methods.

The two-step method involves using a method such as metaheuristics to determine the approximate position (a range) of the GMPP in the first step, using traditional MPPT methods to determine the precise position of the GMPP. Therefore, the key to the success of the two-stage method is the accuracy of the GMPP range obtained in the first stage.

In the study of Patel and Agarwal (2006), it was determined that the minimum distance between the local maximum power points occurring in the P-V characteristic of a PV source under partial shading is $0.8V_{OC}$, and the local maximum power points can be located at $0.8V_{OC}$ or its integer multiples.

In the method proposed by Patel & Agarwal (2006), firstly, the total open-circuit voltage of the series-connected string is found, and the search is started at the point of $0.8V_{OC(TOTAL)}$ with the P&O algorithm. The first peak is found, and the power value is recorded. The other peak is found by shifting the search point of the P&O algorithm $0.7V_{OC(MODULE)}$, and the power point is recorded. The process continues in this way until the next power value is less than the previous one. As shown in Figure 3.17, if the power value of the previous peak is greater, it is necessary to return to that point since it is the global maximum.

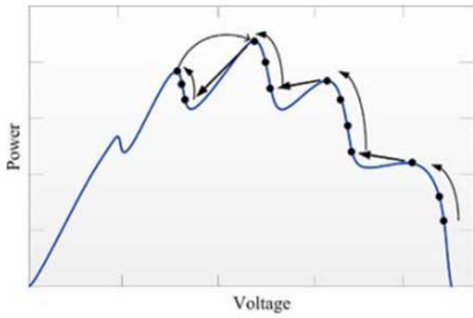

Figure 3.17 Method proposed by Patel (Patel & Agarwal, 2008).

In the study by Koutroulis & Blaabjerg (2012), to roughly determine the location of the GMPP, they used a similar method to scan the entire P-V curve with constant ΔP (called as *Global Biased Search*) as shown in Figure 3.18, As can be seen from the flowchart given in the figure, in this method, after the global scan, a local search is performed using another method around the highest value found in the previous global scan in order to pinpoint the location of the GMPP.

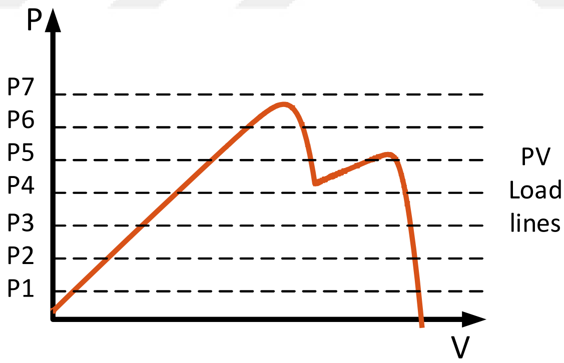

Figure 3.18 Method proposed by by Koutroulis & Blaabjerg (2012)

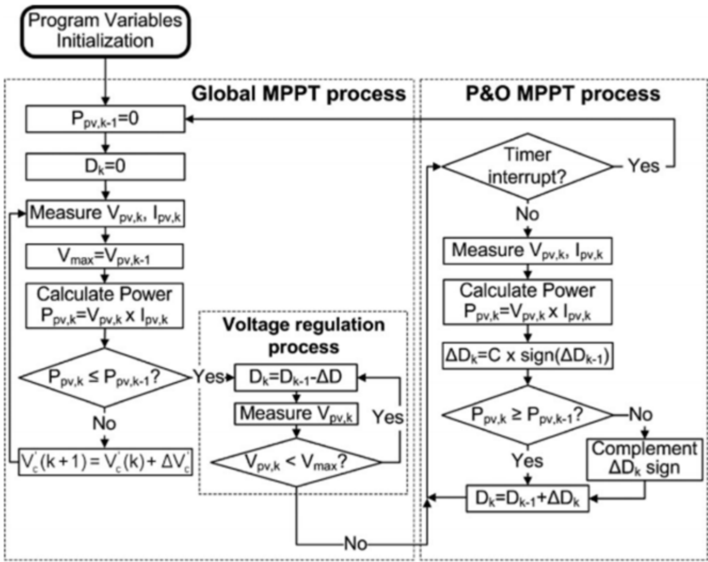

Figure 3.19 Flowchart of the Method proposed by Koutroulis

In the study by Kumar, Prabhakaran, & Balasubramanian (2022), an area whose boundaries are changed dynamically is searched instead of searching the entire I-V or P-V curve to find the GMP point. The boundaries of the searching area are updated using Equation (3.20) at each sampling.

$$V_{MIN} = \frac{P_{MAX}}{I_{MPP,STC}} \qquad\qquad (3.20)$$
$$I_{MIN} = \frac{P_{MAX}}{0.9V_{OCSTRING}}$$

P_{MAX} is the highest power value obtained during the scan so far, and V_{MIN} and I_{MIN} are limit values in this equation. On the other hand, using the difference of the power values obtained in two consecutive samples, it is determined in which region of the I-V curve (constant current or constant voltage) the current operating point is located. A constant increase in current or voltage is made according to the region where the operating point is located. When the stopping criteria, which is set as $0.9I > I_{MIN}$, is reached, the operating point of the array is brought to the voltage value of the highest power value obtained during the scan. From this point on, the location of the GMP point is determined using the classical P&O algorithm.

In a similar study by Deboucha, Kermadi, Mekhilef, & Belaid (2021), an algorithm named Voltage Track Optimizer MPPT was proposed. As in the previous study, this study is also based on the principle of not doing a search in an area that is thought not to contain GMP point. The key parameters of the proposed method are given in Equation (3.21). The parameters given in Equation (3.21) are dynamically updated according to the data obtained at the end of each sample.

$$\begin{aligned} V_{MIN} &= \frac{P_{GMPP}}{I_{GMPP,STC}} \\ V_{MAX} &= 0.9V_{OC,STC} \\ I_{MIN} &= \frac{P_{GMPP}}{V_{MAX}} \\ V_{START} &< 0.5V_{MAX} \\ V_{START} &< V_{MIN} \\ V_{SKIP} &= \frac{P_{GMPP}}{I_{SDP}} \end{aligned} \tag{3.21}$$

where, P_{GMPP} is the highest power value obtained during the scan so far, V_{START} is the starting point voltage of the scan, V_{SKIP} is the ending voltage of the area that will not be scanned. I_{SDP} is the current value of the transition point of the I-V curve from the current source region to the voltage source region, also called the section dividing point (SDP). The first point where the difference between the current values read in two consecutive samples falls below a particular value is recorded as the SDP point. The proposed algorithm works as follows.

Suppose the difference between the power values obtained from the array as a result of two consecutive samplings is above a particular threshold value. In that case, a new scanning process is started because the PV system's operating conditions change. The initial power value is recorded as the current G_{MPP} value, and then, V_{MAX}, V_{MIN} and I_{MIN} values are calculated using Equation (3.21). If the starting point is in the range of $[0 - 0.5V_{MAX}]$, scanning is performed to the left side of the P-V curve, otherwise to the right side.

If the $V_{REF} < V_{MIN}$, the condition is met in the scans to the left side, and the scanning process is terminated. Then the conditions given in Equation (3.22) are tested. If both conditions are not met, scanning continues in the $[V_{START} - V_{OC}]$ interval. Otherwise, the scan process starts from V_{SKIP} voltage. The scanning process continues in scans made to the right side until any of the conditions given in Equation (3.22) are met. When the V_{MAX} is reached, the P&O algorithm is run to find the exact location of the GMPP.

$$\begin{aligned} I_{START} &< I_{MIN} \\ V_{SKIP} &\geq V_{MAX} \end{aligned} \tag{3.22}$$

Karabacak, Kesilmiş, & Aksoy (2022), in their study, proposed a new method to avoid the erroneous results of the inflection voltages method. In the proposed method, the voltages of the inflection points and the local maximum power points are calculated as given in Equations 3.17 and 3.18. Then, the power values of all local maximum power points are measured, and the exact location of the GMP point is found by running the P&O algorithm around the point estimated to be the GMP point.

3.8. Hybridized MPPT Methods Under PSC

A method capable of finding the global maximum power point can often be combined with another conventional or non-conventional method to increase its efficiency/accuracy. These methods are called hybrid methods.

Alik et al. (2015) proposed a method combining NN and P&O algorithms. In this method, NN gives an initial reference for the P&O algorithm, and P&O performs a precise search according to this reference. The system's performance is increased by combining the speed of NN and the accuracy of P&O.

Mohanty et al. (2017) proposed P&O and GWO algorithms, Lian et al. (2014), Suryavanshi et al. (2012) proposed P&O and PSO algorithms, Sundareswaran et al. (2015), proposed P&O and ACO, Pilakkat & Kanthalakshmi, (2019) proposed methods combining P&O and ABCO algorithms.

In the case of partial shading in these proposed methods, the global maximum point is approximately determined using one of the metaheuristic methods. Then the P&O algorithm is used to determine the exact location of the GMPP. The convergence speed of metaheuristic algorithms increases with fewer iterations using the P&O algorithm.

Rahman & Islam (2020) proposed a new hybrid method (PSO-ANN) in which PSO and ANN algorithms are used together, which can find the global maximum among multiple maximum power points that occur in the case of partial shading.

Gawande, Ghulaxe, Mahatme, Salvi, & Bagewadi (2021) proposed a method (INC-PSO) in which the INC algorithm is run in the absence of partial shading, and the PSO algorithm is run in the case of partial shading, thereby increasing the efficiency of the MPPT system.

<u>3. MPPT ALGORITHMS/ METHODS for PV SYSTEMS Bülent BÜYÜKGÜZEL</u>

4. BD CURRENT BASED GMPP ESTIMATOR

The position of the global maximum power point on a P-V curve is first roughly estimated by the *global search* process and can then be located using the *local search* process within the expected range, as with Two Stage MPPT systems. Most of the GMPPT systems discussed in the preceding sections search the whole P-V curve for the GMPP point. For this reason, the PV source is also operated at operating points quite far from the GMP point. On the other hand, even if various procedures, such as heuristic algorithms, are employed to minimize the search time, obtaining the GMP point takes a long time because the search space covers the whole P-V curve. All of these have a degrading effect on system efficiency. As a result, determining the range where GMPP can be found and searching only that region produces results much faster than searching algorithms that search for the entire P-V curve.

In this thesis, a new system is designed to determine the relative irradiance values of PV modules in a series connected array by measuring the currents passing through the bypass diodes and estimating the GMPP's location using these values.

4.1. Analysis of the P-V Curve of the PV String

Figure 4.1 shows the I-V curve obtained in STC one PV module under uniform irradiance of a PV array consisting of 4 PV modules connected in series. The parameters obtained in STC of the PV module used in the simulations are given in Table 4.1. As can be easily seen from Figure 4.1, the I-V curve on the far right, that is, the I-V curve of the PV array; actually, consists of the sum of the I-V curves of 4 single modules.

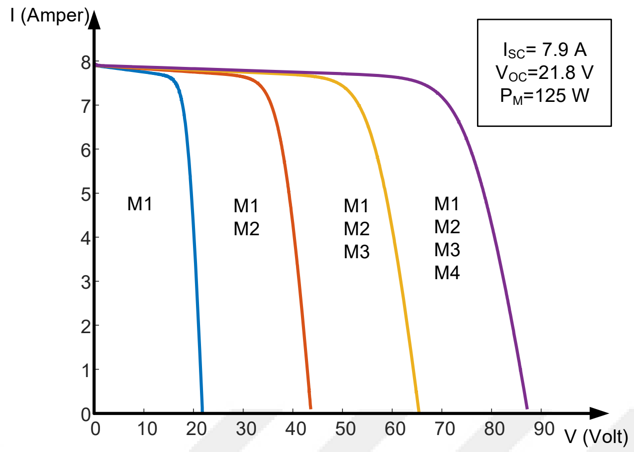

Figure 4.1 I-V curve of the PV string consisting of four modules under uniform irradiance

Figure 4.2 shows the I-V curve of the same string under partial shading and the amount of irradiance to which the PV modules are exposed, and Figure 4.3 shows the P-V curve under partial shading.

In the first region (S1) located at the far right of the I-V curve given in Figure 4.2, the string current is smaller than the short circuit current that can be produced by the M4 module with an irradiance value of 500 W/m^2. For this reason, the bypass diode of all modules is cut off, and all four panels produce an energy proportional to the irradiance value they receive. As a result, all four panels help to produce the local maximum power point in this region.

In the second region, the by-pass diode of the M4 module turns on since the string current is greater than the short-circuit current that the M4 module can produce. Therefore, the M4 module can no longer generate energy and it does not help to establish the local maximum power point in this region.

When the array current surpasses the short circuit current of the M2 and M3 modules, which receive 700 W/m^2 irradiance, the bypass diodes of these modules turn on, and the third region (S3) is entered. The local maximum power point in this region will be determined only by the M1 module, as other modules cannot produce energy.

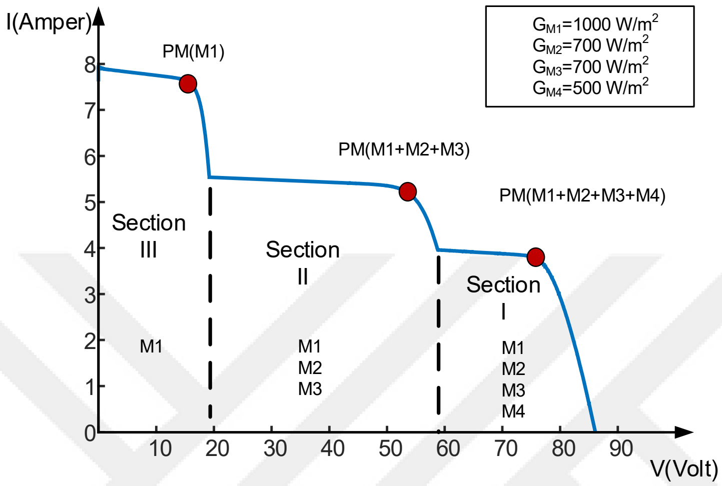

Figure 4.2 I-V curve of the PV string consisting of four modules under PS

Table 4.1 Parameters of the PV string used in simulations

Parameter	Value (@STC)
V_{OC} (V)	21.80
V_{MPP} (V)	17.30
I_{SC} (A)	7.90
I_{MPP} (A)	7.23
P_{MPP} (W)	125
αISC (% °C)	0.0428
α VOC (%°C)	-0.3627
NS	36

A power of 125 W (P_{MPP}=125 W in STC) can be produced because only the M1 module, which receives 1000 W/m^2 irradiance, is active in the S3 region, as shown in Figure 4.3.

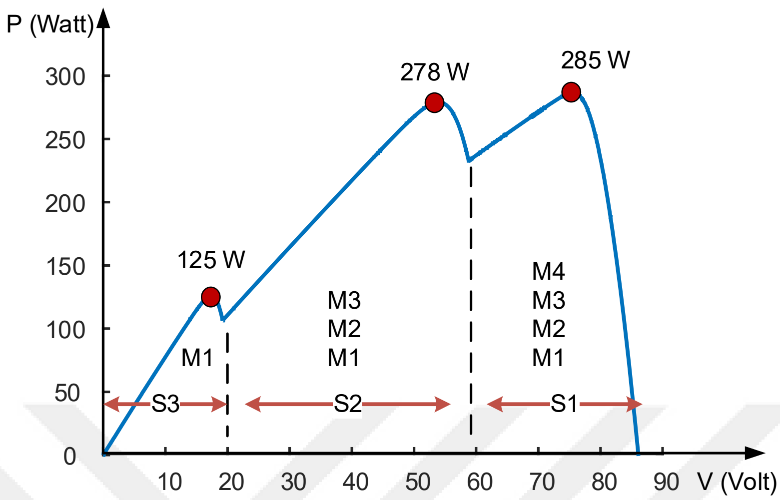

Figure 4.3 P-V curve of the PV string consisting of four modules under PS

In the S2 region, all modules except the M4 module contribute to energy production according to their irradiance and operating points. Although the M1 module receives full irradiance, it contributes to energy production with a power of less than 125 W as the operating point moves away from the maximum power point due to the decrease in the string current. This situation can be easily understood from Figure 4.4, which shows the change of current and voltage in the entire P-V region of the M1 module.

All modules are active in the S1 region due to the decrease of the string current. However, although modules other than the M4 module, which can operate at the maximum power point, contribute to power generation, as they move away from the maximum power points, they can no longer produce the power they could produce in the previous regions.

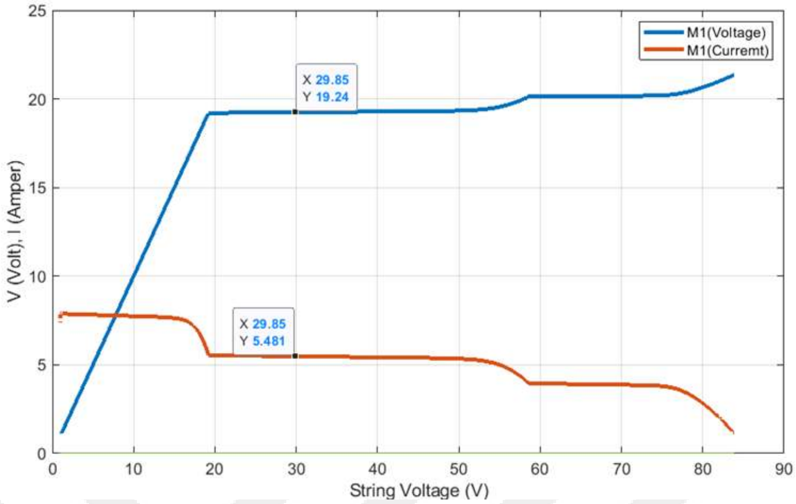

Figure 4.4 Voltage and current of the M1

In Figure 4.5, the P-V curve of the array and P-V curves of the modules consisting of this string are shown on the same graph. When the figure is examined, the contribution of each module to the local maximum formation in the S1 region can be easily seen. The contribution of the modules to the local maximum power point of 285 W in the S1 region is 76 W, 73 W, 73 W and 63 W, respectively.

As a result, the power that can be obtained for any operating point from a PV string with a bypass diode operating under partial shading is the sum of the power that each module consisting of that string can produce at that operating point.

On the other hand, if the power that modules with different irradiance values can produce at any operating point of the string can be determined, the location of the local maximums can also be determined.

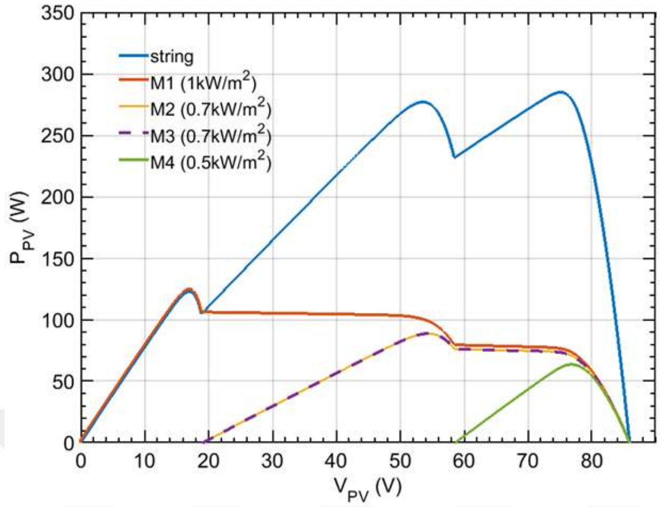

Figure 4.5 P-V Curves of the String and Modules

4.2. Maximum Power-Irradiance Relation

There is various research in the literature that investigates the relations between the maximum power generated from a PV source and the irradiance.

Outdoor measurements were performed in the study conducted by King et al. (2002) for amorphous silicon (a-Si) and multi-crystalline silicon (mc-Si) PV modules at Sandia National Laboratories (SNL). According to the measurement results of this study, the relation between maximum power and irradiance is linear. In another study conducted by King et al. (2004) at the Sandia Laboratory to develop a PV performance model, outdoor measurements made on the mc-Si PV module also showed that this relationship is linear, as shown in Figure 4.6.

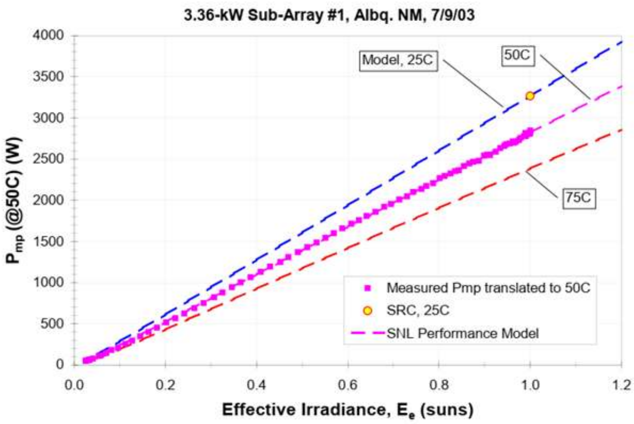

Figure 4.6 Maximum Power- Irradiance relation of the PV Module (King, Kratochvil, & Boyson, 2004)

Marion (2008) created a PV performance model, commonly known as the PVFORM model, at the National Renewable Energy Laboratory (NREL). This model works with PV WATTS, NREL's web-based program, for calculating the power generation of grid-connected PV installations. The relation between the maximum power generated from the PV module and the irradiance and temperature is specified in the PVFORM model by splitting the irradiance into two distinct areas;

$$
\begin{aligned}
&\text{if } G \geq 125 \text{ W/m}^2; \\
&P_{M(G,T)} = \frac{G}{G_{STC}} P_{M(STC)} \left(1 + \gamma \left(T - T_{STC}\right)\right) \\
&\text{if } G < 125 \text{ W/m}^2; \\
&P_{M(G,T)} = \frac{0.008 G^2}{G_{STC}} P_{M(STC)} \left(1 + \gamma \left(T - T_{STC}\right)\right)
\end{aligned}
\tag{4.1}
$$

In this equation, γ donates the temperature coefficient of P_M, G denotes irradiance, and T denotes temperature. The STC index indicates that these are the values at the STC.

Since the efficiency of PV sources decreases significantly at low irradiance values, the irradiance range of 200-1000 W/m^2 is considered the effective range (Grunow, ve diğerleri, 2004; Mavromatakis, Vignola, & Marion, 2017). As shown in Equation 4.1, the relationship between maximum power and irradiance is linear in the 200-1000 W/m^2 irradiance range.

Huld et al. (2011) analysed the performance of crystalline silicon (c-Si) PV modules based on their irradiance and temperature values. The coefficients in the proposed model were discovered utilizing data from indoor and outdoor measurements as well as the curve-fitting approach. In this model, the relationship between power, temperature and irradiance is defined as follows.

$$P_{MP(G,T)} = P_{MP(STC)} \frac{G}{G_{STC}} \begin{pmatrix} 1 + k_1 \ln\left(\frac{G}{G_{STC}}\right) + k_2 \ln\left(\frac{G}{G_{STC}}\right)^2 \\ +k_3\left(T - T_{STC}\right) + k_4\left(T - T_{STC}\right)\ln\left(\frac{G}{G_{STC}}\right) \\ +k_5\left(T - T_{STC}\right)\ln\left(\frac{G}{G_{STC}}\right)^2 + k_6\left(\frac{T}{T_{STC}}\right)^2 \end{pmatrix} \tag{4.2}$$

If the temperature value is the same as in the STC, Equation (4.2) becomes the following equation since only the components with irradiance are effective.

$$P_{MP(G,T)} = P_{MP(STC)} \frac{G}{G_{STC}} \left(1 + k_1 \ln\left(\frac{G}{G_{STC}}\right) + k_2 \ln\left(\frac{G}{G_{STC}}\right)^2\right) \tag{4.3}$$

There is a 15% deviation between the coefficients determined to be k_1=-0.01724, k_2=-0.04047, and k_6=5.0×110^{-6} by Huld et al. (2011) and the calculation for 200 W/m^2 using Equation (4.3) and the calculation using Equation (4.1).

However, the same research also indicated that this proposed approach produced excessive spikes at irradiance values of less than 300 W/m^2 in some PV modules.

If the relationship between the maximum power obtained from a PV source and the irradiance is considered linear, the maximum power that can be obtained for any irradiance value can be found by using the irradiance value to which the PV source is exposed and the maximum power at the STC. The maximum power obtained by this method will be valid for the STC temperature value. As shown in Figure 4.7, the maximum power of two PV sources with the same temperature but different irradiance may be determined by referring to the irradiance values and the maximum power in the STC.

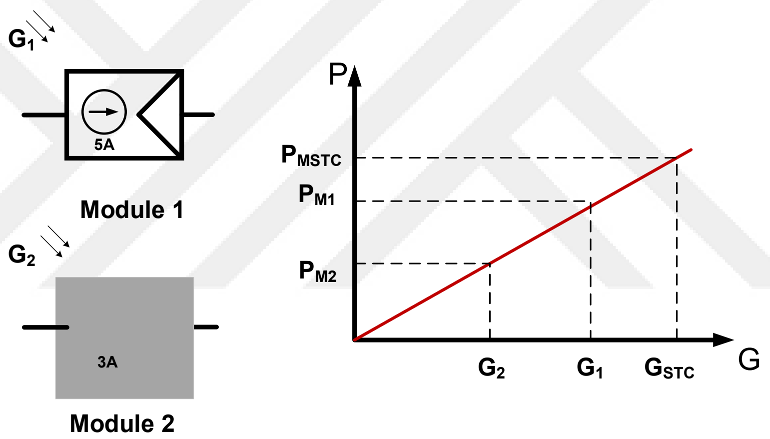

Figure 4.7 Maximum Power- Irradiance relation

At the same time, the P_M value of one of the modules can be normalized and used as a reference, and the P_M value of the other can be found relatively. For example, if the maximum power that can be obtained from Module-1 in Figure 4.7 at G_1 irradiance value is accepted as 1 unit, the maximum power that can be obtained from Module-2 operating under partial shading at G_2 irradiance value will be $P_{M2} = G_2 / G_1$ unit.

On the other hand, as mentioned before in Section 1.5, when the terminals of the PV panel are short-circuited, the short-circuit current I_{SC} produced by the PV panel is equal to the current produced by the light, I_{PH}, if the effect of the series resistance is neglected. Since I_{PH} changes linearly with irradiance, I_{SC} also changes linearly with irradiance as expressed in Equation (4.4).

$$I_{SC(G)} = \left(\frac{G}{G_{STC}}\right) I_{SC(STC)} \tag{4.4}$$

$$\frac{I_{SC(G)}}{I_{SC(STC)}} = \frac{G}{G_{STC}} \tag{4.5}$$

Equation (4.5) obtained by arranging Equation (4.4) shows that since the relationship between short-circuit current and irradiance is linear, the irradiance value can be used instead of the current value normalized with the $I_{SC\,(\mathrm{STC})}$ value.

The P-I curve of the EE125MF5 PV panel, whose model is used in this thesis study, obtained from the simulation in the MATLAB environment at a constant temperature of 25 °C and different irradiance values, is given in Figure 4.8.

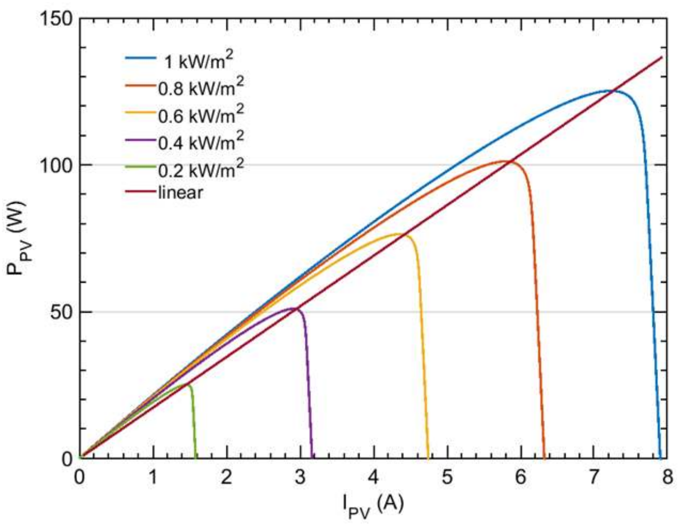

Figure 4.8 P-I curve of the EE125MF5 PV panel

4.3. Relation Between Irradiance and Bypass Diode Current

Figure 4.9 depicts two series-connected PV modules, one of which is partially shaded. The first one of these modules is exposed to G_1 irradiance and can generate the I_{SC1} short circuit current. Because the second module is partially shaded, it gets irradiance with a G_2 value lower than the G_1 value and can generate I_{SC2} short-circuit current that is lower than I_{SC1}. Because the PV array's output is short-circuited and a bypass diode is attached to the modules, a current equal to I_{SC1} current runs through the array. The bypass diode of the second module will activate because the short circuit current produced by partial shade is less than the string current.

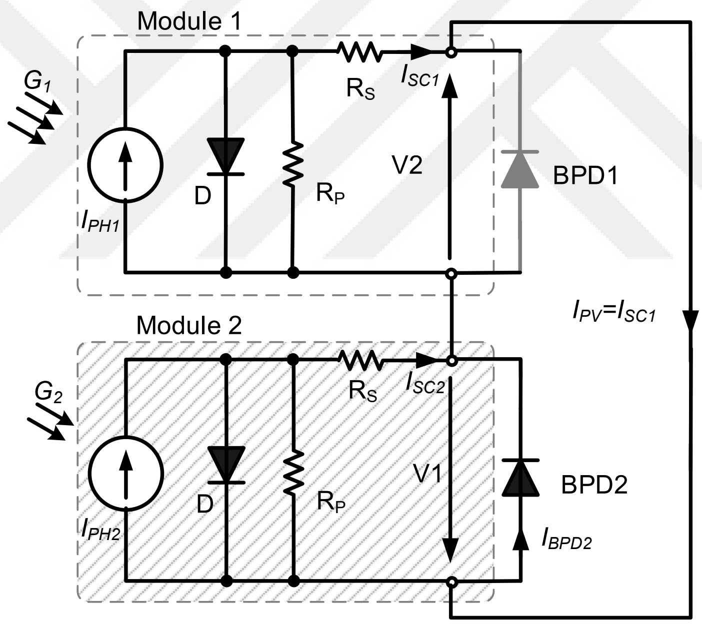

Figure 4.9 Bypass diode current of the PV under PS

If both modules are assumed to have identical properties, the current flowing through the second module's bypass diode BPD_2 will be as follows;

$$\begin{aligned} I_{BD2} &= I_{PV} - I_{SC2} \\ &= I_{SC1} - I_{SC2} \end{aligned} \tag{4.6}$$

Equation (4.4) expresses the relationship between short-circuit current and irradiance. If both modules are identical and at the same temperature, then using this equation, the following statement can be made;

$$\begin{aligned} I_{BD2} &= \frac{G_1}{G_{STC}} I_{SC(STC)} - \frac{G_2}{G_{STC}} I_{SC(STC)} \\ &= I_{SC(STC)} \left(\frac{G_1 - G_2}{G_{STC}} \right) \end{aligned} \tag{4.7}$$

Since a current equal to the short-circuit current of the first module receiving G_1 irradiance from the PV array passes;

$$\begin{aligned} I_{PV} &= I_{SC1(G1)} \\ &= I_{SC(STC)} \frac{G_1}{G_{STC}} \end{aligned} \tag{4.8}$$

From the Equation (3.18);

$$I_{SC(STC)} = I_{PV} \frac{G_{STC}}{G_1} \tag{4.9}$$

If Equation (4.9) is written in Equation (4.7);

$$\begin{aligned} I_{BD2} &= I_{PV} \frac{G_{STC}}{G_1} \left(\frac{G_1 - G_2}{G_{STC}} \right) \\ &= I_{PV} \left(1 - \frac{G_2}{G_1} \right) \end{aligned} \tag{4.10}$$

Editing the expression in Equation (4.10) yields Equation (4.11).

$$\frac{G_2}{G_1} = 1 - \frac{I_{BD2}}{I_{PV}} \tag{4.11}$$

In fact, Equation (4.11) shows that the irradiance values of PV modules with and without partial shading can be found relatively if the bypass diode and PV array current are known. It is clear that the value obtained by Equation (4.11) is a ratio and dimensionless. Therefore, the unit of the calculated irradiance values is the unit.

4.4. Estimation of the GMPP Using Bypass Diode Current

Figure 4.10 shows the P-I curve of the PV string mentioned in Section 4.1. For any operating point or string current, the power to be obtained can be calculated if the power to be produced from each module at that current value is determined.

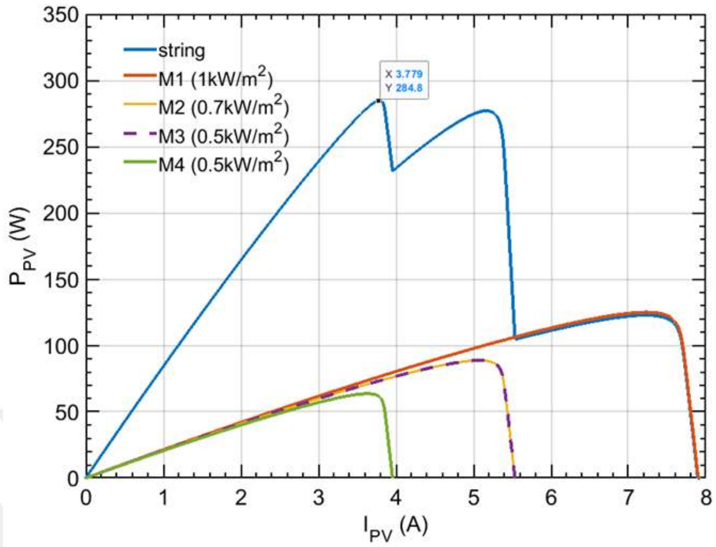

Figure 4.10 P-I Curves of the String and Modules

For example, a power of 285 W can be obtained at the operating point where the string current is 3.78 A. This point is also the global maximum power point, at which the modules produce 76 W, 73 W, 73 W and 63 W, respectively. At this point in the P-V curve, it can be seen that only one module is operating at the maximum power point, while other modules are not operating at maximum power because they are far from their maximum power points.

In order to determine the GMP point, first of all, it is necessary to determine the irradiance value to which each module forming the array is exposed, using the method described in Section 4.3. For this purpose, both the string current and the bypass diode currents are measured by short-circuiting the ends of the PV string. After the current values are obtained, the irradiance values are found by the ratio of the bypass diode currents to the string current. In the case of a short circuit, no current will flow through the bypass diodes of the modules with the highest irradiance value. In this method, the irradiance values of the modules whose bypass diodes in the off state are accepted as 1 *Unit* irradiance.

The measurement values obtained in the short circuit condition of the string mentioned in section 4.1 and the irradiance values obtained using Equation (4.9) are given in Table 4.2. In this table, Shading Pattern 1 (SP1) indicates that the modules are exposed to 1, 0.7, 0.7, and 0.5 kW/m^2, respectively, and SP2 indicates that they are exposed to 0.8, 0.7, 0.7, and 0.5 kW/m^2, respectively. As can be seen from Table 4.2, although the highest irradiance values were 1 and 0.8 kW/m^2 in different shading patterns applied to the string, the calculated irradiance values are found to be 1 unit for both.

At irradiance values lower than STC, the string current will decrease. However, the module with the highest irradiance value in the string also has the highest short-circuit current. The bypass diode of these modules will not turn on in the case of a short circuit. Therefore, the irradiance value of the module with the highest irradiance value in a string is always considered as 1 unit. The irradiance values of other modules are found by comparing the irradiance value of this module.

Table 4.2 Current and Irradiance values of the PV string

SP1	Current (A)	I_{PV}	I_{BD1}	I_{BD2}	I_{BD3}	I_{BD4}
		7.9240	0	2.3712	2.3712	3.9523
	Irradiance (kW/m^2) (Applied)	-	M1	M2	M3	M4
		-	1	0.7	0.7	0.5
	Irradiance (Unit) (Calculated)	-	1	0.7007	0.7007	0.5012
SP2	Current (A)	I_{PV}	I_{BD1}	I_{BD2}	I_{BD3}	I_{BD4}
		6.3423	0	0.7769	0.7769	2.3644
	Irradiance (kW/m^2) (Applied)	-	M1	M2	M3	M4
		-	0.8	0.7	0.7	0.5
	Irradiance (Unit) (Calculated)	-	1	0.8775	0.8775	0.6272

This value actually shows the panel that produces the highest power in the array as it has the highest irradiance value considering Equation (4.1). The maximum power produced by the other modules of the string can be found relatively by referencing this module.

Using the given data in Table 4.2, it is conceivable that the following methods could be used to determine which region contains the global maximum power point. As given in Table 4.3, assuming that each bypass diode forms a different region in the P-V curve, the maximum power that the active modules can produce in these regions can be summed, and the region of the global maximum point can be found.

Table 4.3 Two different approaches for GMPP

Section	Module Power (Unit)				Estimated Total Power (unit)	Estimated Total Power (W)
	M1	M2	M3	M4		
S4	1	-	-	-	1	125
S3	1	0.7	-	-	1.7	212.5
S2	1	0.7	0.7	-	2.4	300
S1	1	0.7	0.7	0.5	2.9	362
S4	1	-	-	-	1	125
S3	0.7	0.7	-	-	1.4	175
S2	0.7	0.7	0.7	-	2.1	262
S1	0.5	0.5	0.5	0.5	2	250

The most important problem to be overcome is to accurately determine the contribution of a module that produces maximum power in one region to power generation in another region.

For example, the module on the far left in the P-V curve given in Figure 4.5 is the module with the maximum irradiance and produces maximum power in the 0-21V region. When moving to the next region, the contribution of this module can be taken as "1" unit, since the irradiance does not change. Or, it can be taken as “0.7” unit since it has the same current as the module with less irradiance in the next region. But both approaches will produce erroneous results, as shown in Table 4.3.

In fact, it is clearly seen in Figure 4.11 that the calculation cannot be done in these ways. It can be seen that the module with the highest irradiance in the array produces only 76 W instead of 125 W at the global maximum power point. This is because the module is not operating at its maximum operating point. Therefore, for any irradiance value, the power produced by a module must be calculated according to the operating point of the PV string.

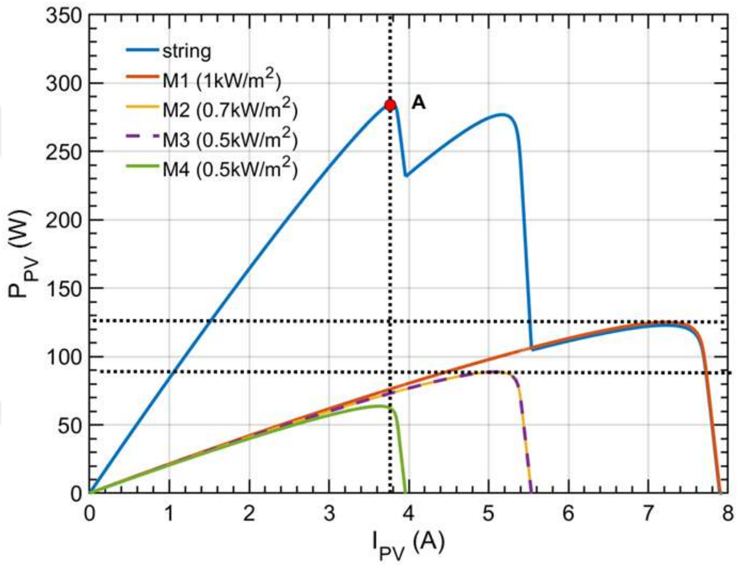

Figure 4.11 P-I data of String and its Modules

The direct calculation of the contribution of modules exposed to different irradiance values in a PV string to the power produced at any operating point of the string is difficult because the characteristics of I-V, P-V and P-I are not linear. Compared to the I-V and P-V curves, the shape in which the P-I curve is relatively linear, at least in the range [0-*MPP*], can be seen in Figure 4.11. On the other hand, as previously mentioned, the x-axis of the P-I curve can be converted into the irradiance axis with a suitable normalization process. Although relatively linear, using the P-I curve to mathematically calculate the power to be obtained from a PV array at any operating point would be a rather erroneous approach. After applying the piecewise linearization process, the use of the P-I curves in the calculation of the power that can be obtained according to the operating point is a method that will minimize the errors.

The P-I curve of the PV module, which is exposed to 1 kW/m^2 and 0.4 kW/m^2 irradiance values, whose basic parameters are given in Table 4.1, is given in Figure 4.12._Actually, this curve is the P-I curve of a PV string consisting of two modules and exposed to different irradiance values. The P-I curve of the PV module operating at 1 kW/m^2 irradiance value is linearized using the B line between the P_{MP1} and P_{C1} points and the A line between the P_{C1} and 0 points. The same process is done for the other curve using lines A and C. So; the curves are linearized using the piecewise linearization process.

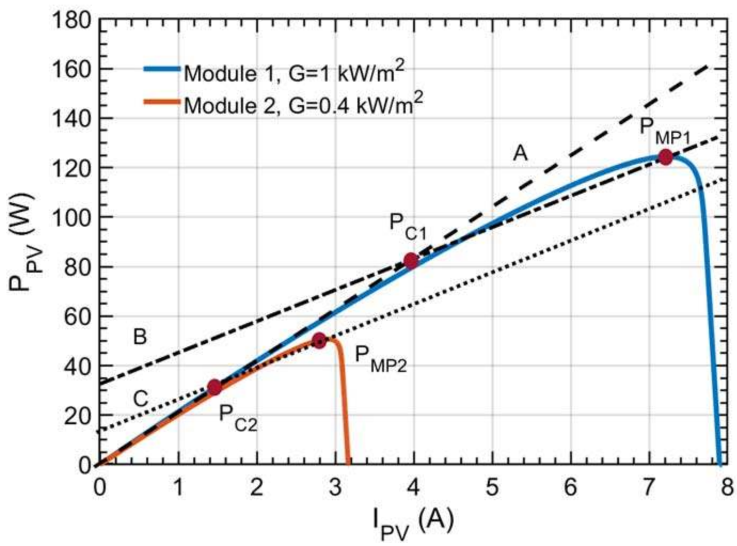

Figure 4.12 P-I curve of the PV module under different irradiance

The equations of the lines A, B and C for the module whose parameters are given in the Table 4.1 are given below.

$$\begin{aligned} y_A &= 20.62x \\ y_B &= 32.5 + 12.7x \\ y_C &= 12.5 + 12.7x \end{aligned} \tag{4.12}$$

Since the irradiance-maximum power relationship is linear, as explained in Section 4.2, it is clear that these lines belonging to two panels with different irradiance values will be parallel, and only the offset values will change according to the irradiance. For this reason, the general equation of this trend line passing through the maximum power point can be written as follows since the coefficients given for the B line in Equation (4.12) are obtained for STC.

$$y(G) = 32.5G + 12.7x \tag{4.13}$$

Using the A and B lines to find the power that a module exposed to irradiance at the value of 1 kW/m^2 can produce at any operating point by using the mathematical method will enable it to overcome the difficulties arising from the nonlinearity in the P-I curve. It is clear that if the operating point is between the P_{MP1} and the PC1 points, line B should be used, and if the current value is smaller than PC1, line C should be used. In fact, the P_{C1} point is the point where the line change should be made._The same is valid for the module exposed to 0.4 kW/m^2 irradiance. If the operating point is between the P_{MP2} and the P_{C2} points, the C line should be used, and beyond this point, the A line should be used. The value of the P_C points, which are the line change points, can be easily determined by using the equation of line C to be used for that irradiance value and the equation of line A.

Using the method described above, the power produced by module 1 can be calculated in addition to the power produced by Module 2 at the P_{MP2} operating point. It can be seen from Figure 4.12 that the power produced by Module2 at the P_{MP2} operating point is 50 W, while the power produced by Module1 is 60 W, and total power of 110 W is produced at this operating point. This value can be calculated using current values and Equation 4.12. At 2.9 A current value, y_A=59.79 W, y_C=49.47 W is found, which confirms the result obtained graphically. On the other hand, the global maximum power value that can be obtained from a PV array in a given partial shading pattern can also be calculated using the same method.

$$\begin{aligned} y_A &= y_B \\ 20.62x &= 32.5 + 12.68x \end{aligned} \tag{4.14}$$

If the x-axis of the P-I curve given in Figure 4.12 is normalized with the I_{MP} value obtained in the STC of Module1, the x-axis values can also be used as the irradiance value for the maximum power points of the PV module. As can be seen in Figure 4.13, as a result of the normalization of the x-axis, the maximum power points of the Modules coincided with the irradiance values they were exposed to.

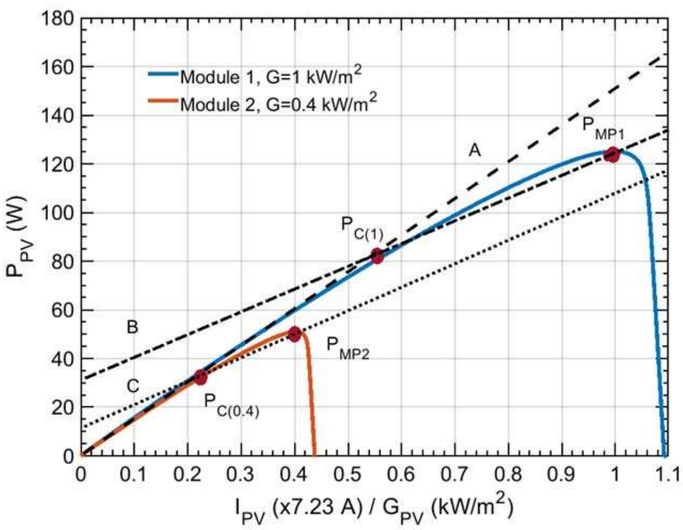

Figure 4.13 P-I curve with normalized x axis

The irradiance value obtained by the method described in Section 4.3 is not an absolute value, but a relative irradiance value obtained according to the highest irradiance value in the string. Therefore, the power values found using this irradiance value are the relative power values found by referencing the module exposed to the highest irradiance value in the string. Therefore, the power axis of the P-I curve given in Figure 4.13 should also be normalized for lines A, B and C. If these lines are normalized with 125 W, which is the maximum power of the module at STC, the equations of the lines given in Equation (4.15) are obtained as follows;

$$
\begin{aligned}
y_A &= 1.2G(x) \\
y_B &= 0.260 + 0.740G(x) \\
y_C &= 0.104 + 0.740G(x) \\
P_{C[G(M)]} &= P_{C(1)} \times G(M)
\end{aligned}
\qquad (4.15)
$$

where, *G(M)* is the irradiance value of the module and *G(x)* is the normalized current value on the x-axis and, indirectly, the irradiance value for maximum power points. $P_{C[G(M)]}$ denotes the irradiance value of *G(M)* and the P_C value of the module.

$P_{C(1)}$ value is found as 0.56 for STC by using y_A and y_B given in Equation (4.15). P_C values required for other irradiance values can be calculated as given in Equation 4.15. For example, $P_C(0.4)$ value required for the irradiance value of G=0.4 kW/m^2 is found as $0.54 \times 0.4 = 0.22$. This value can also be verified graphically from Figure 4.13. It is clear that this value is actually the current value.

The equation y_A of line A in Equation 4.15 is the same for all modules' irradiance values. However, since the expressions of lines such as B and C passing through the maximum power points of the modules depend on the irradiance of the modules. It will be easier to use the general irradiance dependent form of line B as given below.

$$y_{B[G(M)]} = 0.260G(M) + 0.740G(x) \qquad (4.16)$$

After obtaining these values for the PV module used, the location of the global maximum power point of the PV string operating under any shading pattern can be determined by calculating the total power for the irradiance value of each module.

For this purpose, first of all, the PV string is short-circuited, and the current values of the bypass diodes are obtained. And then, the irradiance value of each module is calculated using Equation (4.11) according to the irradiance value of the module with the highest irradiance. Since the calculated irradiance values are not absolute irradiance values, the irradiance value of the module with the highest irradiance is always evaluated as 1 *Unit İrradiance*. For this reason, the power value produced by the module that receives the highest irradiance is always considered as 1 *Unit W*.

After the irradiance values of each module are found, they are sorted from the highest to the lowest. The purpose of this operation is actually to obtain an ordered array, as in the P-I curve. Then, using Equation (4.15), P_C values, which are the change points of linearization lines, are calculated according to the irradiance value of each module.

The power that can be obtained from the string at the maximum operating point of any module can be calculated as follows:

$$P(i) = P(1) \times G(i) + \sum_{j=1}^{i-1} E(j,i) \tag{4.17}$$

where, the values of i and j refer to the position of the modules in the order of irradiance, not their position in the string. *E(j,i)* indicates the contribution of modules that receive higher irradiance but do not operate at their maximum power point to the power produced by the module operating at any irradiance value and at its maximum power point. For example, *E(1,4)* represents the contribution of the module, which is the first in the irradiance ranking because it receives the highest irradiance, to the power produced by the module, which is the 4th in the irradiance ranking.

This contribution is calculated as:

$$E(j,i)=\begin{cases}0.260G(j)+0.740G(i) & \text{, if } G(i)>P_{C[G(j)]} \\ 1.2G(i) & \text{, otherwise}\end{cases} \tag{4.18}$$

To give an example, the components that make up the power at point A on the I-P curve shown in Figure 4.11 are the contributions made by the M4 module operating at its maximum power point and the M1, M2 and M3 modules which are not operating at their maximum power points.

The operation of the Global Maximum Power Point estimator described in this section is summarized in the flowchart given in Figure 4.14.

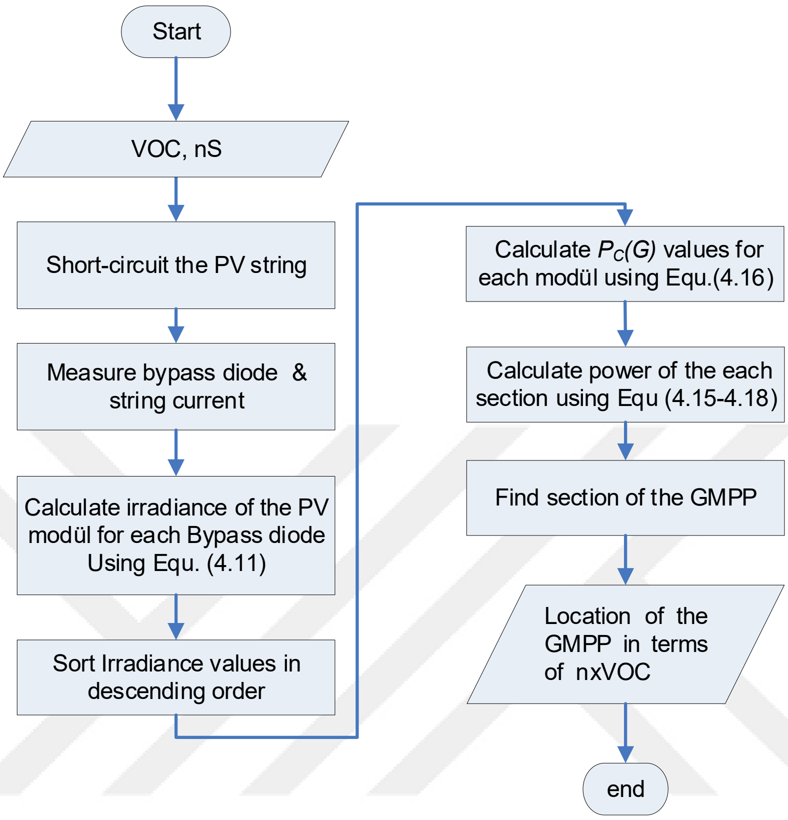

Figure 4.14 Flow chart of the GMPPT location process

4.5. Relationship of V_{OC} with Temperature and Radiation

The relationship of V_{OC} with temperature and radiation is given below.

$$V_{OC}(G,T) = V_{OC,(STC)} + \frac{n_s kTn}{q} \ln\left(\frac{G}{G_{(STC)}}\right) + \alpha_{VOC}\left(T - T_{(STC)}\right) \qquad (4.19)$$

where, α_{VOC} is the temperature coefficient for V_{OC}. As can be seen from the given equation, V_{OC} changes with both radiation and temperature._The I-V curves obtained for different radiation and temperature values obtained as a result of the simulation using the MATLAB model is given in the Figure 4.15. From the obtained I-V curves, when the STC values are taken as a reference, it is seen that the maximum deviation occurs in the minimum temperature/maximum irradiance and maximum temperature/minimum irradiance conditions. From the I-V curves given in Figure 4.15, it has been determined graphically that the total deviation value is 7.73 V.

Although this deviation is not at the predicted power value, it will cause a deviation in the GMP point pointed out by the estimator since the V_{OC} value is taken as a constant. However, this deviation will have no effect on the exact determination of the GMP point if the MPTT system is allowed to search within a sufficiently wide range centred on the given point.

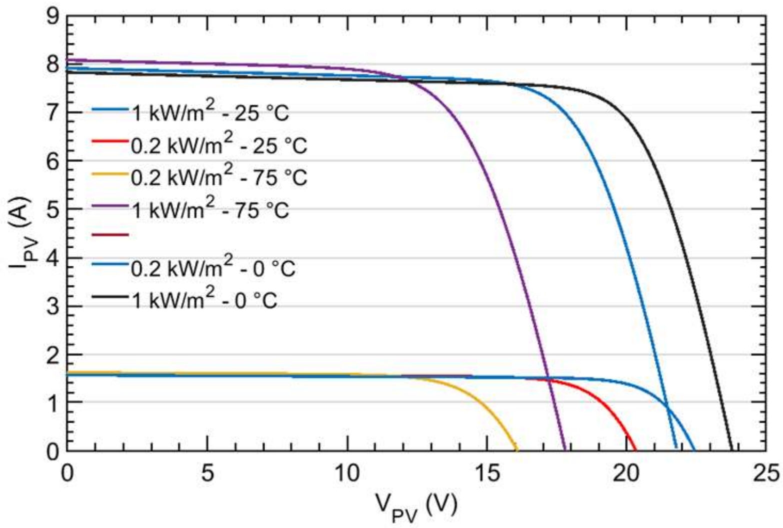

Figure 4.15 I-V curves at different irradiance and temperature values.

4. MPPT ALGORITHMS/ METHODS for PV SYSTEMS Bülent BÜYÜKGÜZEL

5. BDC BASED GMPP TRACKING SYSTEM

In order to locate the GMP point, it is necessary to scan the entire area of the P-V curve in many GMPPT systems given in the literature. Instead, roughly determining the location of the GMP point using an estimator and then reaching the result using a search algorithm around this determined location will shorten the search time considerably. In this thesis, the GMPPT system designed for PV sources operating under partial shading is given in Figure 5.1.

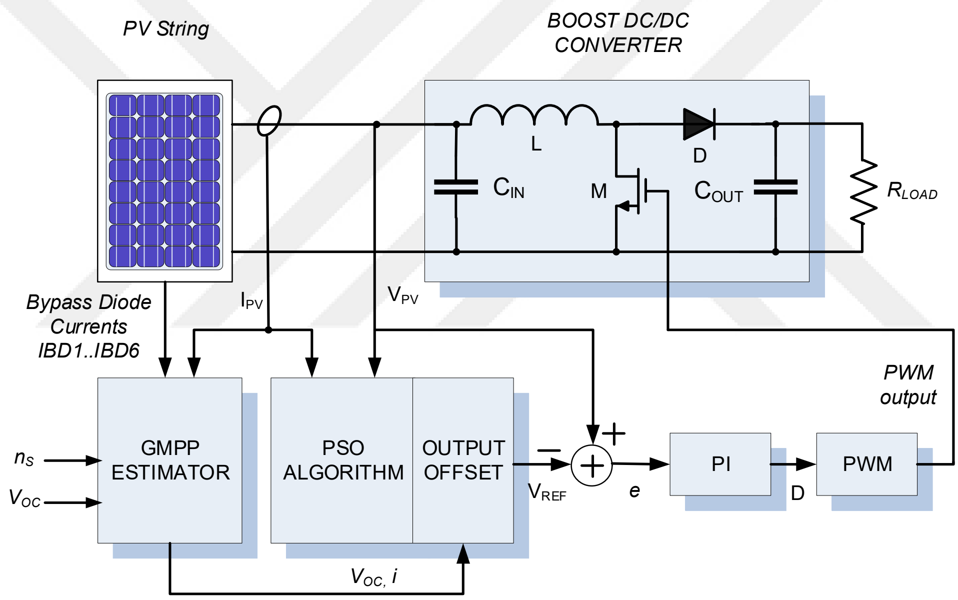

Figure 5.1 Block diagram of the GMPPT System

The system is intended for six series-connected 125 W Mitsubishi PV-UE125MF5N PV module, each with a bypass diode connected in parallel. As a DC/DC converter, a boost type converter is utilized where the input resistance can be modified in the R_L-0 range by adjusting the duty cycle value. Basically, the system works as follows;

First of all, the voltage of the PV array is brought to the $V_{OC}/4$, which is very close to the short-circuit condition, in order to turn the bypass diodes of the panels into conduction, except for those exposed to maximum irradiance. Then, both the array current and the bypass diode currents are measured.

As can be seen from Figure 5.2 and described in the previous section, the GMPP Estimator Algorithm determines the estimated location of the GMP point as $i \times V_{OC}$. The i value here, actually indicates how many modules should be active for GMPP if the modules are ordered from largest to smallest according to their irradiance values.

Using this value and Equation (5.1), the PSO algorithm output in the range [0 1] is transformed to the voltage range where the GMP point is located and applied as a reference voltage to the PI controller. As a result, the PSO algorithm is guaranteed to search inside this voltage range.

$$V_{REF} = i \times V_{OC} + V_{OC}\left(2\left(O_{PSO} - k_W\right)\right) \quad (5.1)$$

In this equation, O_{PSO} represents the PSO algorithm output value, and k_W is the offset value of the voltage search window. When this value is set to 0.5, the search range to the right and left of the point indicated by the GMPP Estimator will be equal.

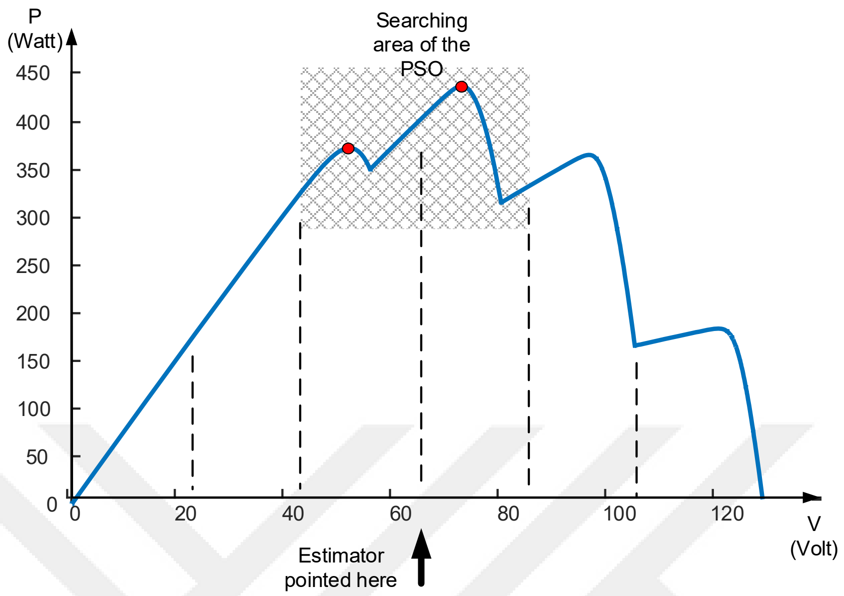

Figure 5.2 Searching area of the PSO pointed by GMPP Estimator

For the purpose of finding the GMP point, giving a range determined by the GMPP Estimator as a search area to the PSO algorithm allows searching in a much smaller area than the [0 $V_{OC(STRING)}$] range.

If the estimator is pointing to the last section, only the left side of the centre point will be scanned, as the centre point of the scan area will be the $V_{OC(STRING)}$. Therefore only for the last section, the centre point of the scan window will be shifted one section before.

The search area of the PSO algorithm is reduced by two-thirds in a string with six bypass diodes, as demonstrated in this study. It is clear that this ratio will be much higher as the number of bypass diodes increases.

5.1. DC/DC Converter

The relation between the input and output voltage of the Boost DC/DC converter;

$$V_{OUT} = \frac{V_{IN}}{1-D} \tag{5.2}$$

where, D is duty cycle value. Using this equation, the relation between the load resistance and the input resistance of the Boost DC/DC converter can be expressed as follows;

$$R_i = (1-D)^2 R_L \tag{5.3}$$

Equation (5.3) demonstrates that when the D value changes in the [0 1] range, the R_{IN} value changes in the [R_L 0] range. The load resistance of the PV array is also the input resistance of the DC/DC converter. Therefore, since it is necessary to operate the PV array at a point close to the short-circuit condition, the boost topology, whose input resistance can be changed in the [R_L 0] range, is preferred as a DC/DC converter in the design of the GMPPT system. In this way, the short-circuit current of the PV array can be measured without the need for additional equipment.

As can be seen from Figure 5.3, the optimum load resistance reaches its maximum value when all modules receive equal and minimum radiation. The minimum value of the optimum load resistance occurs when a single module receives maximum radiation, and the other modules do not receive any radiation. The range of variation of the optimum load resistance is 2.5-72 Ω.

In order to keep this value within the range of the input resistance of the DC/DC converter, the load resistance was chosen as 100 Ω. Using Equation (5.3), at a load resistance of 100 Ω, the duty cycle value that will provide 2.5 Ω input resistance is found as D=0.84 and the output voltage is $V_{OUT} = 106$ V. If the optimum load resistance is 72 Ω, these values are D=0.15, V_{OUT}=123 V.

The critical inductance value required for the boost converter to work in continuous current mode will be determined by the highest power value transferred by the DC/DC converter. This power value can be produced when all modules receive equal irradiance under STC conditions. The minimum value of the inductor and output capacitor used in the boost converter is found using the equations given below (Erickson & Maksimovic, 2007; Rashid, 2017).

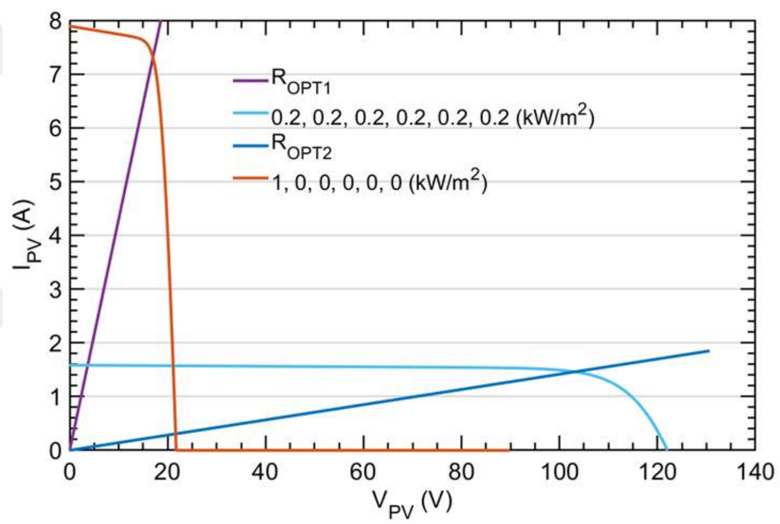

Figure 5.3 I-V curves of the PV string and optimum load lines

$$L = \frac{V_{IN}(V_{OUT} - V_{IN})}{\Delta I_L \times F_S \times V_{OUT}}$$
$$C_{OUT} = \frac{I_{OUT(MAX)} \times D}{F_S \times \Delta V_{OUT}} \tag{5.4}$$

If the switching frequency, the ripple of the coil current and the ripple of the output voltage are chosen as 50 kHz,× 0.30×I_{IN}, and 0.10×$V_{OUT\,(MAX)}$, respectively, then L_{MIN} is found to be 1.65 mH, and C_{OUT} is to be 4 µF. Table 5.1 depicts the design values used for the boost type DC/DC converter as well as the appropriate component values.

Table 5.1 Design values of the DC/DC converter

f_S	50 kHz
R_L	75 Ω
ΔIL	2 A
ΔV_{OUT}	20 V
L_{MIN}	2.2 mH
C_{OUT}	47 uF
C_{IN}	10 uF

5.2. PI Controller

In many GMPPT systems, the outputs of PSO and similar search algorithms in the range of [0 1] are used to directly control the duty cycle value of the PWM generator. However, in the designed system, since the location of the GMPP is determined as the voltage value of the PV array, first of all, the output value in the [0 1] range of the PSO algorithm is converted into the $[(i-1)\times V_{OC}\ \ (i+1)\times V_{OC}]$ range.

In order to bring the operating point of the PV array to the desired voltage value and keep it constant at this point, it is necessary to use a PI (Proportional Integral) controller between the PSO and the PWM generator. The PSO output as the reference value and the voltage of the PV array as the feedback value are applied to the PI controller.

A classical PI controller was used in the designed system, and its parameters were adjusted by the Ziegler- Nichols method (Meshram & Kanojiya, 2012; Valério & Da Costa, 2006) using the SIMULINK/MATLAB model given in Figure 5.3.

With the help of the simulation of the system using the SIMULINK model given in Figure 5, it was determined that the K_P and K_I values should be 0.81 and 110, respectively, for stable operation.

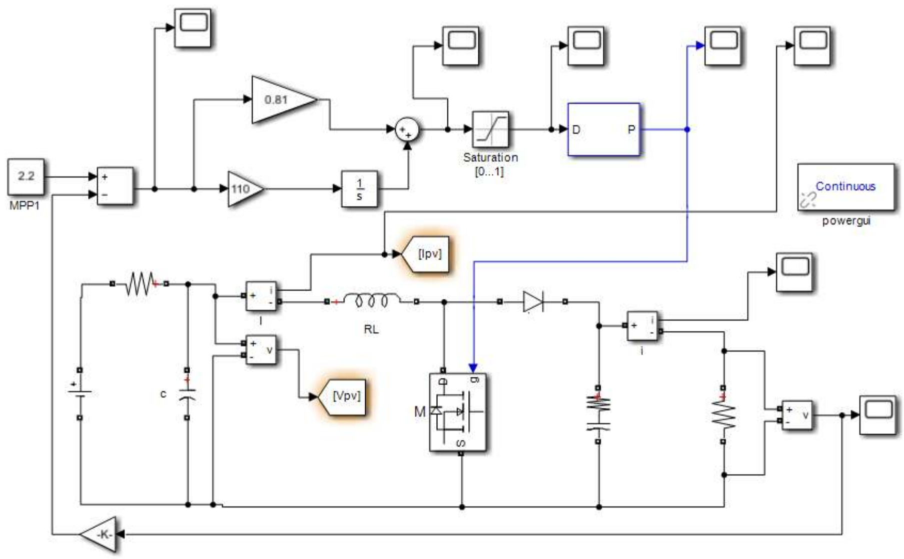

Figure 5.4 Simulink model of the PID controller

5.3. PSO Algorithm

The classical PSO algorithm is used in the GMPPT system. The coefficients used in the algorithm were determined as $c1 = 1, c2 = 1.5, w = 0.5$, by using the simulation. The number of particles is chosen as 4 for optimum convergence.

6. SIMULATION RESULTS

The designed GMPP Estimator and BDC Based GMPPT System were modelled and simulated using MATLAB/SIMULINK.

6.1. Simulation and Validation of the GMPP Estimator

The validation of the GMPP Estimator algorithm, designed to predict the location of the global maximum power point of the PV array operating under partial shading, has been tested in the SIMULINK environment using different shading patterns (SP). The SIMULINK model used in the simulation is shown in figure x. The partial shading patterns used to test the accuracy of the algorithm are given in Table 6.1. Shading patterns were obtained randomly using the *rand* command in the MATLAB environment. Provided that the irradiance values in the shading pattern remain the same, the I-V, P-V and P-I curves obtained as a result of changing the modules to which these irradiance values are applied will be the same. For this reason, in order to increase the intelligibility of the applied pattern, the irradiance values were applied in order from smallest to largest.

The P-V curve obtained by applying SP6 to the PV array is given in Figure 6.1. In Figure 6.1, the voltage and power values of the local maximum power points that occur due to partial shading and the power values calculated by the Estimator are shown on the P-V curve for each section separately. When Figure 6.1 is examined, it can be seen that both the location of the MPP point is correctly determined and the power values calculated with reference to the actual power value in S1 are compatible with the local maximum power values obtained by simulation.

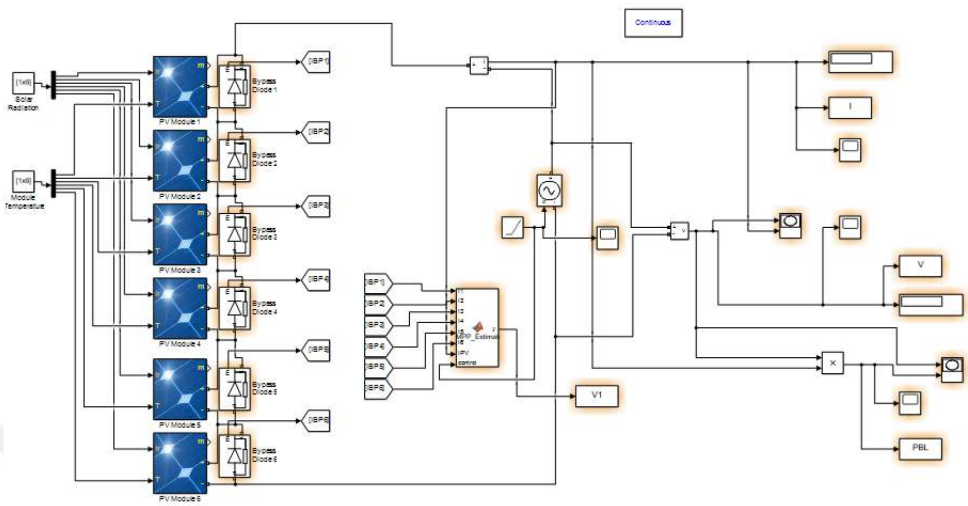

Figure 6.1 SIMULINK model of GMPP Estimator

Table 6.1 Shading Patterns Used for Testing

Module Number	Shading Pattern (SP)									
	1	2	3	4	5	6	7	8	9	10
M1	0.1	0.2	0.2	0.2	0.2	0.1	0.2	0.1	0.45	1
M2	0.1	0.2	0.3	0.2	0.3	0.2	0.4	0.8	0.5	1
M3	0.15	0.2	0.5	0.5	0.4	0.3	0.4	0.8	0.6	1
M4	0.2	0.2	1	0.5	0.5	0.4	0.5	1	0.65	1
M5	0.3	1	1	0.7	0.6	0.5	0.8	1	0.68	1
M6	1	1	1	0.7	0.7	1	1	1	1	1

In order to comply with the working principle of the Estimator and to make a correct comparison, the power values of the LMP points obtained from the P-V curve given in Figure 6.1 and the maximum power value occurring in S1 are proportioned, and the results are given in Table 6.2 for each section. Values calculated by the estimator are also given in the same table for comparison.

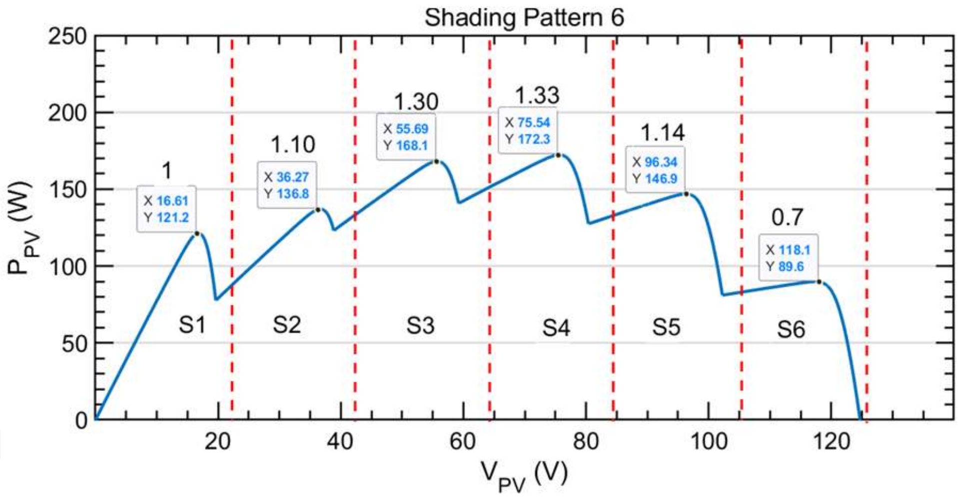

Figure 6.2 P-V curve of the string under PS6

Table 6.2 Power of the local maximums and sections

	Power of the Local Maximum (W) / Section Power					
	S1	S2	S3	S4	S5	S6
P_{LM} (W)	121	137	168	172	147	90
$P_{LM-S(i)}$ /$P_{LM-S(1)}$	1.00	1.13	1.38	1.42	1.21	0.74
Estimator result	1.00	1.10	1.30	1.33	1.14	0.70
Absolute Error	0	0.07	0.08	0.09	0.07	0.04
Relative Error (%)	0	6.19	5.79	6.33	5.78	5.40

The resulting error between the Estimator result and the results obtained directly from the P-V curve is due to the fact that the power loss in the bypass diodes is not taken into account by the Estimator in the calculations. The power loss caused by the bypass diodes can be understood from the fact that the power value obtained from the PV array at S1 should be 125 W while it is 121 W.

The Global maximum power values (GMP) given in Table 6.2 and the voltage (V_{GMP}) values at which these powers occur, the section values of the global maximum power point estimated by the Estimator and the voltage range of this point calculated as [$(i-1) \times V_{OC}$ $i \times V_{OC}$] are given in Table 6.3. The i value is the value pointing to the section number on the P-V curve. The P-V curves, obtained by applying the shading patterns given in Table 6.1, and the string voltages indicated by the Estimator are given in Figures 6.2 and 6.3.

Table 6.3 Estimated location of the GMP, GMP and range of V_{OC}

Shading Pattern	Normalized Power of the Section						Pointed Section	Estimated GMP (W)	$V_{OC}(i-1)$	$V_{OC}(i)$	V_{GMP} (V)	GMP (W)
	S1	S2	S3	S4	S5	S6						
SP1	1.00	0.22	0.32	0.42	0.52	0.61	1	125	0	21	16	118
SP2	1.00	1.99	0.68	0.88	1.07	1.27	2	248	21	42	34	247
SP3	1.00	1.99	2.99	2.30	1.73	1.38	3	372	42	63	51	373
SP4	1.00	1.99	2.29	3.00	1.65	1.94	4	262	63	84	73	270
SP5	1.00	1.75	2.25	2.51	2.42	1.98	4	219	63	54	75	226
SP6	1.00	1.10	1.30	1.33	1.14	0.70	4	166	63	84	75	172
SP7	1.00	1.65	1.67	1.78	2.18	1.40	5	273	84	105	93	279
SP8	1.00	1.99	2.99	3.35	4.15	0.70	5	519	84	105	89	537
SP9	1.00	1.43	2.04	2.53	2.71	2.95	6	369	105	126	112	344
SP10	1.00	2	3	4	5	6	6	750	105	126	106	750

The data in Table 6.3 shows that the GMPP Estimator algorithm, which uses bypass currents to give a specific range where the GMP point can be found, does not fail in any of the partial shadowing patterns used in the testing process.

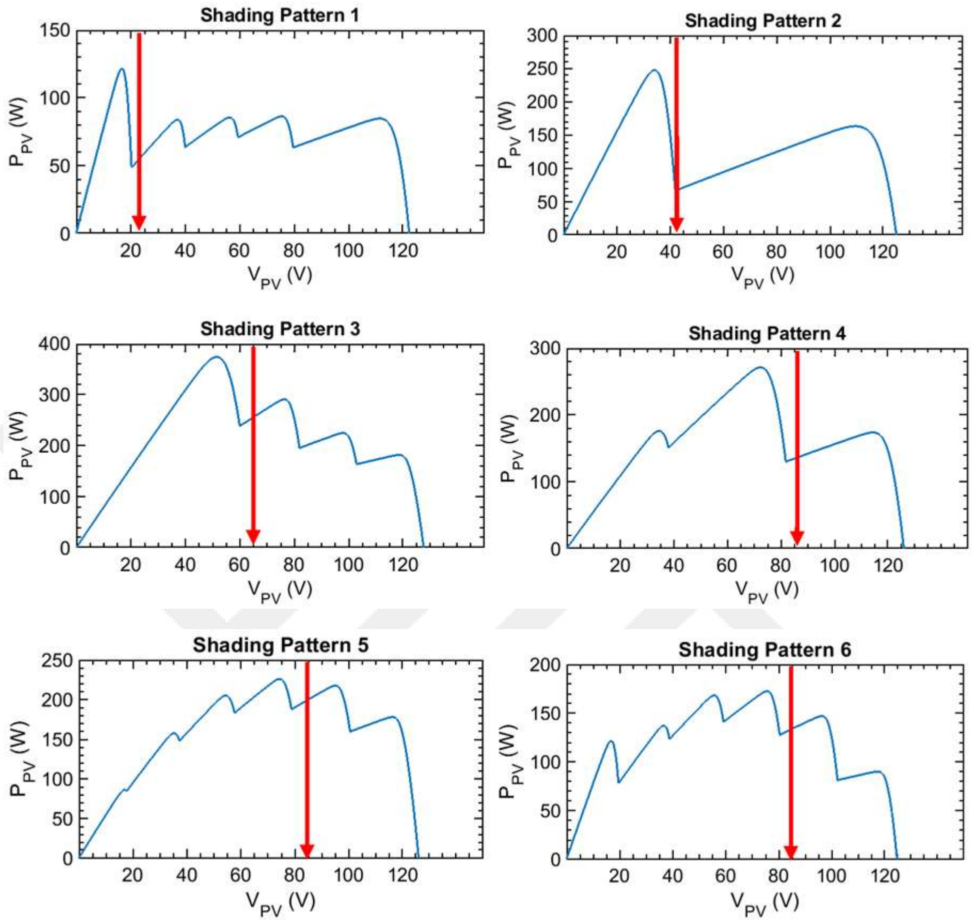

Figure 6.3 P-V curve of the PV string under PS1-PS6

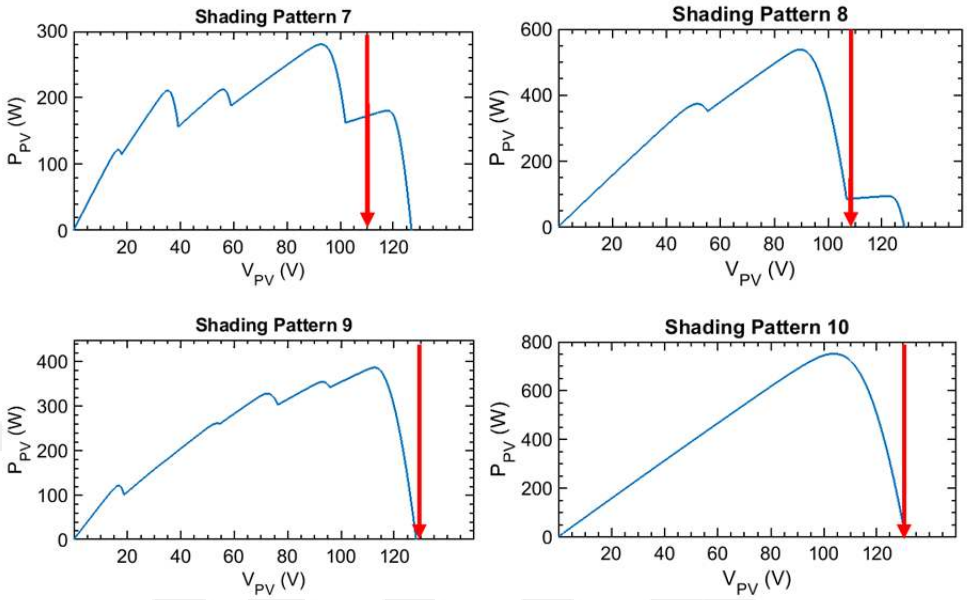

Figure 6.4 P-V curve of the PV string under PS7-PS10

6.2. Simulation Results of the GMPPT System

The model of the GMPPT System realized using SIMULINK models is given in Figure 6.5. GMPPT System performance was investigated by applying the shading patterns given in Table 6 to the PV array. The results of SP2 and SP3 are given in Figure 6.6 and Figure 6.7.

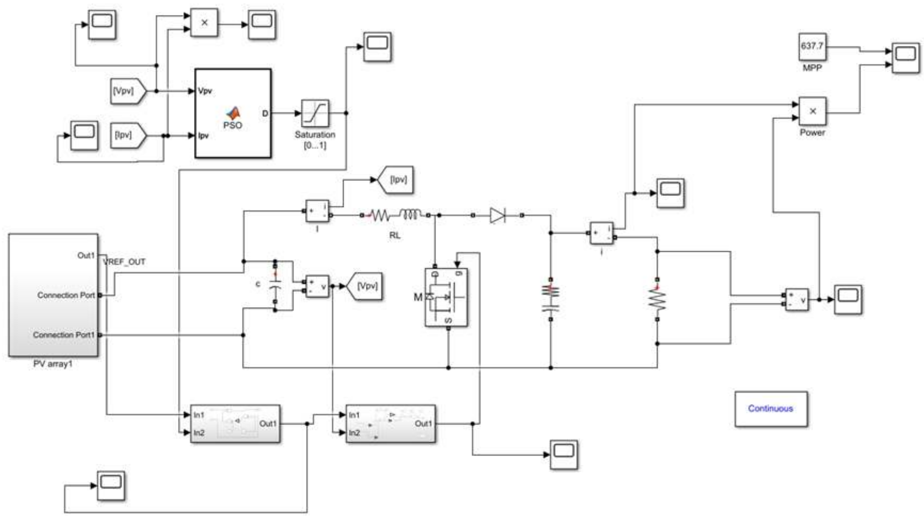

Figure 6.5 SIMULINK Model of the GMPPT System

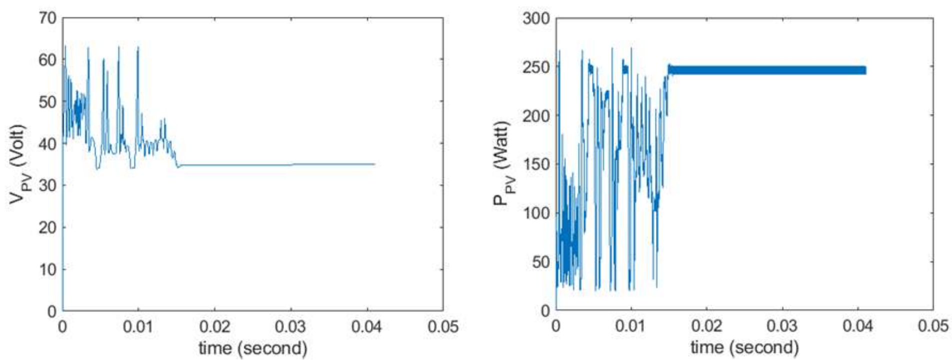

Figure 6.6 Voltage-time and power-time waveform for SP2

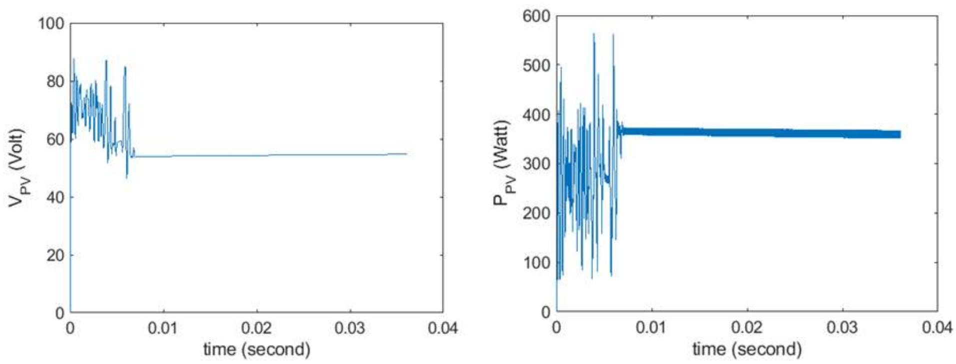

Figure 6.7 Voltage-time and power-time waveform for SP3

The simulation results show that the MPPT system finds the GMPP point without error by searching within the range specified by the estimator. The static MPPT error of the proposed GMPPT System defined as in Equation (5.5) is 1.6 % for SP2 and 1% for SP3.

$$e_{MPTT}\% = \frac{P_{theoretical} - P_{actual}}{P_{theoretical}} \times 100 \tag{6.1}$$

On the other hand, it is seen that the GMPPT system reaches the GMP point in 15 ms for SP2, and 8 ms for SP3. The PSO system reaches the value determined by the GMPPT estimator in an average of 50 iterations.

7. CONCLUSION AND FUTURE WORK

Partial shading is one of the important problems that negatively affects the efficiency of PV systems and needs to be solved. Many methods have been proposed in the literature to overcome this problem. However, an effective solution has not been found by the researchers yet. In recent years, studies on hybrid systems that use both heuristic and classical search algorithms to determine the GMP point have been increasing.

In this thesis, in order to overcome the partial shading problem, a hybrid system has been implemented with a new approach different from the existing methods. Determining the radiations of the modules exposed to different radiations due to partial shading and giving a range where the GMP point can be found to the main search algorithm as the search space will provide convenience for the main algorithm. In order to determine the GMP point, searching only two V_{OC} ranges instead of searching a very wide range will increase the speed of the tracking system to reach the GMP point.

The GMPP estimator is realized using the parameter and characteristic curves of a particular PV panel. This situation can be considered as a disadvantage. However, the model of the PV panel is not used in the GMPP estimation calculations. Therefore, the computational load is quite low. This allows it to be run on low-cost microcontrollers. The most important disadvantage of the proposed method is that the calculations are made by assuming that the module temperatures are equal.

There will be no difficulty in assembling the circuit board to the panels, which is required for measuring the currents of the bypass diodes, which are located in the junction box of the PV panel and can be removed when necessary.

The GMPP estimator can be integrated into any heuristic or conventional searching algorithm that can search the entirety of a specified search space. Since the search space is limited, it is even possible to use a modified P&O algorithm to work across the entire search space.

The simulation results given in the previous section show that both the GMPP Estimator and the GMPPT System are working in accordance with the theory put forward. As can be seen in Figure 6.6 and Figure 6.7, PSO, which is the main search part of the system, searches in the interval determined by the Estimator instead of scanning in the [0-V_{OC}] range.

As can be seen from the simulation results, the GMP point can be reached in a short time, like 50 iterations on average, as a result of the search made in the range indicated by the GMPP Estimator. During the simulation period until the GMP point is reached, 14% energy loss occurs for SP2 and 10% for SP3. In addition, the static error of the system is very low, such as 1.6%, depending on the shading pattern. The most important reason why the energy loss is so low is that the search is only done around the GMP point, thanks to the GMPP Estimator used.

On the other hand, the proposed system seems to be a suitable area for improvement. For example, measuring the currents of bypass diodes in a PV array allows the detection of modules that are permanently under partial shade due to contamination and the generation of warning notifications.

In the future, for the development of the designed GMPP Estimator system, studies will be continued on developing different methods for measuring bypass diode currents and transferring these measurement data to the upper system over a network.

REFERENCES

AbdulHadi, M., Al-Ibrahim, A. M., & Virk, G. S. (2004). Neuro-fuzzy-based solar cell model. *IEEE Transactions on Energy Conversion, 19*, 619-624. doi:10.1109/TEC.2004.827033

Ahmed, J., & Salam, Z. (2014). A Maximum Power Point Tracking (MPPT) for PV system using Cuckoo Search with partial shading capability. *Applied Energy, 119*, 118–130.

Alam, D. F., Yousri, D. A., & Eteiba, M. B. (2015). Flower pollination algorithm based solar PV parameter estimation. *Energy Conversion and Management, 101*, 410–422.

Ali, A., Almutairi, K., Padmanaban, S., Tirth, V., Algarni, S., Irshad, K., . . . Malik, M. Z. (2020). Investigation of MPPT Techniques Under Uniform and Non-Uniform Solar Irradiation Condition–A Retrospection. *IEEE Access, 8*, 127368-127392. doi:10.1109/ACCESS.2020.3007710

Anani, N., & Ibrahim, H. (2020). Adjusting the single-diode model parameters of a photovoltaic module with irradiance and temperature. *Energies, 13*, 3226.

André, T., & Guerra, F. (2020). Renewables 2020 global status report. *Mastny, L., Brumer, L., Eds*.

Andrei, H., Ivanovici, T., Predusca, G., Diaconu, E., & Andrei, P. C. (2012). Curve fitting method for modeling and analysis of photovoltaic cells characteristics. *Proceedings of 2012 IEEE International Conference on Automation, Quality and Testing, Robotics*, (s. 307-312). doi:10.1109/AQTR.2012.6237722

Anoop, K., & Nandakumar, M. (2018). A novel maximum power point tracking method based on particle swarm optimization combined with one cycle control. *2018 International Conference on Power, Instrumentation, Control and Computing (PICC)*, (s. 1–6).

Arora, S., & Singh, S. (2019). Butterfly optimization algorithm: a novel approach for global optimization. *Soft Computing, 23*, 715–734.

Askarzadeh, A., & dos Santos Coelho, L. (2015). Determination of photovoltaic modules parameters at different operating conditions using a novel bird mating optimizer approach. *Energy Conversion and Management, 89*, 608–614.

Askarzadeh, A., & Rezazadeh, A. (2013). Artificial bee swarm optimization algorithm for parameters identification of solar cell models. *Applied Energy, 102*, 943–949.

Awadallah, M. A. (2016). Variations of the bacterial foraging algorithm for the extraction of PV module parameters from nameplate data. *Energy conversion and management, 113*, 312–320.

Aygül, K., Cikan, M., Demirdelen, T., & Tumay, M. (2019). Butterfly optimization algorithm based maximum power point tracking of photovoltaic systems under partial shading condition. *Energy Sources, Part A: Recovery, Utilization, and Environmental Effects*, 1–19.

Ayodele, T. R., Ogunjuyigbe, A. S., & Ekoh, E. E. (2016). Evaluation of numerical algorithms used in extracting the parameters of a single-diode photovoltaic model. *Sustainable Energy Technologies and Assessments, 13*, 51–59.

Barukčić, M., Ćorluka, V., & Miklošević, K. (2015). The irradiance and temperature dependent mathematical model for estimation of photovoltaic panel performances. *Energy conversion and management, 101*, 229–238.

Bonanno, F., Capizzi, G., Graditi, G., Napoli, C., & Tina, G. M. (2012). A radial basis function neural network based approach for the electrical characteristics estimation of a photovoltaic module. *Applied Energy, 97*, 956–961.

Büyükgüzel, B., & Aksoy, M. (2016). A current-based simple analog MPPT circuit for PV systems. *Turkish Journal of Electrical Engineering & Computer Sciences, 24*, 3621–3637.

Carrero, C., Ramírez, D., Rodríguez, J., & Platero, C. A. (2011). Accurate and fast convergence method for parameter estimation of PV generators based on three main points of the I–V curve. *Renewable Energy, 36*, 2972–2977.

Celikel, R., Yilmaz, M., & Gundogdu, A. (2022). A voltage scanning-based MPPT method for PV power systems under complex partial shading conditions. *Renewable Energy, 184*, 361–373.

Chatterjee, A., & Keyhani, A. (2011). Thevenin's equivalent of photovoltaic source models for MPPT and power grid studies. *2011 IEEE Power and Energy Society General Meeting*, (s. 1-7). doi:10.1109/PES.2011.6039203

Chin, V. J., Salam, Z., & Ishaque, K. (2015). Cell modelling and model parameters estimation techniques for photovoltaic simulator application: A review. *Applied Energy, 154*, 500–519.

Daraban, S., Petreus, D., & Morel, C. (2014). A novel MPPT (maximum power point tracking) algorithm based on a modified genetic algorithm specialized on tracking the global maximum power point in photovoltaic systems affected by partial shading. *Energy, 74*, 374–388.

De Soto, W., Klein, S. A., & Beckman, W. A. (2006). Improvement and validation of a model for photovoltaic array performance. *Solar energy, 80*, 78–88.

Deboucha, H., Kermadi, M., Mekhilef, S., & Belaid, S. L. (2021). Voltage track optimizer based maximum power point tracker under challenging partially shaded photovoltaic systems. *IEEE Transactions on Power Electronics, 36*, 13817–13825.

Desai, H. P., & Patel, H. K. (2007). Maximum power point algorithm in PV generation: An overview. *2007 7th International Conference on Power Electronics and Drive Systems*, (s. 624–630).

Di Piazza, M. C., & Vitale, G. (2013). *Photovoltaic sources: modeling and emulation.* Springer.

Di, X., Yundong, M., & Qianhong, C. (2014). A global maximum power point tracking method based on interval short-circuit current. *2014 16th European Conference on Power Electronics and Applications*, (s. 1–8).

Duy, C., Ho, L. D., & Dunnigan, M. W. (2020). Parameter Estimation of Solar Photovoltaic Cells Using an Improved Artificial Bee Colony Algorithm. *Computational Intelligence Methods for Green Technology and Sustainable Development: Proceedings of the International Conference GTSD2020*, *1284*, s. 281.

Erickson, R. W., & Maksimovic, D. (2007). *Fundamentals of power electronics.* Springer Science & Business Media.

Esram, T., & Chapman, P. L. (2007). Comparison of Photovoltaic Array Maximum Power Point Tracking Techniques. *IEEE Transactions on Energy Conversion, 22*, 439-449. doi:10.1109/TEC.2006.874230

Fan, Y., Wang, P., Heidari, A. A., Chen, H., Mafarja, M., & others. (2022). Random reselection particle swarm optimization for optimal design of solar photovoltaic modules. *Energy, 239*, 121865.

Farzaneh, J., Keypour, R., & Khanesar, M. A. (2018). A new maximum power point tracking based on modified firefly algorithm for PV system under partial shading conditions. *Technology and Economics of Smart Grids and Sustainable Energy, 3*, 1–13.

Fathabadi, H. (2013). Novel neural-analytical method for determining silicon/plastic solar cells and modules characteristics. *Energy conversion and management, 76*, 253–259.

Feldman, D., Dummit, K., Zuboy, J., & Margolis, R. (2022, August). Summer 2022 Solar Industry Update. https://www.osti.gov/biblio/1883384 adresinden alındı

Femia, N., Petrone, G., Spagnuolo, G., & Vitelli, M. (2017). *Power electronics and control techniques for maximum energy harvesting in photovoltaic systems.* CRC press.

Fortunato, M., Giustiniani, A., Petrone, G., Spagnuolo, G., & Vitelli, M. (2008). Maximum power point tracking in a one-cycle-controlled single-stage photovoltaic inverter. *IEEE Transactions on Industrial Electronics, 55*, 2684–2693.

Galtieri, J., & Krein, P. T. (2018). Ripple correlation control with capacitive compensation for photovoltaic applications. *2018 IEEE 19th Workshop on Control and Modeling for Power Electronics (COMPEL)*, (s. 1–7).

Gawande, M. K., Ghulaxe, S. G., Mahatme, T. R., Salvi, A. S., & Bagewadi, M. D. (2021). Modern approach for hybridization of PSO-INC MPPT methods for efficient solar power tracking. *2021 2nd Global Conference for Advancement in Technology (GCAT)*, (s. 1–6).

Gibb, D., Ledanois, N., Ranalder, L., Yaqoob, H., Murdock, H. E., Achury, N., . . . others. (2022). Renewables 2022 global status report+ Renewable energy data in perspective+ Press releases+ Regional fact sheets+ Country fact sheets.

Gilbert, M. (2004). *Renewable and Efficient Electric Power Systems.*

Grunow, P., Lust, S., Sauter, D., Hoffmann, V., Beneking, C., Litzenburger, B., & Podlowski, L. (2004, January). Weak light performance and annual yields of PV modules and systems as a result of the basic parameter set of industrial solar cells. *Proc. 19th European Photovoltaic Solar Energy Conf.*

Guo, L., Meng, Z., Sun, Y., & Wang, L. (2016). Parameter identification and sensitivity analysis of solar cell models with cat swarm optimization algorithm. *Energy conversion and management, 108*, 520–528.

Hansen, C. W. (2015). Parameter Estimation for Single Diode Models of Photovoltaic Modules.

Hilali, A., Mardoude, Y., Essahlaoui, A., Rahali, A., & El Ouanjli, N. (2022). Migration to solar water pump system: Environmental and economic benefits and their optimization using genetic algorithm Based MPPT. *Energy Reports, 8*, 10144–10153.

Ho, B. M., Chung, H. S., & Lo, W. L. (2004). Use of system oscillation to locate the MPP of PV panels. *IEEE Power Electronics Letters, 2*, 1–5.

Ishaque, K., & Salam, Z. (2012). A deterministic particle swarm optimization maximum power point tracker for photovoltaic system under partial shading condition. *IEEE transactions on industrial electronics, 60*, 3195–3206.

Ismail, M. S., Moghavvemi, M., & Mahlia, T. M. (2013). Characterization of PV panel and global optimization of its model parameters using genetic algorithm. *Energy Conversion and Management, 73*, 10–25.

Jain, S., & Agarwal, V. (2004). A new algorithm for rapid tracking of approximate maximum power point in photovoltaic systems. *IEEE power electronics letters, 2*, 16–19.

Jiang, L. L., Srivatsan, R., & Maskell, D. L. (2018). Computational intelligence techniques for maximum power point tracking in PV systems: A review. *Renewable and Sustainable Energy Reviews, 85*, 14–45.

Kaced, K., Larbes, C., Ramzan, N., Bounabi, M., & elabadine Dahmane, Z. (2017). Bat algorithm based maximum power point tracking for photovoltaic system under partial shading conditions. *Solar Energy, 158*, 490–503.

Karabacak, M. A., Kesilmiş, Z., & Aksoy, M. (2022). A novel two-stage MPPT method based on inflection voltages. *Energy Sources, Part A: Recovery, Utilization, and Environmental Effects, 44*, 591–612.

Karaboga, D. (2005). *An idea based on honey bee swarm for numerical optimization.* Tech. rep., Technical report-tr06, Erciyes university, engineering faculty, computer ….

Karatepe, E., Boztepe, M., & Colak, M. (2006). Neural network based solar cell model. *Energy conversion and management, 47*, 1159–1178.

Kennedy, J., & Eberhart, R. (1995). Particle swarm optimization. *Proceedings of ICNN'95 - International Conference on Neural Networks*, *4*, s. 1942-1948 vol.4. doi:10.1109/ICNN.1995.488968

Kesilmiş, Z., Karabacak, M. A., & Aksoy, M. (2020). A novel MPPT method based on inflection voltages. *Journal of Cleaner Production, 266*, 121473.

Kharchouf, Y., Herbazi, R., & Chahboun, A. (2022). Parameter's extraction of solar photovoltaic models using an improved differential evolution algorithm. *Energy Conversion and Management, 251*, 114972.

Khatib, T., Elmenreich, W., & Mohamed, A. (2017). Simplified IV characteristic tester for photovoltaic modules using a DC-DC boost converter. *Sustainability, 9*, 657.

Khatib, T., Sopian, K., & Kazem, H. A. (2013). Actual performance and characteristic of a grid connected photovoltaic power system in the tropics: A short term evaluation. *Energy Conversion and Management, 71*, 115–119.

King, D. L., Boyson, W. E., & Kratochvil, J. A. (2002). Analysis of factors influencing the annual energy production of photovoltaic systems. *Conference Record of the Twenty-Ninth IEEE Photovoltaic Specialists Conference, 2002.*, (s. 1356–1361).

King, D. L., Kratochvil, J. A., & Boyson, W. E. (2004). *Photovoltaic array performance model.* United States. Department of Energy.

Kirkpatrick, S., Gelatt, C. D., & Vecchi, M. P. (1983). Optimization by simulated annealing. *science, 220*, 671–680.

Koutroulis, E., & Blaabjerg, F. (2012). A New Technique for Tracking the Global Maximum Power Point of PV Arrays Operating Under Partial-Shading Conditions. *IEEE Journal of Photovoltaics, 2*, 184-190. doi:10.1109/JPHOTOV.2012.2183578

Kumar, N., Nema, S., Nema, R. K., & Verma, D. (2020). A state-of-the-art review on conventional, soft computing, and hybrid techniques for shading mitigation in photovoltaic applications. *International Transactions on Electrical Energy Systems, 30*, e12420.

Kumar, S., Yadav, S., Singh, N., & Tiwari, P. (2018). Evaluation amp; Analysis of MPPT Controller for PV Systems. *2018 International Conference on Computing, Power and Communication Technologies (GUCON)*, (s. 1161-1165). doi:10.1109/GUCON.2018.8674965

Kumar, V., Prabhakaran, K. K., Balasubramanian, V., & others. (2022). A Novel Algorithm based on Voltage and Current Perturbation to track Global peak under Partial Shading Conditions. *IEEE Transactions on Energy Conversion*.

Kuperman, A. (2014). Comments on "An analytical solution for tracking photovoltaic module MPP". *IEEE Journal of Photovoltaics, 4*, 734–735.

Leedy, A. W., Guo, L., & Aganah, K. A. (2012). A constant voltage MPPT method for a solar powered boost converter with DC motor load. *2012 Proceedings of IEEE Southeastcon*, (s. 1–6).

Li, G., Jin, Y., Akram, M. W., Chen, X., & Ji, J. (2018). Application of bio-inspired algorithms in maximum power point tracking for PV systems under partial shading conditions–A review. *Renewable and Sustainable Energy Reviews, 81*, 840–873.

Lian, K. L., Jhang, J. H., & Tian, I. S. (2014). A maximum power point tracking method based on perturb-and-observe combined with particle swarm optimization. *IEEE journal of photovoltaics, 4*, 626–633.

Liu, J., Li, J., Wu, J., & Zhou, W. (2017). Global MPPT algorithm with coordinated control of PSO and INC for rooftop PV array. *The Journal of Engineering, 2017*, 778–782.

Liu, Y.-H., Chen, J.-H., & Huang, J.-W. (2015). A review of maximum power point tracking techniques for use in partially shaded conditions. *Renewable and Sustainable Energy Reviews, 41*, 436-453. doi:https://doi.org/10.1016/j.rser.2014.08.038

Luque, A., & Hegedus, S. (2003). *Handbook of Photovoltaic Scienece and Engineering.* Wiley.

Mahmoud, Y. A., Xiao, W., & Zeineldin, H. H. (2012). A parameterization approach for enhancing PV model accuracy. *IEEE Transactions on Industrial Electronics, 60*, 5708–5716.

Marion, B. (2008). Comparison of predictive models for photovoltaic module performance. *2008 33rd IEEE Photovoltaic Specialists Conference*, (s. 1–6).

Mavromatakis, F., Vignola, F., & Marion, B. (2017). Low irradiance losses of photovoltaic modules. *Solar Energy, 157*, 496–506.

Meshram, P. M., & Kanojiya, R. G. (2012). Tuning of PID controller using Ziegler-Nichols method for speed control of DC motor. *IEEE-international conference on advances in engineering, science and management (ICAESM-2012)*, (s. 117–122).

Mobarak, M. H., & Bauman, J. (2021). A Fast Parabolic-Assumption Algorithm for Global MPPT of Photovoltaic Systems Under Partial Shading Conditions. *IEEE Transactions on Industrial Electronics, 69*, 8066–8079.

Moring, S., & Pols, A. F. (2012). Maximum power point tracking: algorithm and software development.

Muhsen, D. H., Ghazali, A. B., Khatib, T., & Abed, I. A. (2015). Extraction of photovoltaic module model's parameters using an improved hybrid differential evolution/electromagnetism-like algorithm. *Solar Energy, 119*, 286–297.

Mumtaz, S., Ahmad, S., Khan, L., Ali, S., Kamal, T., & Hassan, S. Z. (2018). Adaptive feedback linearization based neurofuzzy maximum power point tracking for a photovoltaic system. *Energies, 11*, 606.

Obaid, Z. A., Cipcigan, L. M., & Muhssin, M. T. (2017). Power system oscillations and control: Classifications and PSSs' design methods: A review. *Renewable and Sustainable Energy Reviews, 79*, 839–849.

Patel, H., & Agarwal, V. (2008). Maximum Power Point Tracking Scheme for PV Systems Operating Under Partially Shaded Conditions. *IEEE Transactions on Industrial Electronics, 55*, 1689-1698. doi:10.1109/TIE.2008.917118

Pradeep, K. P., Mouli, C. C., Reddy, K. S., & Raju, K. N. (2015). Design and implementation of maximum power point tracking in photovoltaic systems. *International Journal of Engineering Science Invention, 4*, 37–43.

Prasad, K. K., Myneni, H., & Kumar, G. S. (2018). Power quality improvement and PV power injection by DSTATCOM with variable DC link voltage control from RSC-MLC. *IEEE Transactions on Sustainable Energy, 10*, 876–885.

Prasanth Ram, J., Pillai, D. S., Rajasekar, N., & Kumar Chinnaiyan, V. (2020). Flower pollination based solar PV parameter extraction for double diode model. *Intelligent Computing Techniques for Smart Energy Systems* (s. 303–312). içinde Springer.

Rahman, M. M., & Islam, M. S. (2020). PSO and ANN based hybrid MPPT algorithm for photovoltaic array under partial shading condition. *Engineering International, 8*, 9–24.

Ram, J. P., & Rajasekar, N. (2017). A new robust, mutated and fast tracking LPSO method for solar PV maximum power point tracking under partial shaded conditions. *Applied energy, 201*, 45–59.

Ramasamy, A., & Suthanthira Vanitha, N. (2014). Maximum power tracking for PV generating system using novel optimized fractional order open circuit voltage- FOINC method. *2014 International Conference on Computer Communication and Informatics*, (s. 1-6). doi:10.1109/ICCCI.2014.6921842

Ramasamy, V., Feldman, D., Desai, J., & Margolis, R. (2021). *US Solar Photovoltaic System and Energy Storage Cost Benchmarks: Q1 2021.* Tech. rep., National Renewable Energy Lab.(NREL), Golden, CO (United States).

Ramli, M. A., Ishaque, K., Jawaid, F., Al-Turki, Y. A., & Salam, Z. (2015). A modified differential evolution based maximum power point tracker for photovoltaic system under partial shading condition. *Energy and Buildings, 103*, 175–184.

Rashid, M. H. (2017). *Power electronics handbook.* Butterworth-Heinemann.

Saadaoui, D., Elyaqouti, M., Assalaou, K., & Lidaighbi, S. (2021). Parameters optimization of solar PV cell/module using genetic algorithm based on non-uniform mutation. *Energy Conversion and Management: X, 12*, 100129.

Sai Krishna, G., & Moger, T. (2020). Enhanced power generation for total-cross-tied PV array using simulated annealing under partial shading conditions. *IET Renewable Power Generation, 14*, 3457–3468.

Salas, V., Olías, E., Barrado, A., & Lázaro, A. (2006). Review of the maximum power point tracking algorithms for stand-alone photovoltaic systems. *Solar Energy Materials and Solar Cells, 90*, 1555-1578. doi:https://doi.org/10.1016/j.solmat.2005.10.023

Sawant, P. T., Lbhattar, P. C., & Bhattar, C. L. (2016). Enhancement of PV system based on artificial bee colony algorithm under dynamic conditions. *2016 IEEE International Conference on Recent Trends in Electronics, Information & Communication Technology (RTEICT)*, (s. 1251–1255).

Sen, T., Pragallapati, N., Agarwal, V., & Kumar, R. (2018). Global maximum power point tracking of PV arrays under partial shading conditions using a modified particle velocity-based PSO technique. *IET Renewable Power Generation, 12*, 555–564.

Sera, D., Teodorescu, R., & Rodriguez, P. (2007). PV panel model based on datasheet values. *2007 IEEE International Symposium on Industrial Electronics*, (s. 2392-2396). doi:10.1109/ISIE.2007.4374981

Shaiek, Y., Smida, M. B., Sakly, A., & Mimouni, M. F. (2013). Comparison between conventional methods and GA approach for maximum power point tracking of shaded solar PV generators. *Solar energy, 90*, 107–122.

Shongwe, S., & Hanif, M. (2015). Comparative analysis of different single-diode PV modeling methods. *IEEE Journal of photovoltaics, 5*, 938–946.

Siddique, H. A., Xu, P., & De Doncker, R. W. (2013). Parameter extraction algorithm for one-diode model of PV panels based on datasheet values. *2013 International Conference on Clean Electrical Power (ICCEP)*, (s. 7–13).

Smida, M. B., & Sakly, A. (2015). Genetic based algorithm for maximum power point tracking (MPPT) for grid connected PV systems operating under partial shaded conditions. *2015 7th International Conference on Modelling, Identification and Control (ICMIC)*, (s. 1–6).

Smith, B. L., Woodhouse, M., Horowitz, K. A., Silverman, T. J., Zuboy, J., & Margolis, R. M. (2021). *Photovoltaic (PV) Module Technologies: 2020 Benchmark Costs and Technology Evolution Framework Results.* Tech. rep., National Renewable Energy Lab.(NREL), Golden, CO (United States).

Soon, J. J., & Low, K.-S. (2012). Photovoltaic model identification using particle swarm optimization with inverse barrier constraint. *IEEE Transactions on Power Electronics, 27*, 3975–3983.

Sundareswaran, K., Peddapati, S., & Palani, S. (2014). MPPT of PV systems under partial shaded conditions through a colony of flashing fireflies. *IEEE transactions on energy conversion, 29*, 463–472.

Sundareswaran, K., Vigneshkumar, V., Sankar, P., Simon, S. P., Nayak, P. S., & Palani, S. (2015). Development of an improved P&O algorithm assisted through a colony of foraging ants for MPPT in PV system. *IEEE transactions on industrial informatics, 12*, 187–200.

Suryavanshi, R., Joshi, D. R., & Jangamshetti, S. H. (2012). PSO and P&O based MPPT technique for SPV panel under varying atmospheric conditions. *2012 International Conference on Power, Signals, Controls and Computation*, (s. 1–6).

Tajuddin, M. F., Ayob, S. M., & Salam, Z. (2014). Global maximum power point tracking of PV system using dynamic population size differential evolution (DynNP-DE) algorithm. *2014 IEEE Conference on Energy Conversion (CENCON)*, (s. 254–259).

Tamrakar, R., & Gupta, A. (2015). A Review: extraction of solar cell modelling parameters. *International journal of innovative research in electrical, electronics, instrumentation and control engineering, 3*, 55–60.

Tauseef, M., & Nowicki, E. (2012). A simple and cost effective maximum power point tracker for PV arrays employing a novel constant voltage technique. *2012 25th IEEE Canadian Conference on Electrical and Computer Engineering (CCECE)*, (s. 1–4).

Tauseef, M., & Nowicki, E. (2012). A simple and cost effective maximum power point tracker for PV arrays employing a novel constant voltage technique. *2012 25th IEEE Canadian Conference on Electrical and Computer Engineering (CCECE)*, (s. 1-4). doi:10.1109/CCECE.2012.6334828

Teshome, D. F., Lee, C. H., Lin, Y. W., & Lian, K. L. (2016). A modified firefly algorithm for photovoltaic maximum power point tracking control under partial shading. *IEEE Journal of Emerging and Selected Topics in Power Electronics, 5*, 661–671.

Tsang, K. M., & Chan, W. L. (2015). Maximum power point tracking for PV systems under partial shading conditions using current sweeping. *Energy conversion and management, 93*, 249–258.

Valério, D., & Da Costa, J. S. (2006). Tuning of fractional PID controllers with Ziegler–Nichols-type rules. *Signal processing, 86*, 2771–2784.

Veerachary, M., Senjyu, T., & Uezato, K. (2001). Maximum power point tracking control of IDB converter supplied PV system. *IEE Proceedings-Electric Power Applications, 148*, 494–502.

Villalva, M. G., Gazoli, J. R., & Filho, E. R. (2009). Comprehensive Approach to Modeling and Simulation of Photovoltaic Arrays. *IEEE Transactions on Power Electronics, 24*, 1198-1208. doi:10.1109/TPEL.2009.2013862

Villalva, M. G., Gazoli, J. R., & Ruppert Filho, E. (2009). Comprehensive approach to modeling and simulation of photovoltaic arrays. *IEEE Transactions on power electronics, 24*, 1198–1208.

Wenham, S. R., Green, M. A., Watt, M. E., Corkish, R., & Sproul, A. (2013). *Applied photovoltaics.* Routledge.

Xiao, W., & Dunford, W. G. (2004). A modified adaptive hill climbing MPPT method for photovoltaic power systems. *2004 IEEE 35th annual power electronics specialists conference (IEEE Cat. No. 04CH37551), 3*, s. 1957–1963.

Yang, B., Zhang, X., Yu, T., Shu, H., & Fang, Z. (2017). Grouped grey wolf optimizer for maximum power point tracking of doubly-fed induction generator based wind turbine. *Energy conversion and management, 133*, 427–443.

Yang, X.-S. (2008). Introduction to Computational Mathematics.

Yang, X.-S., & Deb, S. (2009). Cuckoo search via Lévy flights. *2009 World congress on nature & biologically inspired computing (NaBIC)*, (s. 210–214).

Zhang, Y. (2021). Neural network algorithm with reinforcement learning for parameters extraction of photovoltaic models. *IEEE Transactions on Neural Networks and Learning Systems*.

CURRICULUM VITAE

Bülent BÜYÜKGÜZEL , received a B.Sc. degree in Electronic Engineering Department from Uludağ University, Bursa, in 1985. He worked in Turkish Telekom for many years. He received his M.Sc. degree in the Electrical and Electronics Engineering Department from Çukurova University, Adana, Turkey, in 2011. He is working at Çukurova University as an engineer.